LA-UR-29622

Proton and Ion Linear Accelerators

9. Emittance Growth, Halo Formation, and Beam Loss

Yuri Batygin
Los Alamos National Laboratory

U.S. Particle Accelerator School
Albuquerque, New Mexico, June 17-28, 2019

Operated by Los Alamos National Security, LLC for the U.S. Department of Energy's NNSA

Sources of Beam Loss

1. Misalignments of accelerator channel components
2. Transverse-longitudinal coupling in RF field
3. Particle scattering on residual gas, intra-beam stripping
4. Nonlinearities of focusing and accelerating elements
5. Non-linear space-charge forces of the beam
6. Mismatch of the beam with accelerator structure
7. Instabilities of accelerating and focusing field
8. Beam energy tails from un-captured particles
9. Dark currents (un-chopped beam, RF transients)
10. Excitation of higher-order RF modes
11. Black-body radiation

Requirements on Hands-On Maintenance of Accelerator

Beam loss criteria:

Radioactivation limit of 20 mrem/hour at a distance of 1 m from the accelerator beamline after long operation of linac and after 1 hour of downtime.

Required beam losses: less than 1 W/m

For beam power 1 MW beam losses should be less than 10^{-6}/m.

Requirements on Hands-On Maintenance of Accelerator

Allowable beam power loss versus beam energy to produce an activation of 0.1 mSv/h (10 mrem/h) at 30 cm for the case of copper, after 4 h cool down (M. Plum, CERN-2016-002).

Beam Losses in LANL Linear Accelerator

Drift Tube Linac 0.75 – 100 MeV

Transition Region

Coupled- Cavity Linac (100 MeV – 800 MeV)

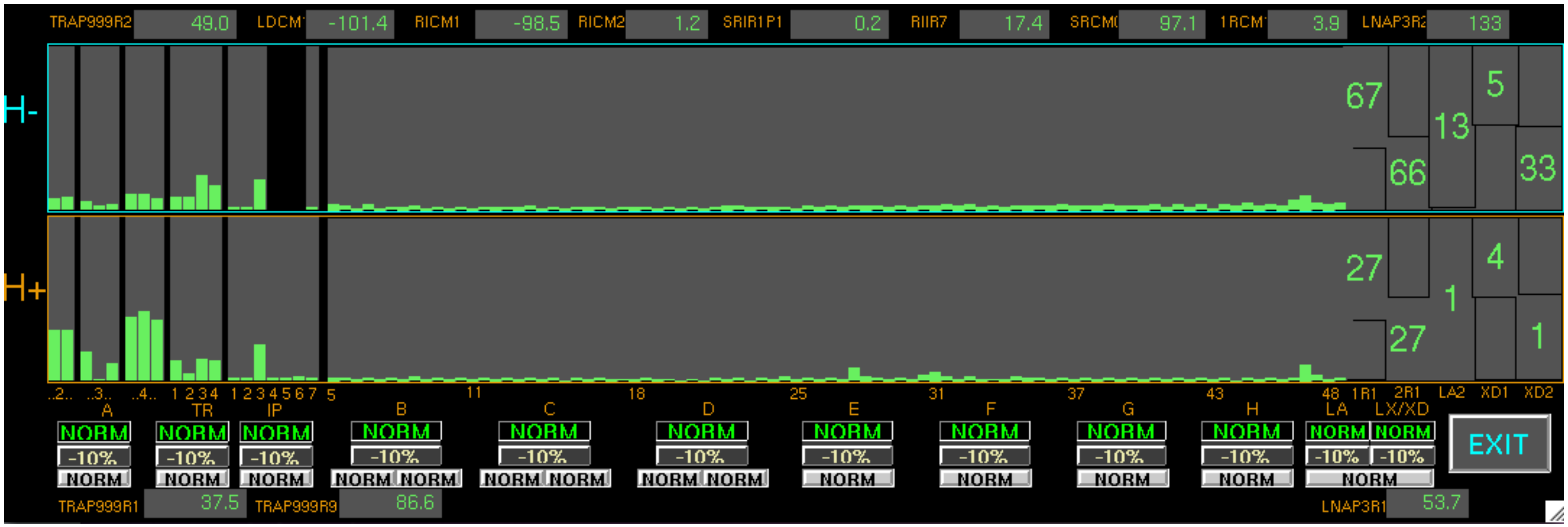

LANL linac loss monitors (Activation Protection devices): liquid scintillator and photomultiplier tube, calibrated against 100 nA point spill. Average beam losses are 0.1 – 0.2 W/m.

Year	Pulse Rate (Hz)	Summed Loss Monitor Reading (A.U.)
2018	120/60	180
2017	120	150
2016	120	190
2015	120	135
2014	60	211
2013	60	190

Beam Loss Monitors

Scintillation based detector

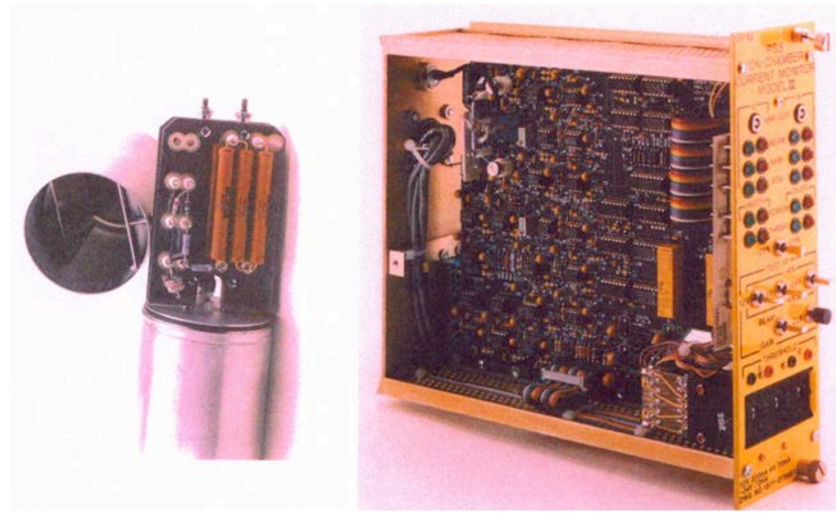

Gamma detector: ion chamber based loss monitor

LANSCE beam spill monitoring along high-energy beamlines

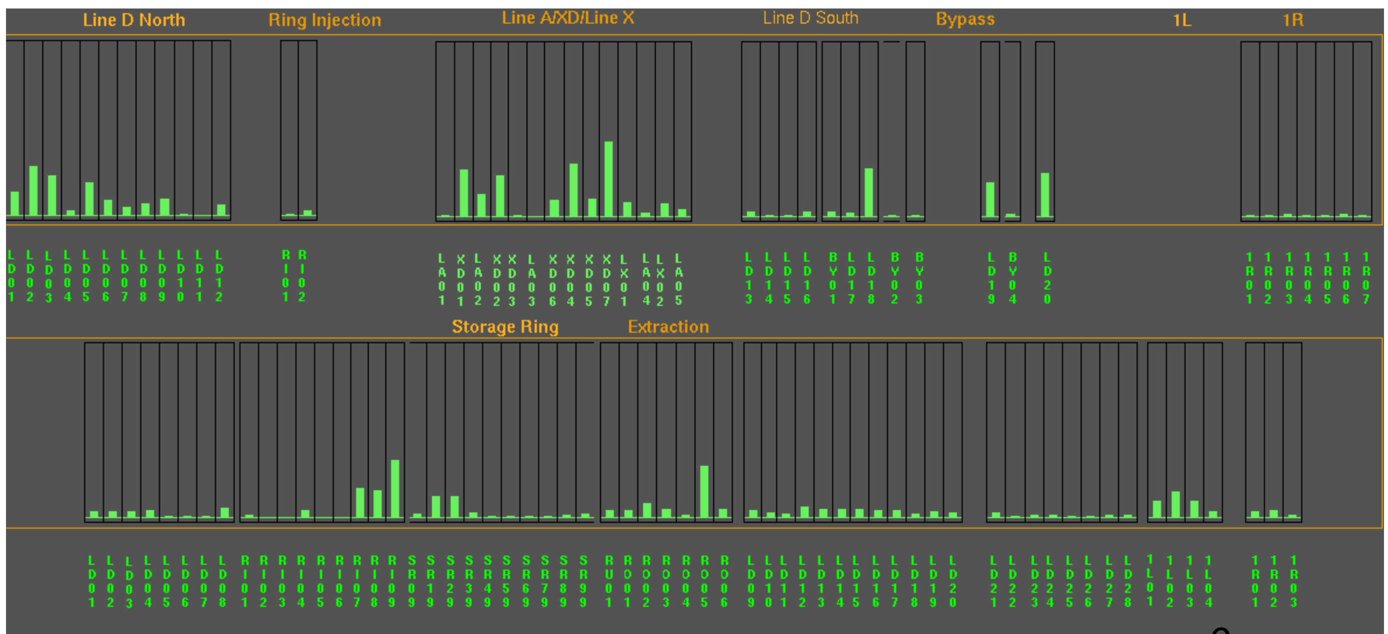

Beam Loss Monitors (cont.)

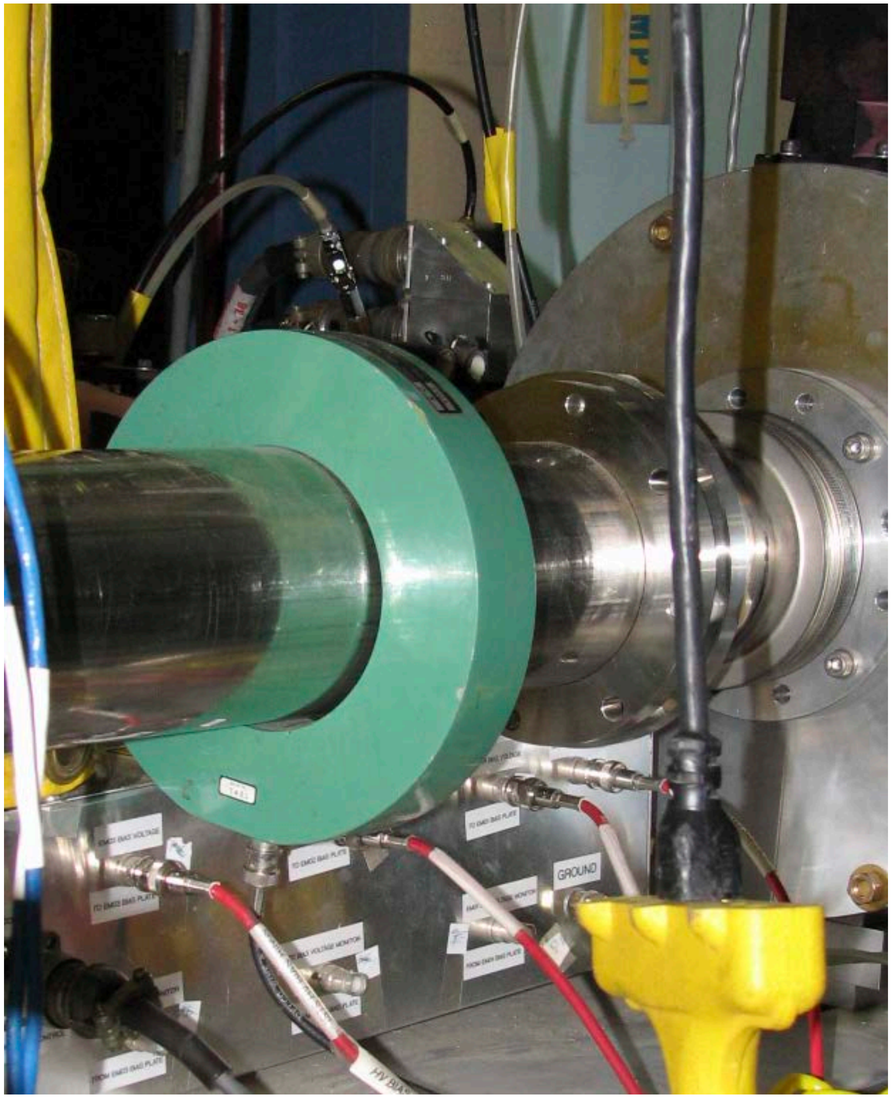

Gamma Detectors feed Radiation Safety System

Hardware Transmission Monitors (HWTM) measures the beam current losses between current monitors and limit beam current to a value at one current monitor.

Vibrating Wire Sensor as a Halo Monitor

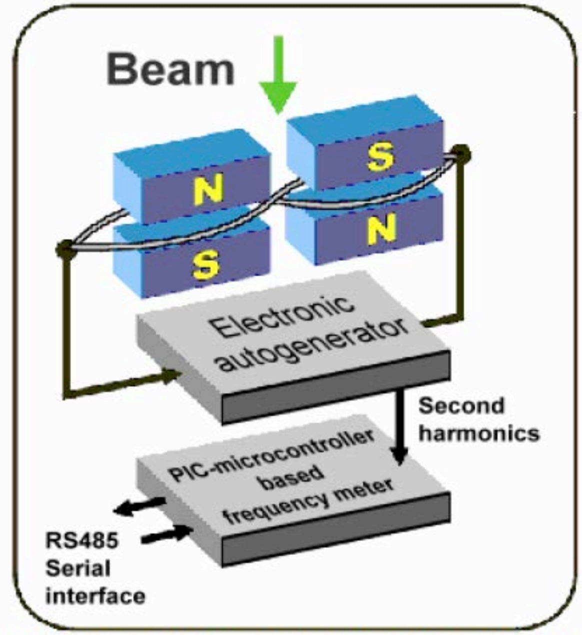

Vibrating wire scanner test in lab [Arutunian et. al., PAC (March 29 - April 2. 1999. New York City)]

The operating principle of vibrating wire sensors is measurement of the change in the frequency of a vibrating wire, which is stretched on a support, depending on the physical parameters of the wire and the environment in

By use of a simple positive feedback circuit, the magnetic system excites the second harmonic of the wire's natural oscillation frequency while keeping the middle of the wire exposed for detection of beam heating.

The interaction of the beam with the wire mainly causes heating of the wire due to the energy loss of the particles

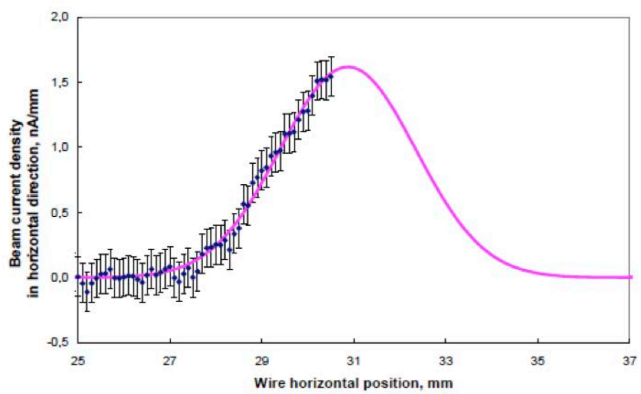

Scan of the electron beam at the Injector of Yerevan Synchrotron with an average current of about 10 nA (after collimation) and an electron energy of 50 MeV

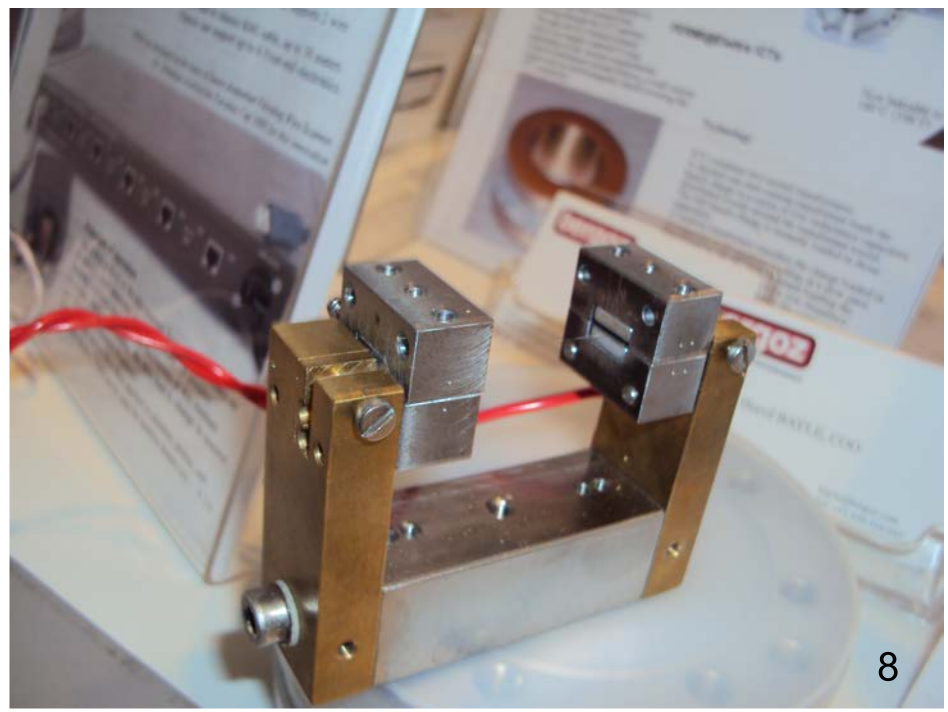

Linac Beam Distribution in Phase Space

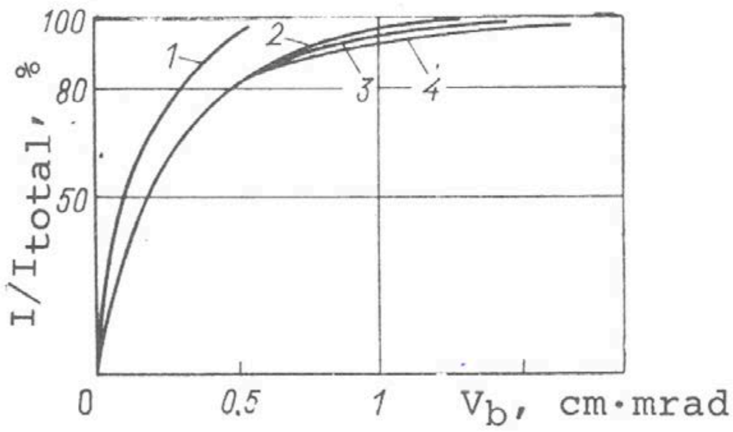

Fig. 4.8 The distribution of the current in the phase space of the beam at different points in the CERN proton accelerator-injector. 1--0.5 MeV, 115 mA; 2--10 MeV; 3--30 MeV; 4--50 MeV, 58 mA.

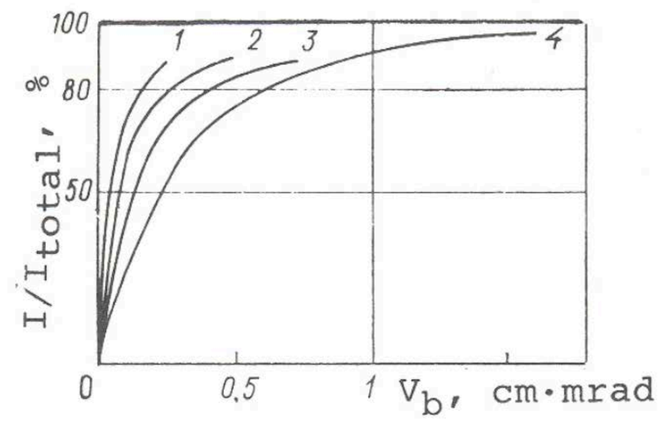

Fig. 4.9 The distribution of the current in the phase space of the beam in the FNAL proton accelerator-injector. 1--0.75 MeV, 150 ma; 2--10 MeV; 3 and 4--200 MeV, 78 mA.

Beam Distribution as a Function of Beam Intensity

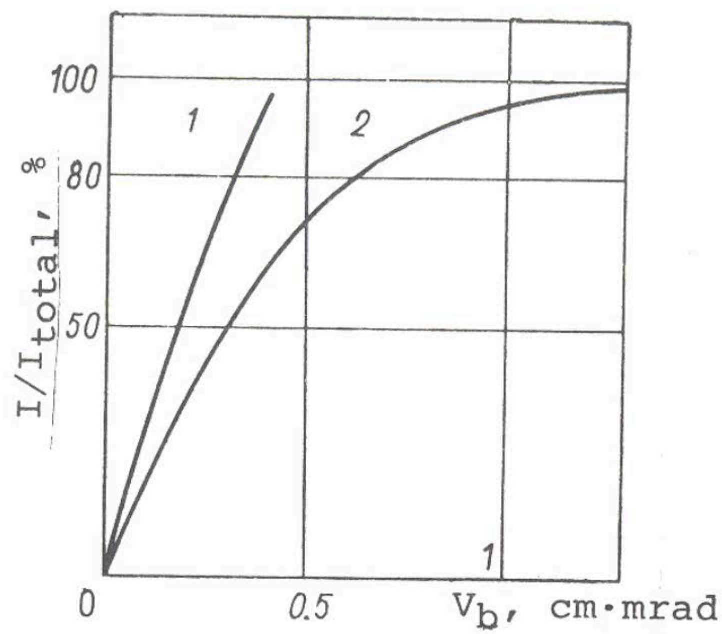

Fig. 4.10 The distribution of the current in the phase space of the beam at the entrance and exit of the ITEP proton accelerator-injector. 1--0.7 MeV, 470-600 mA; 2--25 MeV, 160-200 mA.

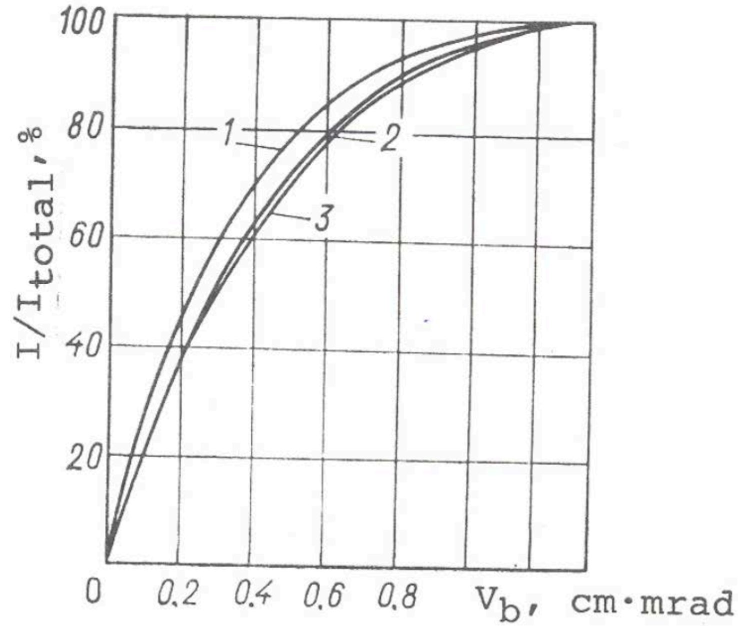

Fig. 4.11 The distribution of the current in the phase space of the beam at the exit of the ITEP accelerator-injector for different values of the total current of the accelerated beam. 1--60-100 mA; 2--100-160 mA; 3--160-200 mA.

Empirical experimental dependence of beam emittance growth in RF linac versus beam current *I* (0.6< n <1.0)

$$\boxed{\varepsilon_{out} = \sqrt{\varepsilon_{in}^2 + kI^n}}$$

Beam Halo

1. Beam halo - a collection of particles which lies outside of beam core and typically contain small fraction of the beam (less than 1%).

2. Beam halo is a main source of beam losses which results in radio-activation and degradation of accelerator components.

3. Modern accelerator projects using high-intensity beams with final energies of 1-1.5 GeV and peak beam currents of 30-100 mA require keeping the beam losses at the level of 10^{-7}/m (less than 1 Watt/m) to avoid activation of the accelerator and allowing hands-on maintenance over long operating periods.

4. Collimation of beam halo cannot prevent beam losses completely, because the halo of a mismatched beam re-develops in phase space after a certain distance following collimation.

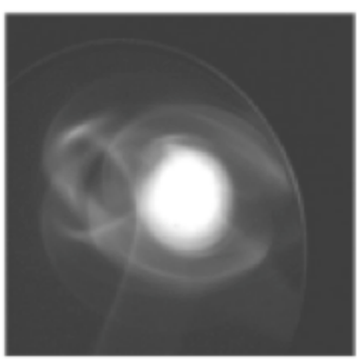

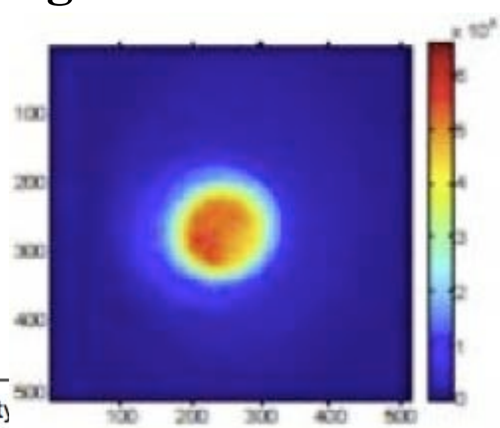

Beam halo monitoring at Liverpool University

http://liv.ac.uk/quasar/research/beam-instrumentation/beam-halo-studies/

Beam Emittance Growth in Low Energy Beam Transport

RF Bunching

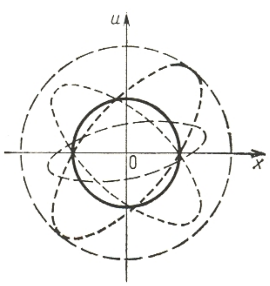

Beam	Emittance Growth $\varepsilon_{RF}/\varepsilon$
H^-	1.1 – 1.2
H^+	1.9 – 2.2

Bunchers Off

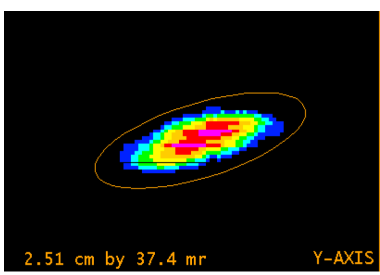

Bunchers On

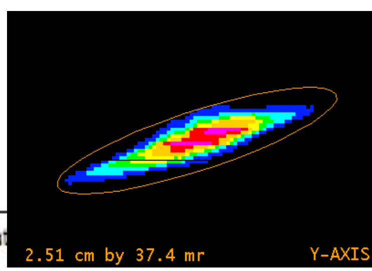

H^- Beam Chopping

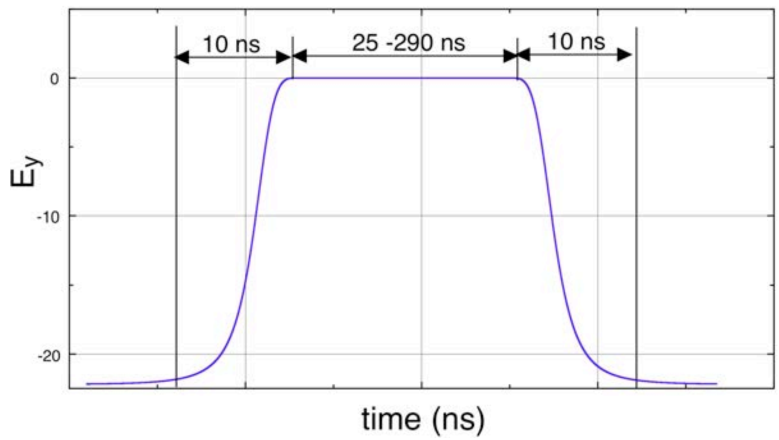

H^- Chopper Pulse	Emittance Growth $\varepsilon_{ch}/\varepsilon$
290 ns	1.1
36 ns	1.3

Chopper Off

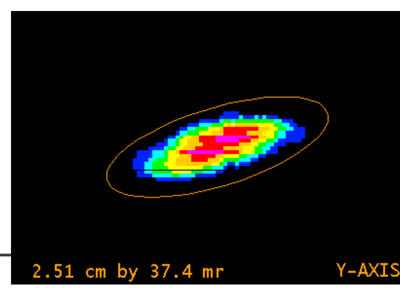

Chopper pulse 290 ns

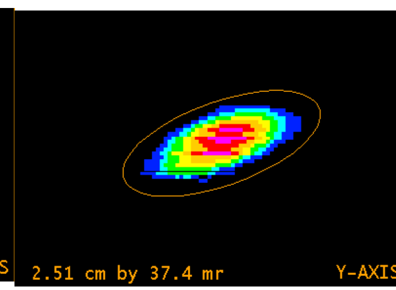

Chopper pulse 36 ns

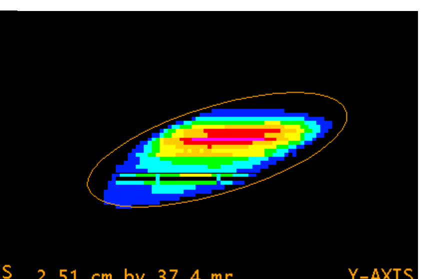

Transverse-Longitudinal Dynamics in RF Field

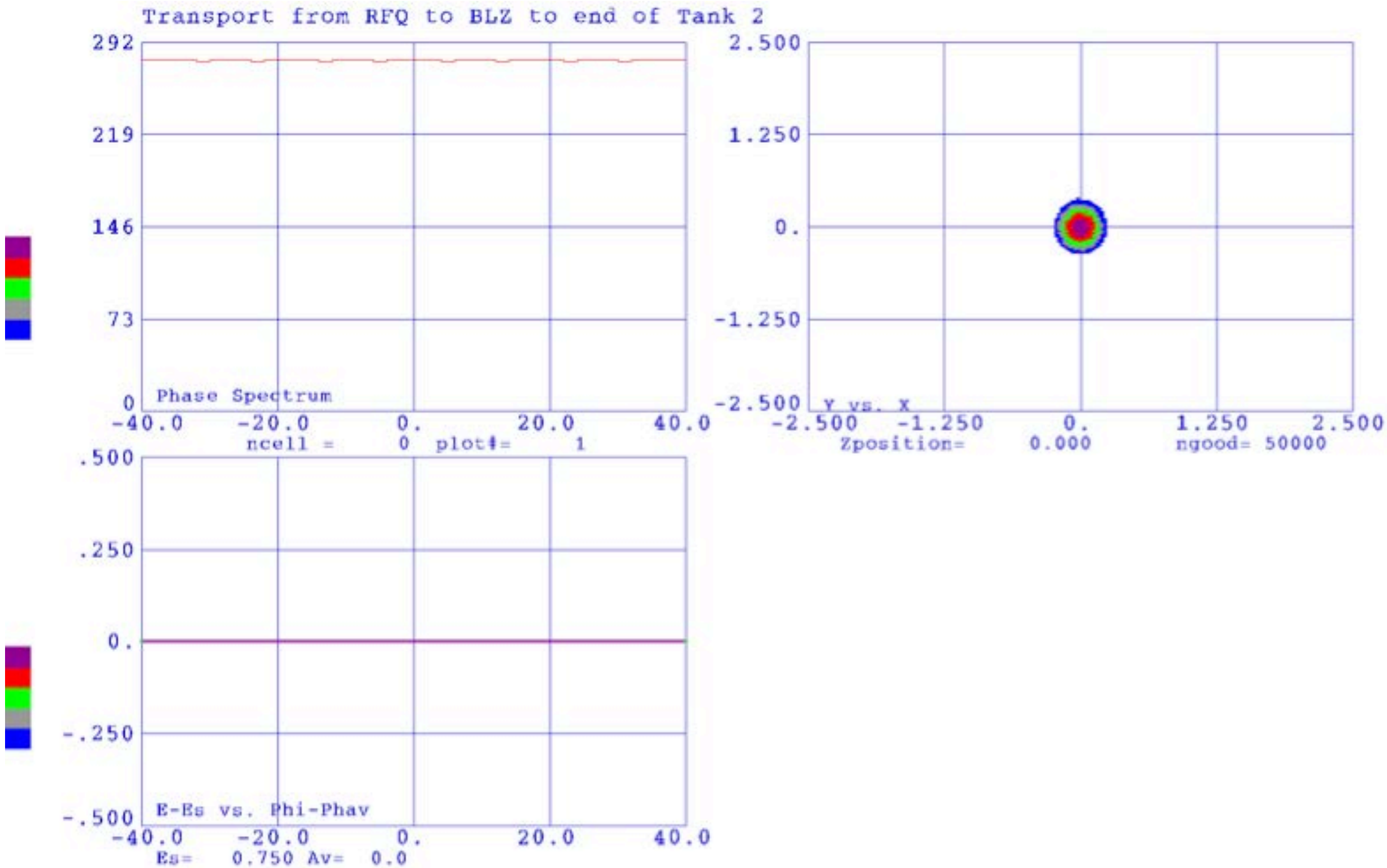

Example of beam dynamics in accelerating structure (courtesy of Larry Rybarcyk).

Emittance Growth due to Transverse-Longitudinal Coupling

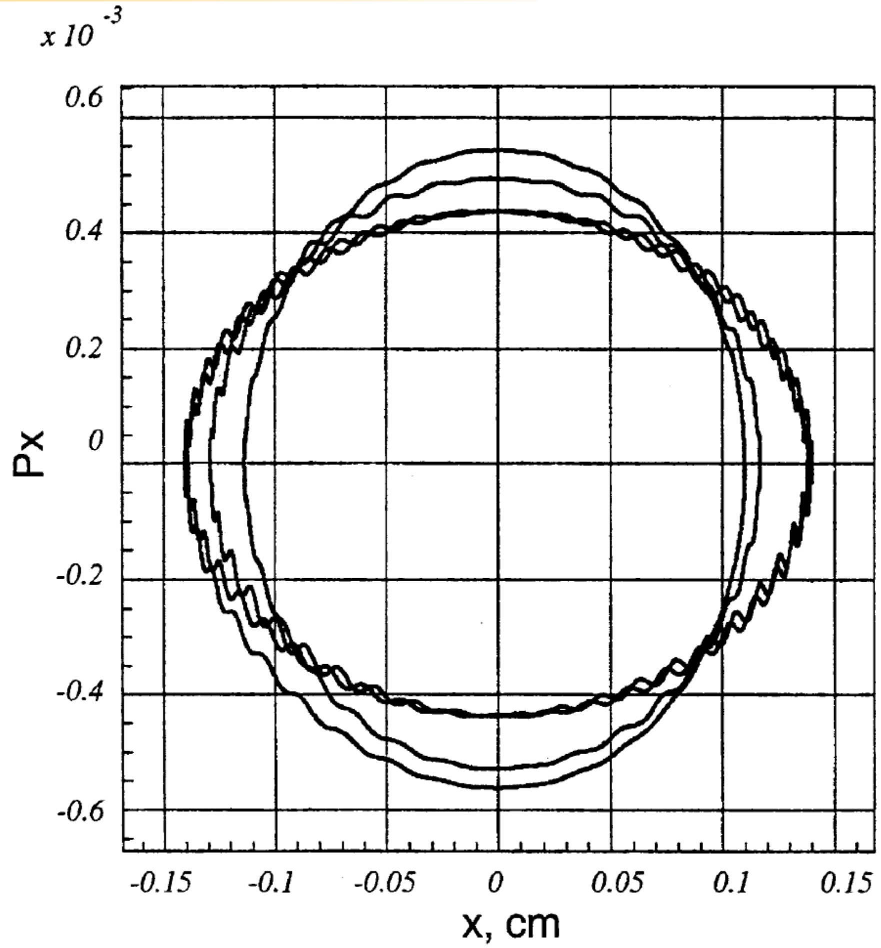

Phase space trajectory of particle in a standing wave RF accelerator.

Emittance Growth due to Transverse-Longitudinal Coupling (cont.)

Transverse oscillations in presence of RF field:

$$\frac{d^2X}{dt^2} + X[\Omega_{rs}^2 - \frac{\Omega^2}{2} h \sin(\Omega t + \psi_o)] = 0$$

Parameter h is proportional to amplitude of longitudinal oscillations Φ.

$$h = \Phi / |\mathrm{tg}\varphi_s|$$

Transverse oscillation equation for synchronous particle

$$\frac{d^2X}{dt^2} + \Omega_{rs}^2 X = 0$$

Solution of equation for synchronous particle:

$$X = A\cos(\Omega_{rs} t + \psi_o)$$

$$\dot{X} = -A\Omega_{rs} \sin(\Omega_{rs} t + \psi_o)$$

Synchronous particle performs oscillations along elliptical phase trajectory in phase space

$$\frac{X^2}{A^2} + \frac{\dot{X}^2}{\Omega_{rs}^2 A^2} = 1$$

Beam emittance

$$Э = \frac{A^2\Omega_{rs}}{v_s}$$

Emittance Growth due to Transverse-Longitudinal Coupling (cont.)

Maximum deviation from axis, A_{max}, is achieved by particles with minimal transverse oscillation frequency, while maximum spread in transverse momentum (and minimal amplitude A_{min}) is achieved by particles with maximal oscillation frequency

$$\Omega_{r\_\min} = \sqrt{\Omega_{rs}^2 - \frac{\Omega^2}{2} h}$$

$$\Omega_{r\_\max} = \sqrt{\Omega_{rs}^2 + \frac{\Omega^2}{2} h}$$

Non-synchronous particle performs transverse oscillations with variable transverse frequency while phase space area comprised by this motion is constant according to adiabatic theorem

$$Э = \frac{A_{\max}^2 \, \Omega_{r\_\min}}{v_s} \qquad Э = \frac{A_{\min}^2 \, \Omega_{r\_\max}}{v_s}$$

Effective emittance is limited by ellipse with semi-axes

$$X = A_{\max} \qquad \dot{X} = A_{\min} \Omega_{r\_\max}$$

$$Э_{eff} = \frac{A_{\max} \, A_{\min} \, \Omega_{r\_\max}}{v_s}$$

$$\boxed{\frac{Э_{eff}}{Э} = \sqrt{\frac{\Omega_{r\_\max}}{\Omega_{r\_\min}}} \approx 1 + \frac{\Omega^2}{4\Omega_{rs}^2} h}$$

$$h = \Phi / \left| \mathrm{tg} \varphi_s \right|$$

Emittance Growth in Drift Tube Linac (0.75 MeV – 100 MeV)

Beam Capture in DTL 75% - 80%
Additional losses 0.1% -1%

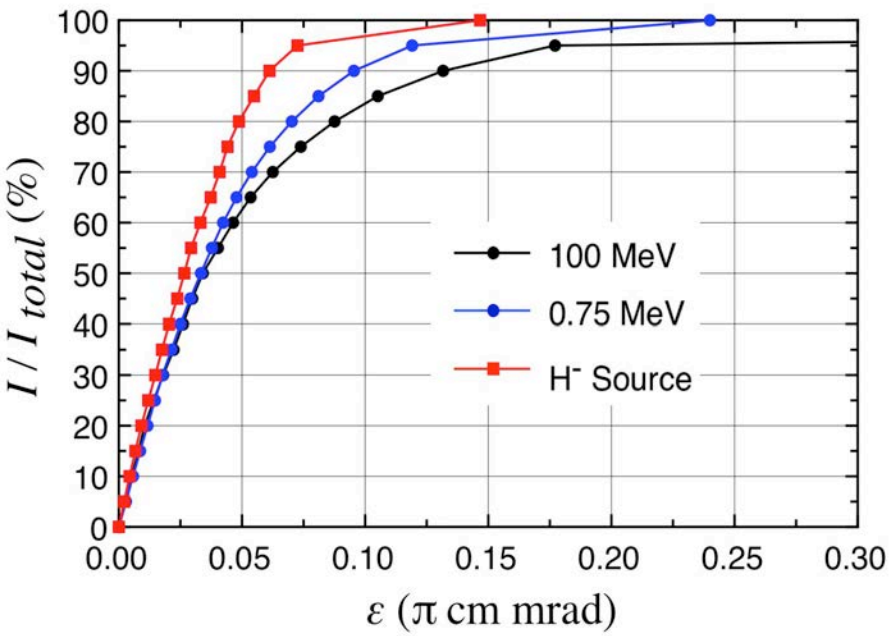

Accelerator Misalignment

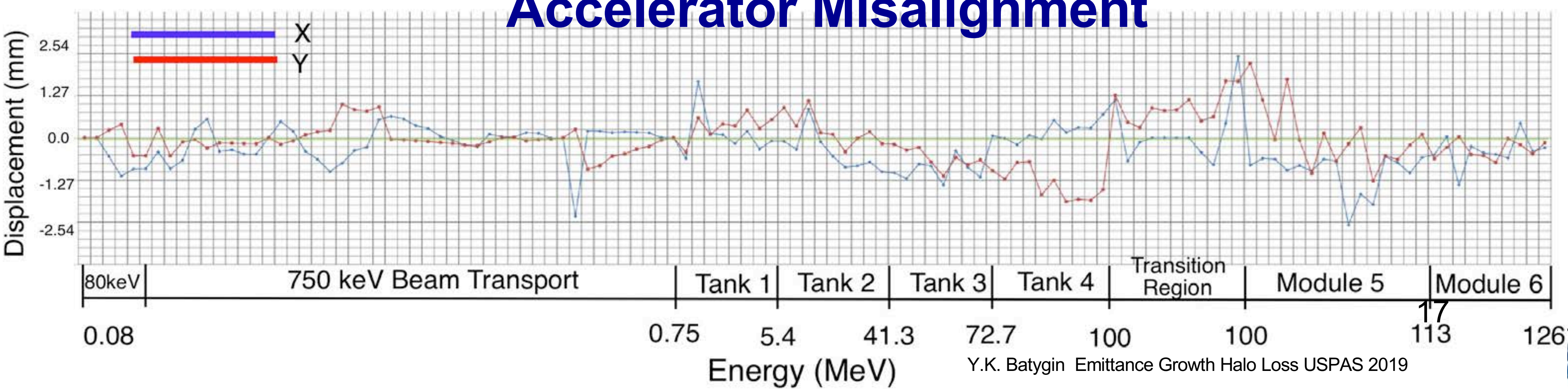

Dynamics of Uncaptured Particles in Drift Tube Linac

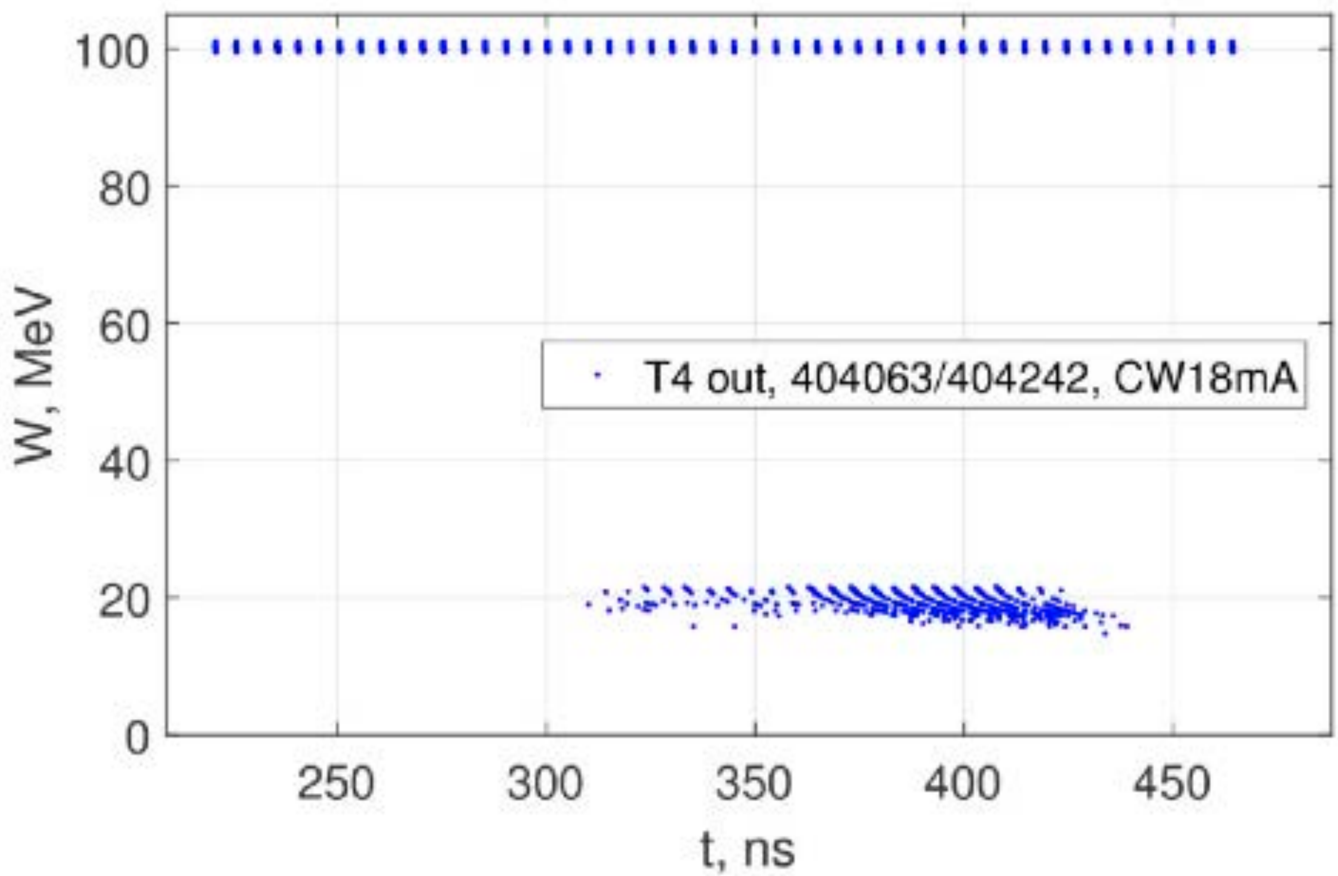

Distance between RF gaps: $L = n\beta\lambda$

***n=1* accelerated particles**

***n=2* non-accelerated particles**

Accelerated and non-accelerated particles after Tank 4 (S.Kurennoy, IPAC16)

Beam Capture in Tank 1 of LANSCE Drift Tube Linac

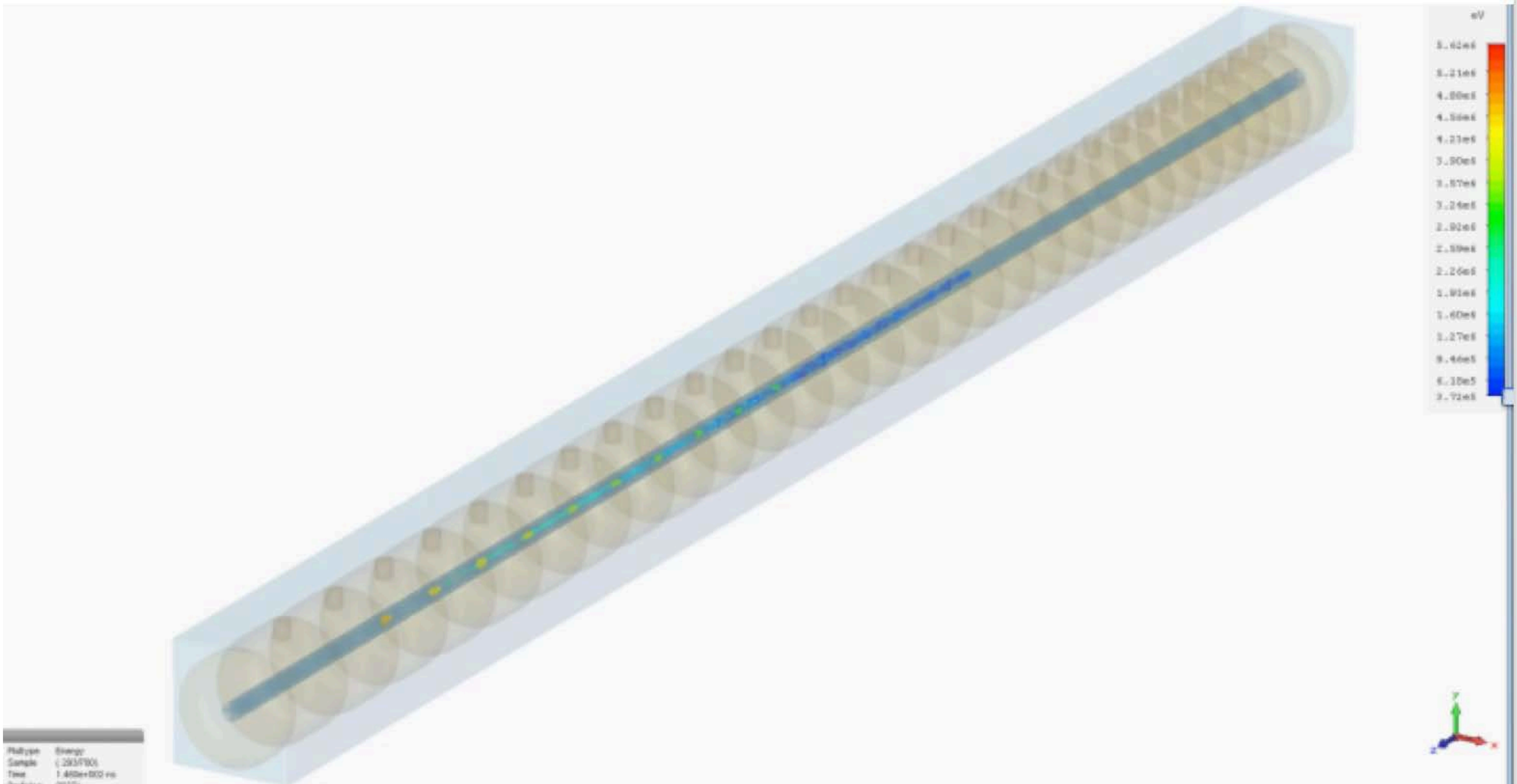

(Courtesy of Sergey Kurennoy)

Acceleration in Non-Ideal Accelerating Structure

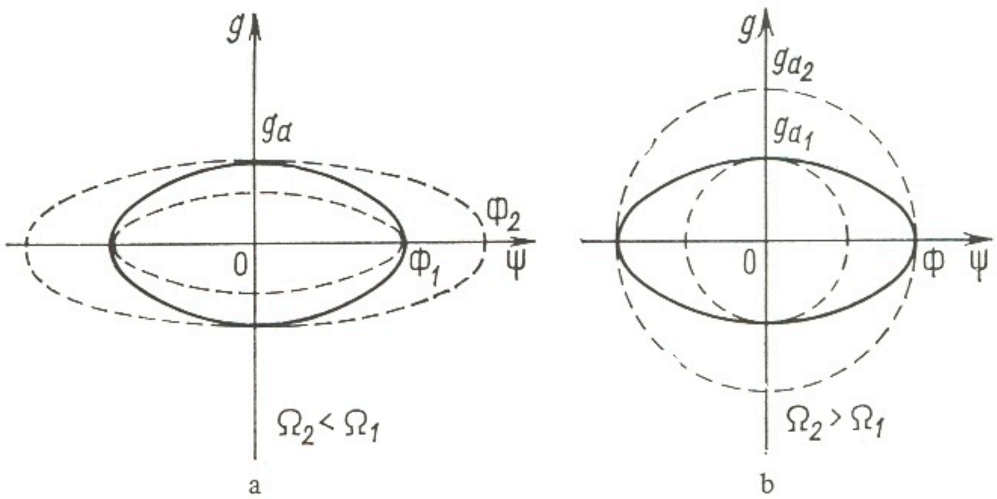

Fig. 1.12 Effect of an abrupt change in frequency on longitudinal oscillations of particles.

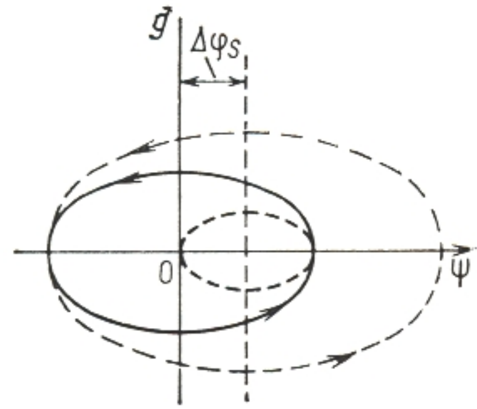

Fig. 1.10 Effect of an abrupt change of the equilibrium phase on the longitudinal oscillations of particles.

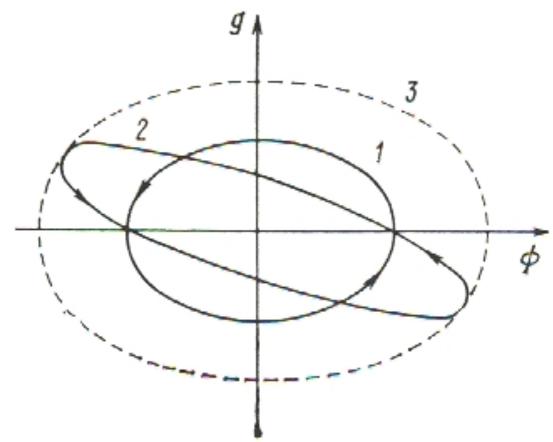

Fig. 1.11 Effect of an empty space on longitudinal oscillations of particles.

Acceleration in Non-Ideal Accelerating Structure (cont.)

Relative momentum deviation from synchronous particle
$$g = \frac{p - p_s}{p_s}$$

Dimensionless longitudinal oscillation frequency
$$\frac{\Omega}{\omega} = \sqrt{\left(\frac{qE\lambda}{mc^2}\right)\frac{|\sin\varphi_s|}{2\pi\beta\gamma^3}}$$

Dimensionless acceleration rate
$$W_\lambda = \frac{eE_o T\lambda\cos\varphi_s}{mc^2}$$

Increase in relative momentum spread

$$\langle \Delta g_a \rangle = \sqrt{\frac{N}{2}\left[\langle \delta g \rangle^2 + \left(\frac{\Omega}{\omega}\right)_N^2 \langle \delta\psi \rangle^2\right]},$$

$$\langle \delta\psi \rangle = 2\pi \left\langle \frac{\delta z}{\beta\lambda} \right\rangle;$$

$$\langle \delta g \rangle = \frac{kW_\lambda}{\beta_N}\sqrt{\left\langle \frac{\delta E_0}{E_0} \right\rangle^2 + 4\pi^2 \operatorname{tg}^2 \varphi_s \left\langle \frac{\delta z}{\beta\lambda} \right\rangle^2}.$$

Acceleration in Non-Ideal Accelerating Structure (cont.)

For LANL 805-MHz linac

$$< \delta(\frac{\Delta p}{p}) >= \sqrt{\frac{N_a}{2}(1.5\cdot 10^{-7} < \frac{\delta E_o}{E_o} >^2 + 4.6\cdot 10^{-6} < \delta\psi >^2)}$$

Typical momentum spread: $\Delta p/p$ = 8x10^{-4}.

For instability of the RF field amplitude

$$< \delta E_o / E_o > \approx 1\%$$

estimated increase of momentum spread of the beam

$$< \delta(\Delta p / p) > \approx 1.7\cdot 10^{-4}$$

Beam Energy Spread Measurements

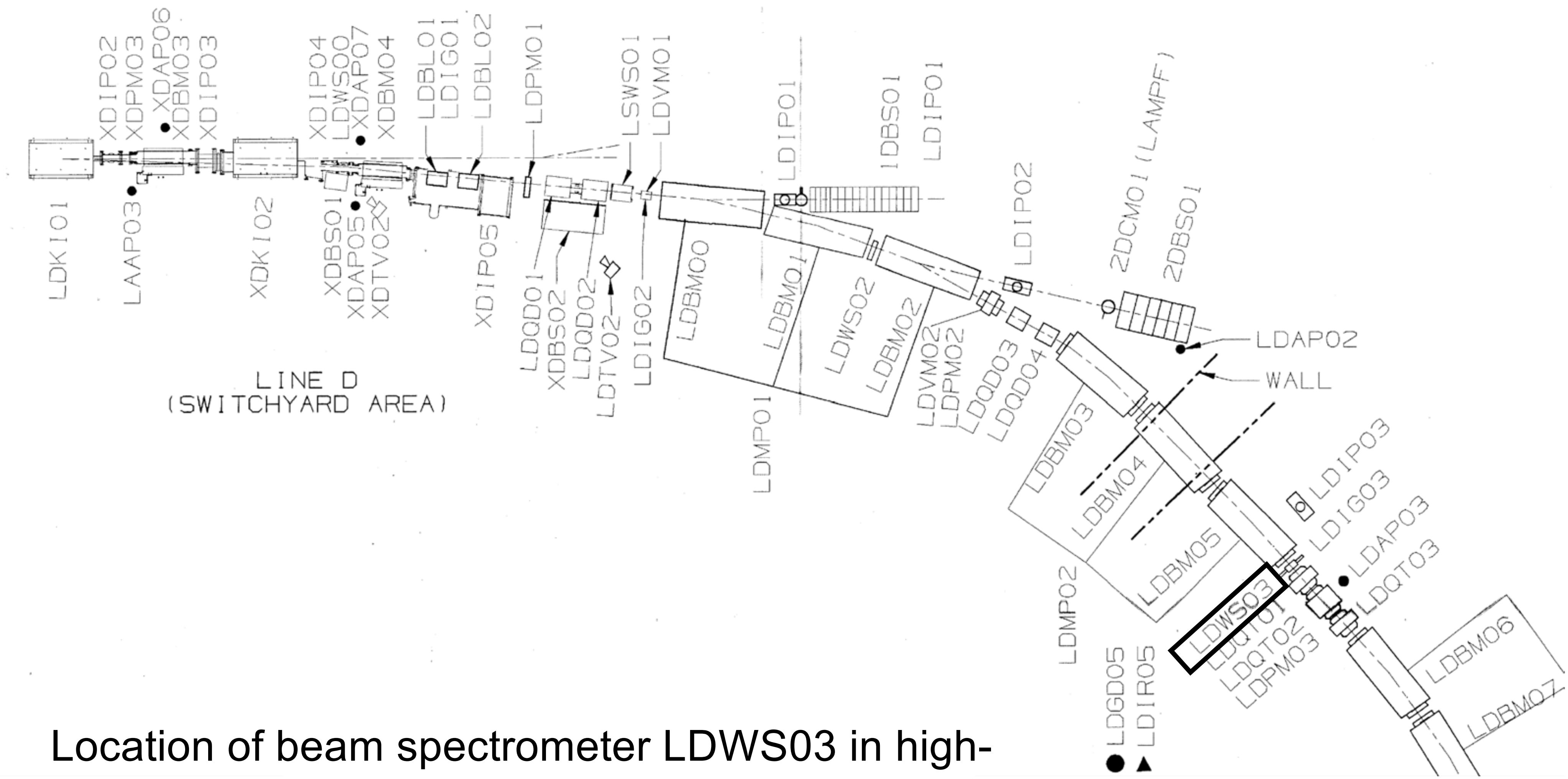

Location of beam spectrometer LDWS03 in high-energy part of accelerator facility

Beam Energy Spread Measurements (cont.)

Beam Momentum Spread

$$\frac{\Delta p}{p} = \frac{\sqrt{R_x^2 - \beta_x (4\, \varepsilon_{x\_rms})}}{\eta}$$

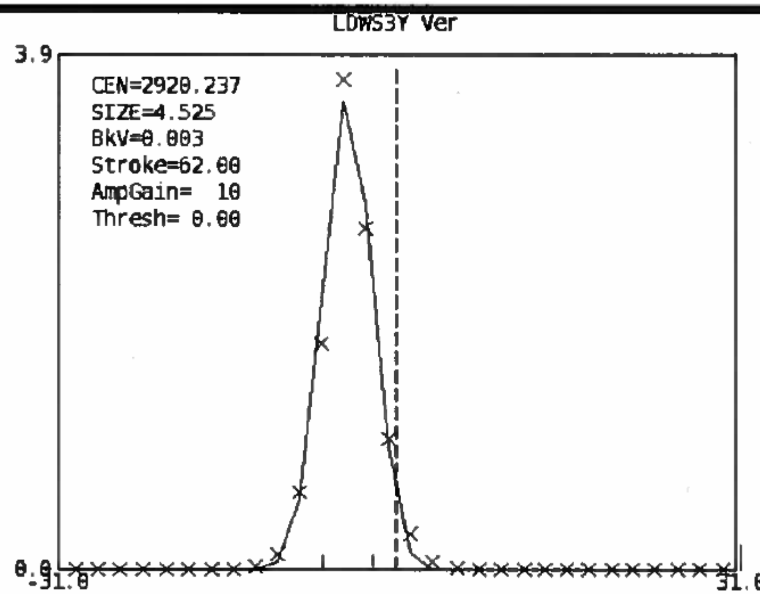

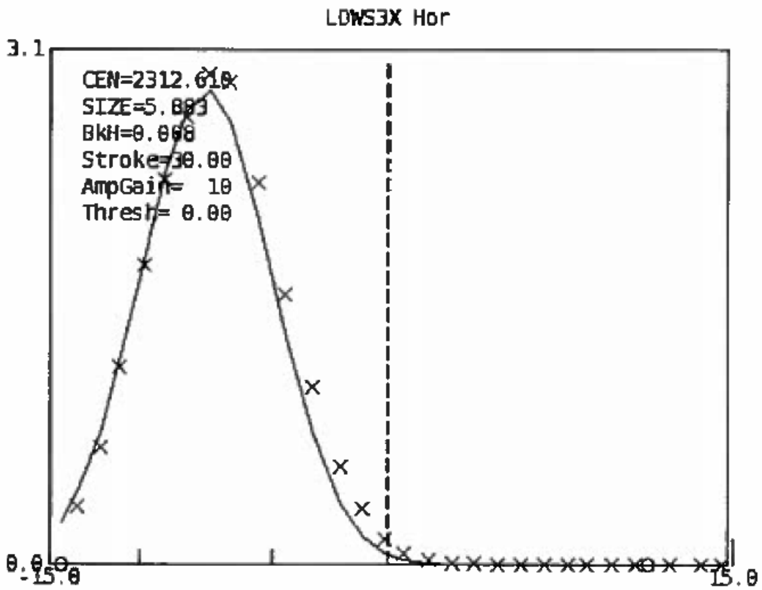

R_x =0.5793 cm

β_x =1.11236 cm /mrad

ε_{x_rms} =0.04 π cm mrad

η =4.8798 m

$$\frac{\Delta p}{p} = 8.13 \cdot 10^{-4}$$

Background Avg = 4, Data Avg = 10, NBins = 30, Mode = STEP, Algorithm = Gauss 0.0, Sequential Scan
WSPSR Wire Scanners -- 2017.01.30-13:02:23.023, Beam Gate = SRT0, Rep Rate = 4, DWSS = 1174, SWSS = 1174, WSDT = 1610

Beam Energy Spread Measurements (cont.)

(a) (b)

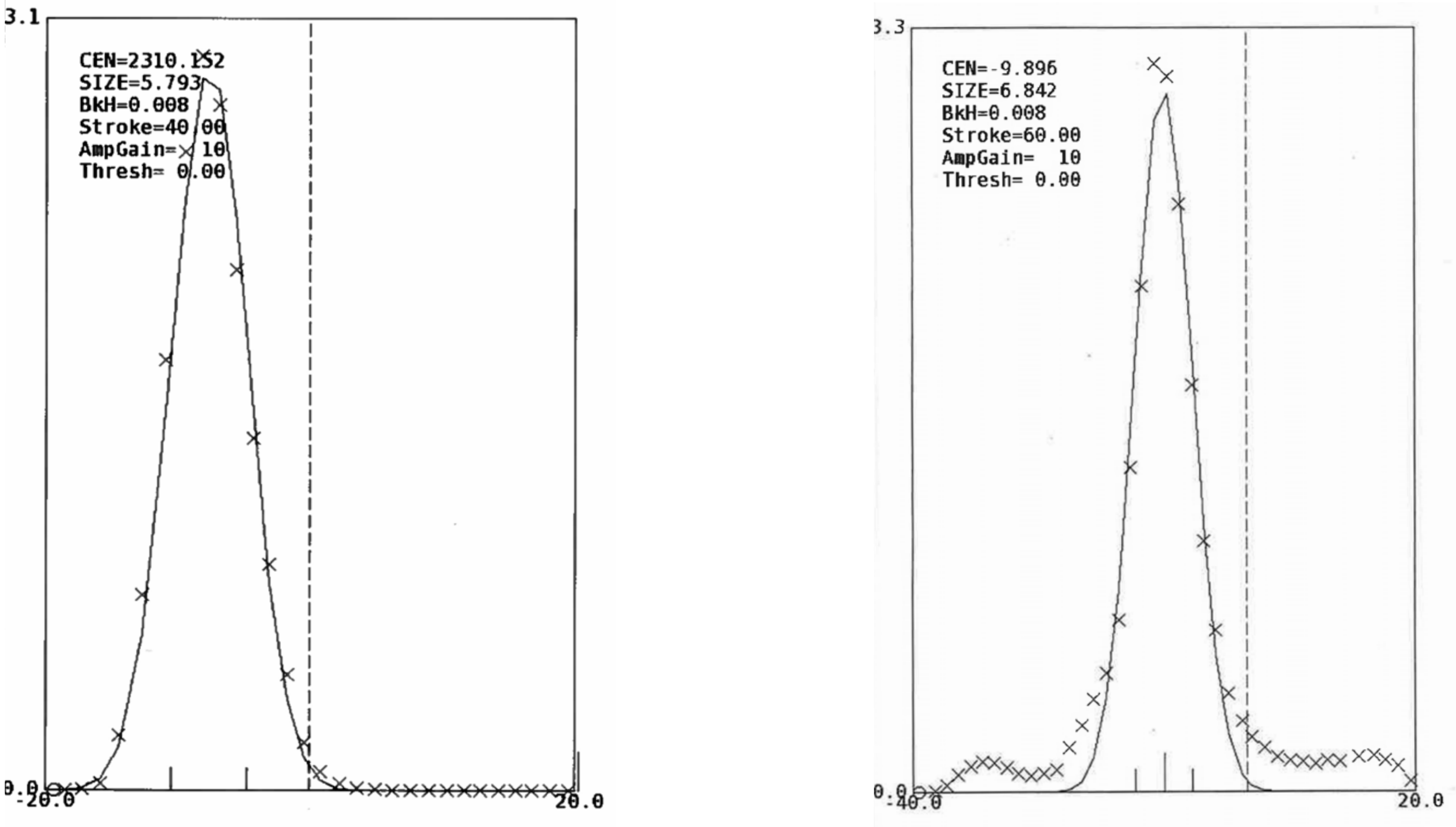

Momentum spread of the beam measured by LDWS03 wire scanner: (a) properly tuned beam, (b) beam with momentum tails due to improper tune.

Effect of DTL Cavity Field Error on Beam Losses

Maximum Spill ≈ $10^{n*Error}$ where n = 3 - 4

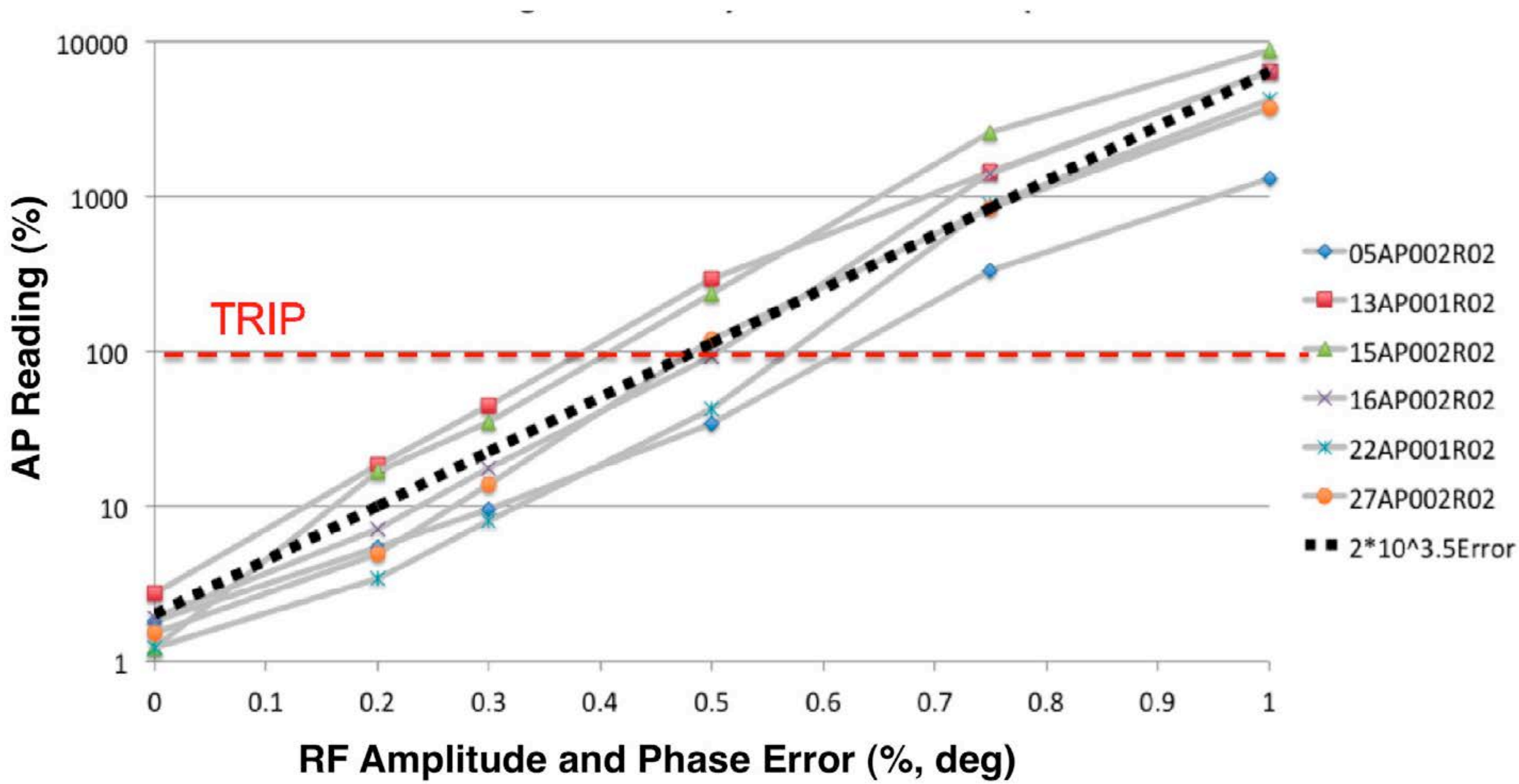

(L.Rybarcyk et al, LINAC 2016)

Observation of Low-Momentum Beam Spill

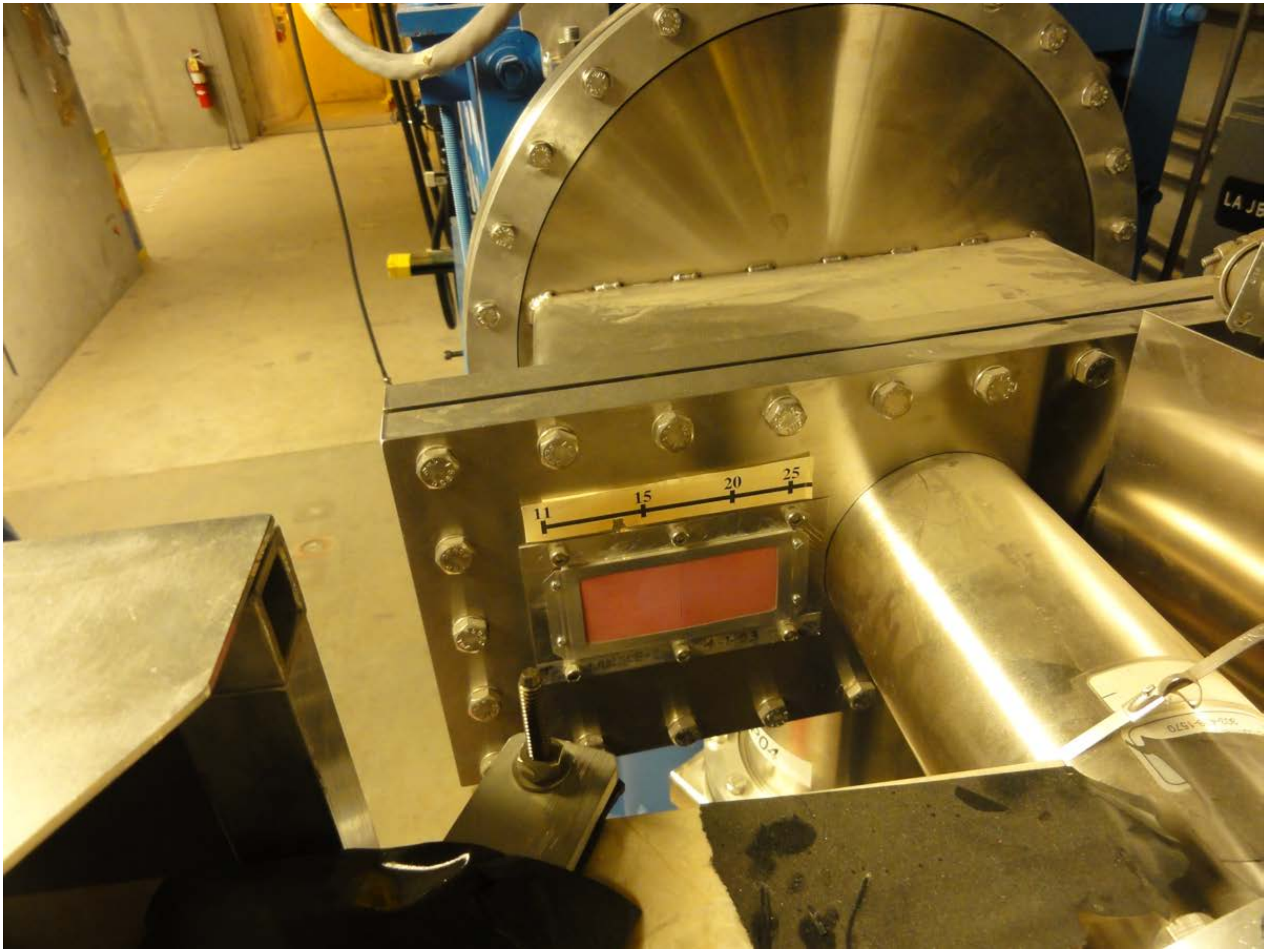

Observation of Low-Momentum Beam Spill

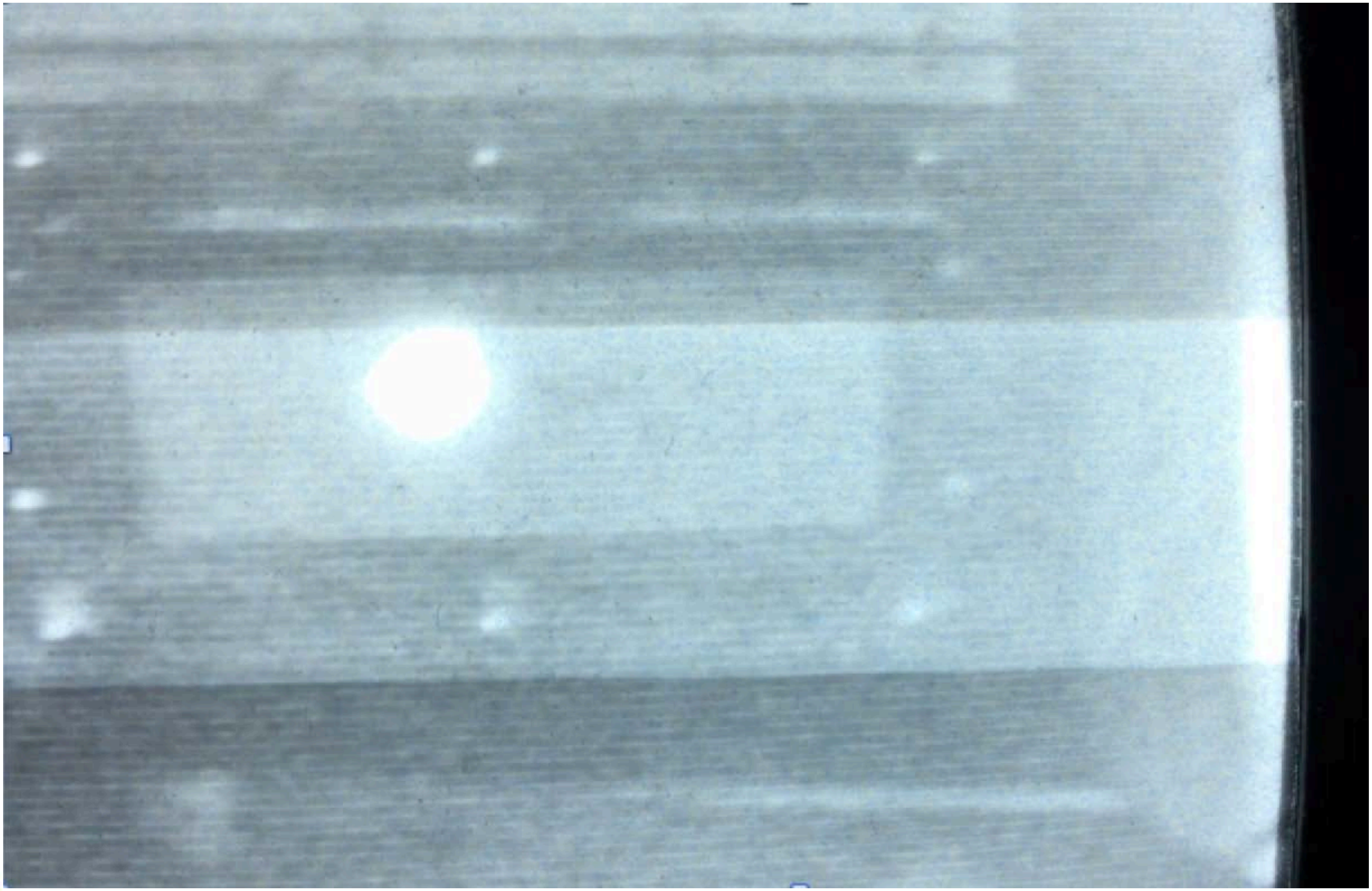

Transverse Oscillations in Non-Ideal Focusing Structure

Rms increase of amplitude of transverse oscillations

$$\langle \Delta A \rangle = \sqrt{\frac{N_\Phi}{2}\left[\Sigma\langle \Delta x^* \rangle^2 + \frac{1}{\nu_\Phi^2}\Sigma\langle \Delta \dot{x}^* \rangle^2\right]}\,.$$

1) slope of longitudinal axis of the lens

$$\langle \Delta x^* \rangle = a_1 K^2 \langle \Delta r_K \rangle; \quad \langle \Delta \dot{x}^* \rangle = b_1 K^2 \langle \Delta r_K \rangle;$$

2) parallel shift of axis of the lens

$$\langle \Delta x^* \rangle = a_2 K^2 \langle \Delta r_0 \rangle; \quad \langle \Delta \dot{x}^* \rangle = b_2 K^2 \langle \Delta r_0 \rangle;$$

3) rotation of transverse axes of the lens

$$\langle \Delta x \rangle^* = 4 a_2 K^2 A \sqrt{\overline{(\Delta\psi)^4}}\,; \quad \langle \Delta \dot{x}^* \rangle = 4 b_2 K^2 A \sqrt{\overline{(\Delta\psi)^4}}\,;$$

For FODO Structure

$$a_1 = \frac{1}{3\sqrt{2}}\left[1 + \frac{K^2}{4}\left(1 + 2\frac{g}{D}\right)\right]^{1/2};$$

$$b_1 = \frac{K^4}{\sqrt{2}}\,10^{-2}\left[1 + \left(1 + 6\frac{g}{D}\right)^2\right]^{1/2};$$

$$a_2 = \left[\left(1 + \frac{g}{D}\right)^2 - \frac{K^2}{6}\left(1 + \frac{5}{2}\frac{g}{D} + \frac{3}{2}\frac{g^2}{D^2}\right)\right]^{1/2};$$

$$b_2 = \sqrt{2}\left[1 - \frac{K^2}{4}\left(1 + 2\frac{g}{D}\right)\right]^{1/2}.$$

$K = D\sqrt{\frac{qG}{mc\beta\gamma}}$ Quadrupole strength

$\frac{g}{D}$ Ratio of drift space to lens length

$\upsilon_\phi \approx$ phase advanve

Δr_o shift of axis of the lens

Δr_k Shift of the end of magnetic axis

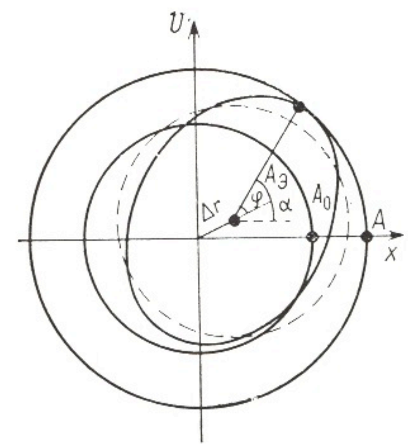

Fig. 2.15 Effective emittance caused by random beam perturbations.

Transverse Beam Matching in Drift Tube Linac

Matched Beam

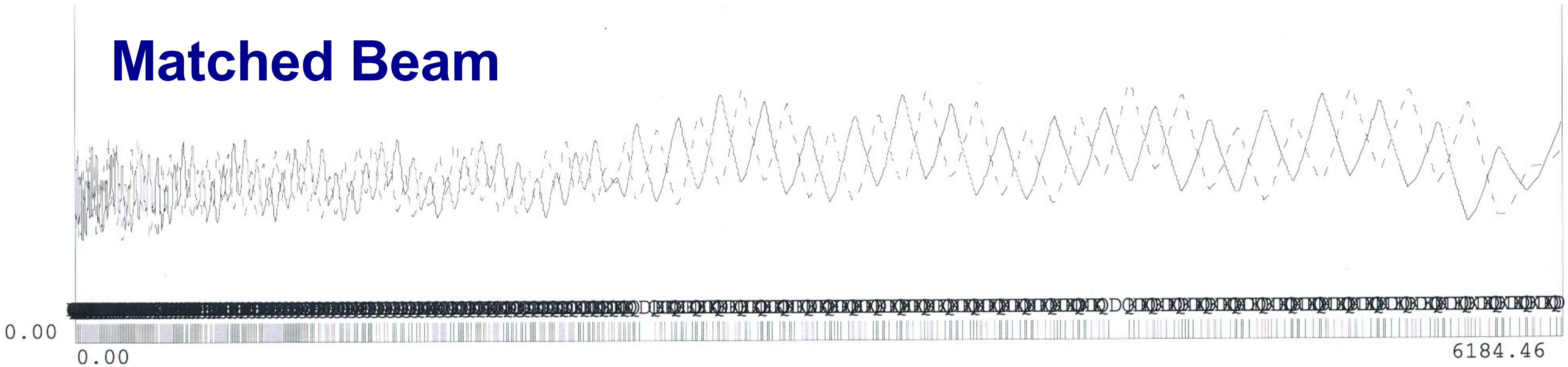

Mismatched Beam

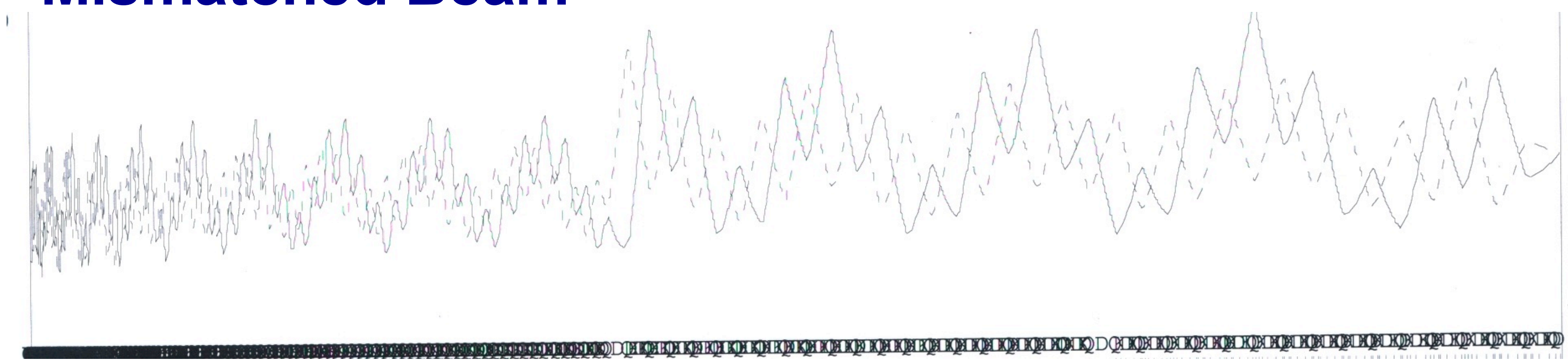

Effect of Beam Mismatch at the Entrance of DTL on Beam Loss in Transition Region (100 MeV)

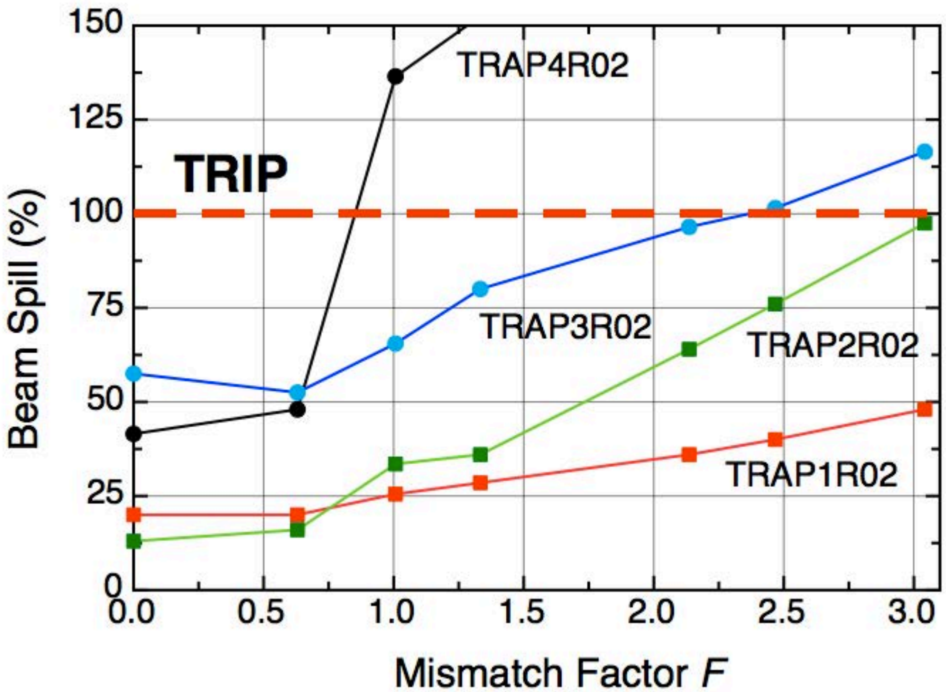

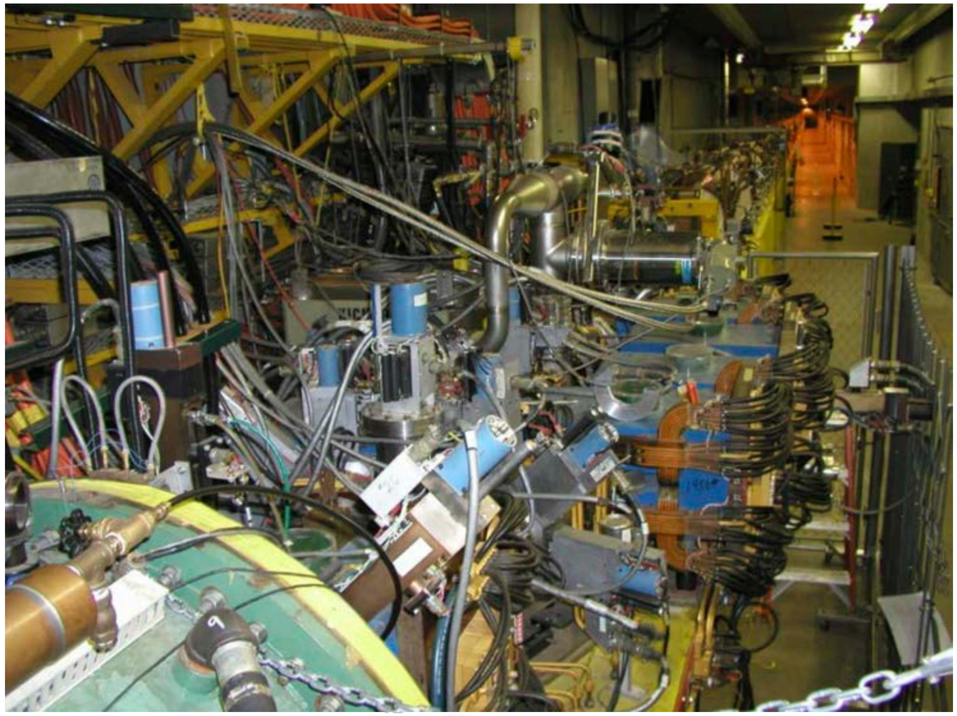

Mismatch Factor:

$$F = \sqrt{\frac{1}{2}(R + \sqrt{R^2 - 4})} - 1$$

Ellipse Overlapping Parameter:

$$R = \beta_1\gamma_2 + \beta_1\gamma_2 - 2\alpha_1\alpha_2$$

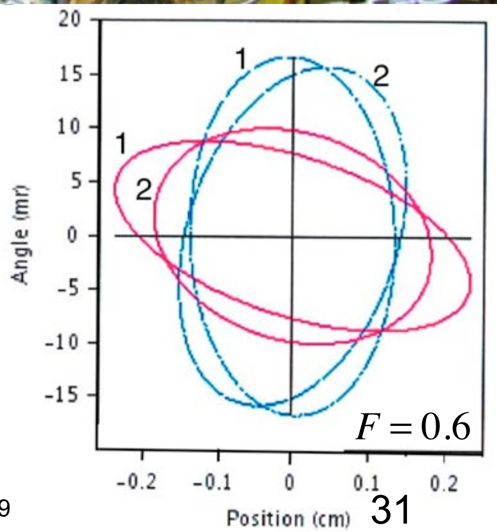

Emittance Growth due to Nonlinearities

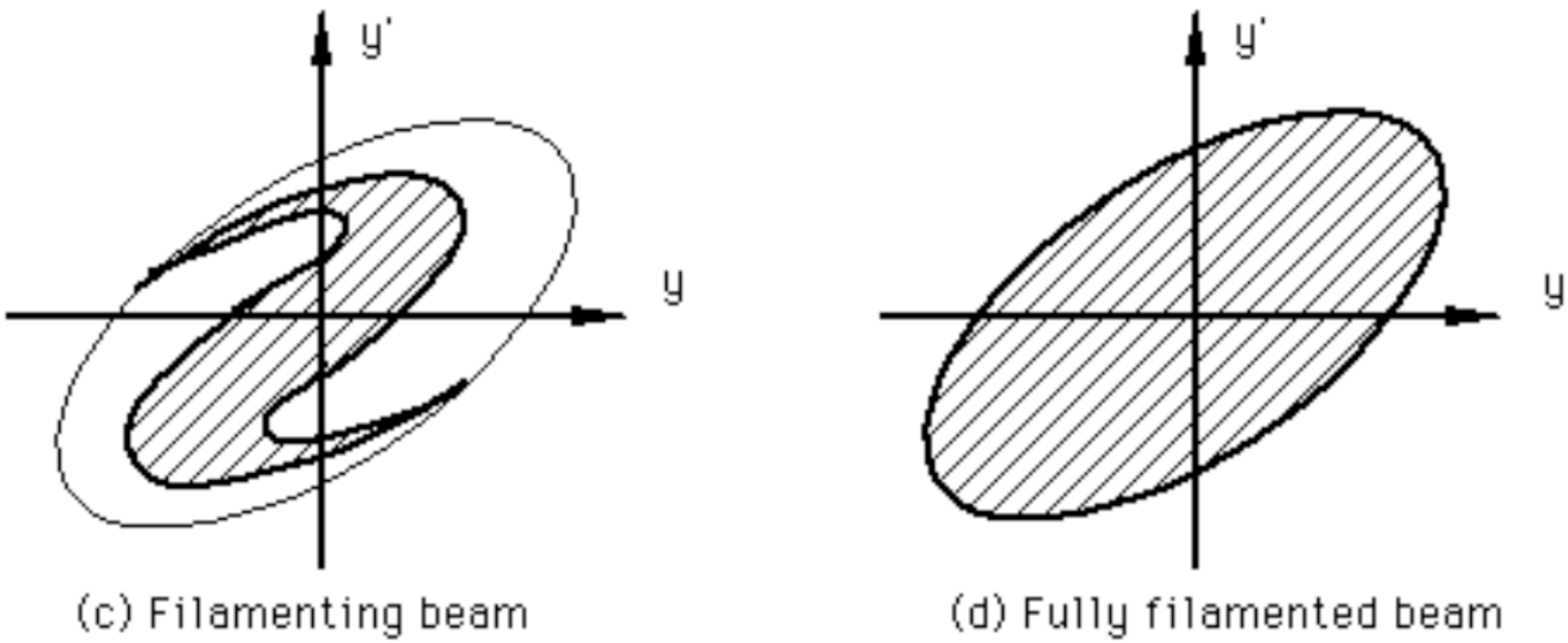

Effect of Random Errors on Emittance Growth

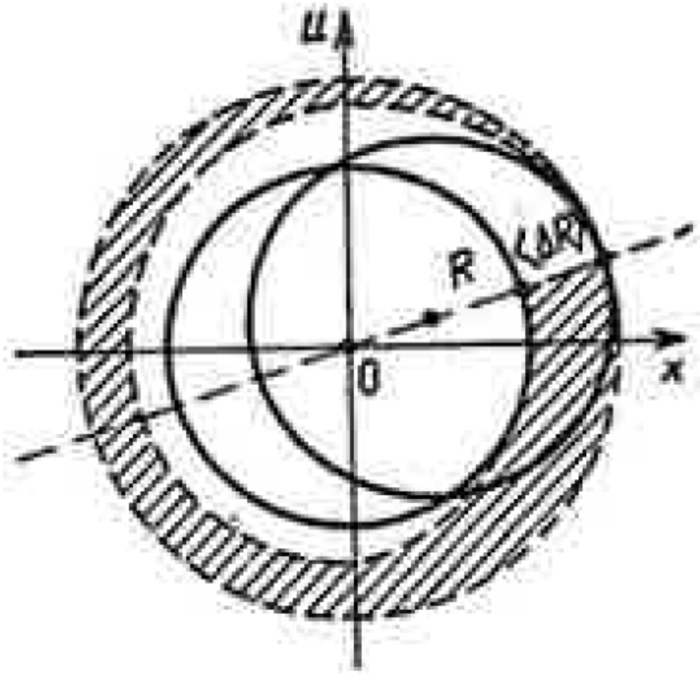

In ideal linear focusing field, beam emittance rotates collectively, and random errors do not result in beam emittance growth.
In presence of frequency dispersion, $d\mu / dR \neq 0$ effective emittance will increase.

If δA is an amplitude perturbation per period, then emittance growth per focusing period:

$$\frac{d\varepsilon}{dn} = 2\beta\gamma \frac{\mu_s R}{S} < \delta A >^{4/3} \sqrt[3]{\frac{1}{2\pi}\left(\frac{d\mu}{dR}\right)}$$

Spreading of effective emittance due to coherent perturbation of the beam in presence of frequency dispersion.

The peripheral part of the emittance increases significantly and the beam halo fill the entire acceptance of accelerator.

Collimation of Beam Phase Space

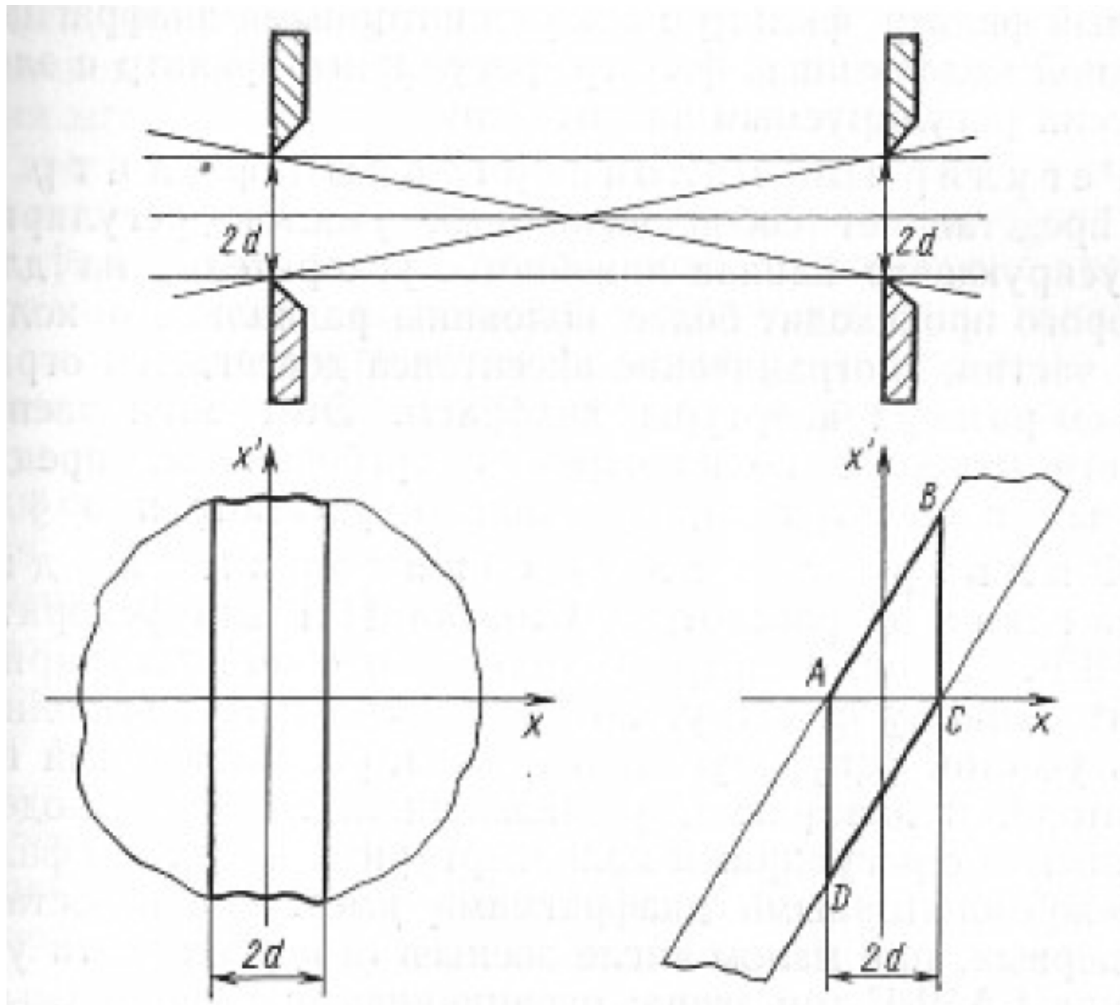

Transverse Beam Dynamics in Drift Tube Linac

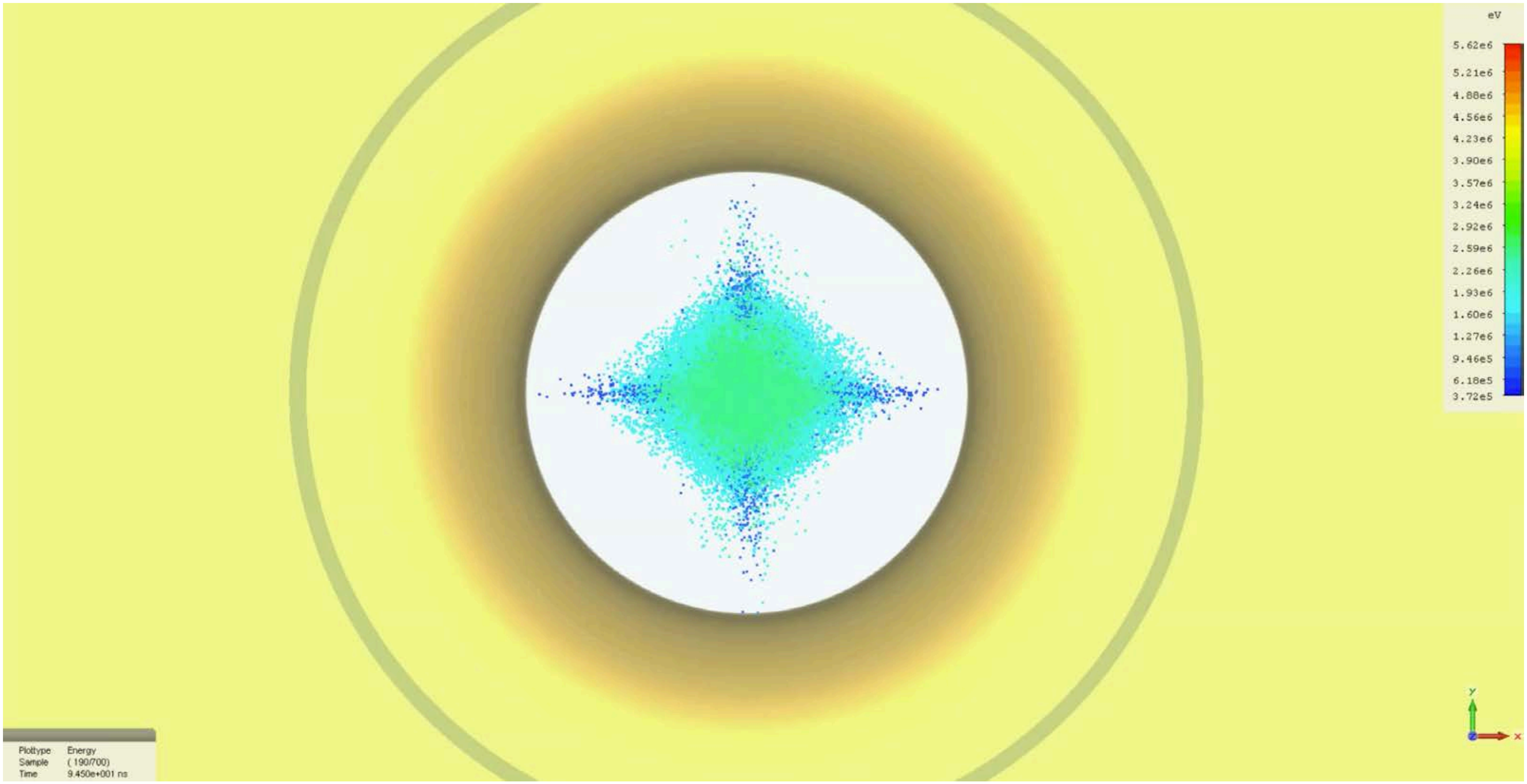

(Courtesy of Sergey Kurennoy)

Beam Losses versus Lattice Phase Advance

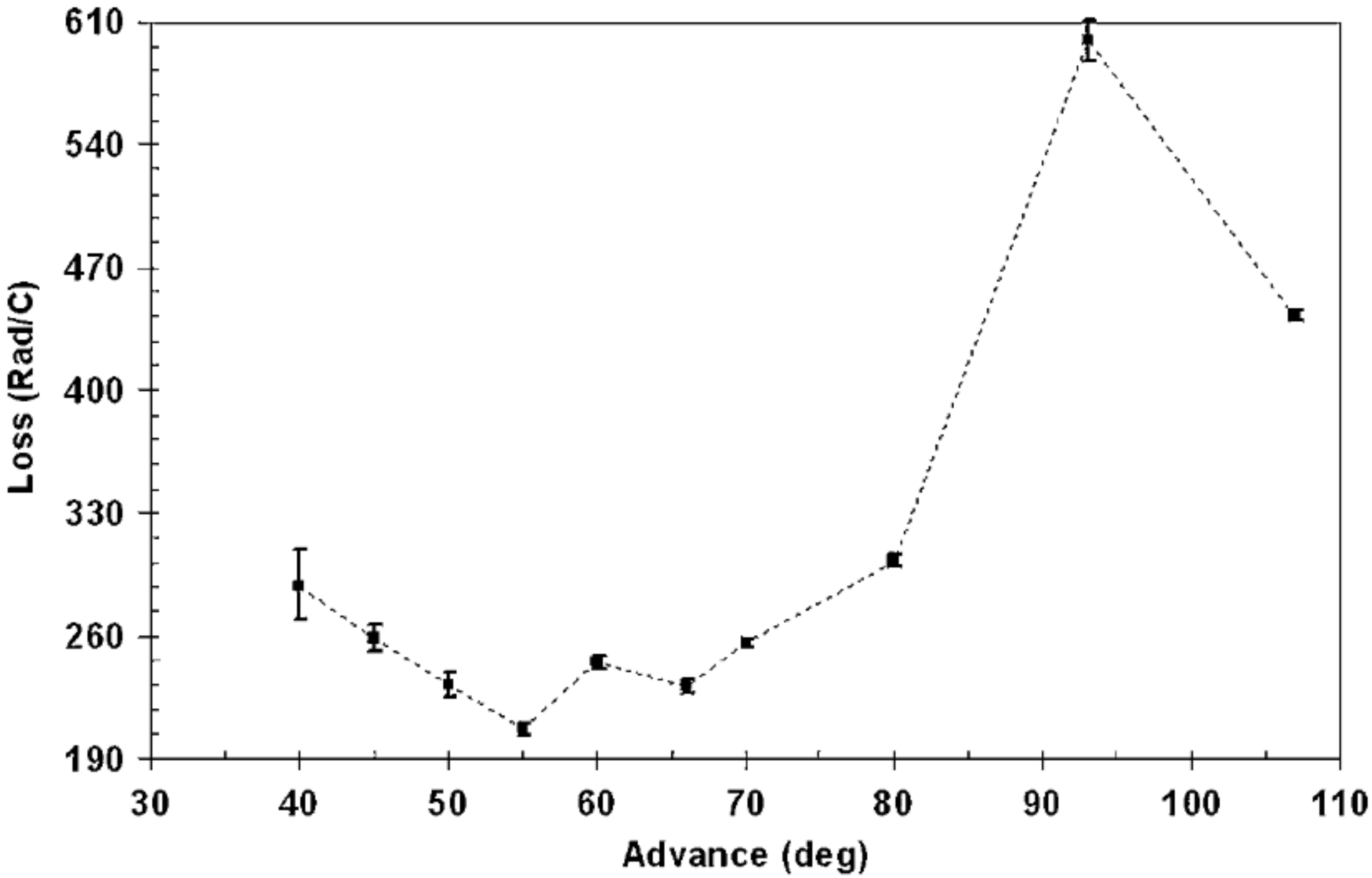

Beam losses in SNS accelerator versus zero-current phase advance (Y. Zhang et al., 2010)

Effect of Lattice Resonance

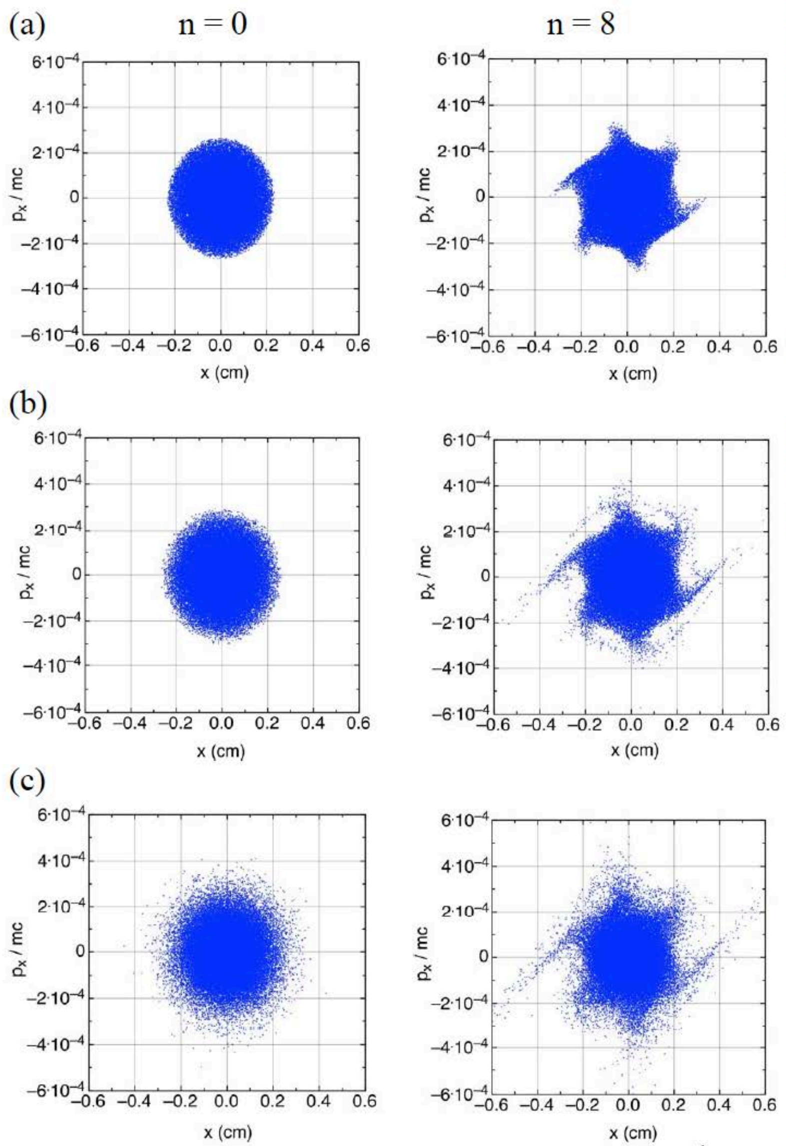

Figure 5: Dynamics of the beam in the vicinity of 6th order resonance for different beam distributions in the lattice with μ_o= 86° : (a) water bag, μ=58° (b) parabolic, μ=54° , (c) Gaussian, μ=38°.

The vector-potential of the magnetic field of a lens with quadrupole symmetry

$$A_z = -[\frac{G_2}{2} r^2 \cos 2\theta + \frac{G_6}{6} r^6 \cos 6\theta + \frac{G_{10}}{10} r^{10} \cos 10\theta + ..]$$

Hamiltonain of averaged particle motion in the vicinity of 6th order resonance:

$$H(J,\psi) = J\vartheta - \frac{\delta_5}{4} J^3 - \frac{\delta_5}{24} J^3 \cos 6\psi \,,$$

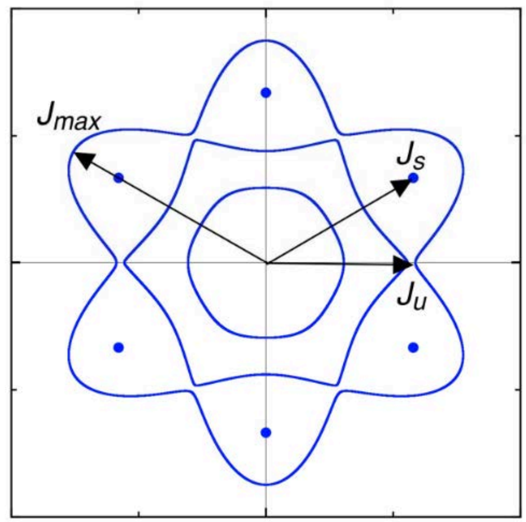

Increase of amplitude of particle trapped into resonance (TUPOB26, NA-PAC 2016)

$$\boxed{\frac{x_{max}}{x_u} = \sqrt{\frac{J_{max}}{J_u}} = 1.24}$$

Excitation of 6th order resonance in quadrupole lattice with phase advance $\mu_o \approx 60^o$

Dark Currents

1. Unchopped beam which comes through chopper due to unsufficient transverse voltage deflecting particles in chopper.

2. Continuous “dark current” of ion source between pulses

3. Beam accelerated during RF turn on/turn off transients.

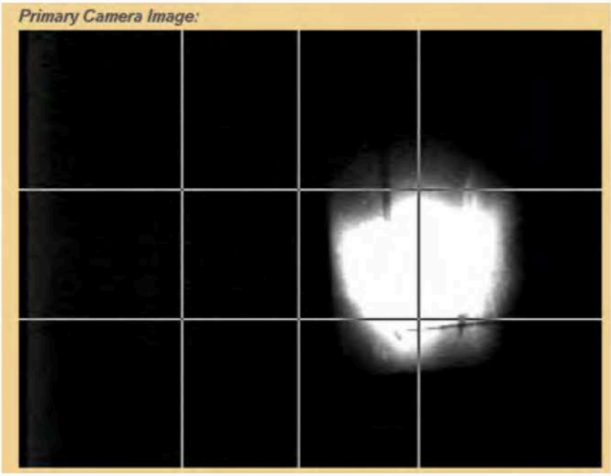

Fig. 15: Example of dark current at a view screen located at the SNS ring injection point. The beam is turned off, yet the dark current is present at levels sufficient to light up the view screen. The phase of the first DTL tank is *not* reversed for this image.

(M.Plum, CERN-2016-002)

Acceleration of H^- Beam

Advantage of H^- beam: multi-turn low-loss beam injection into storage rings and synchrotrons through charge exchange to accumulate large beam charge. Example applications: spallation neutron sources and neutrino production facilities.

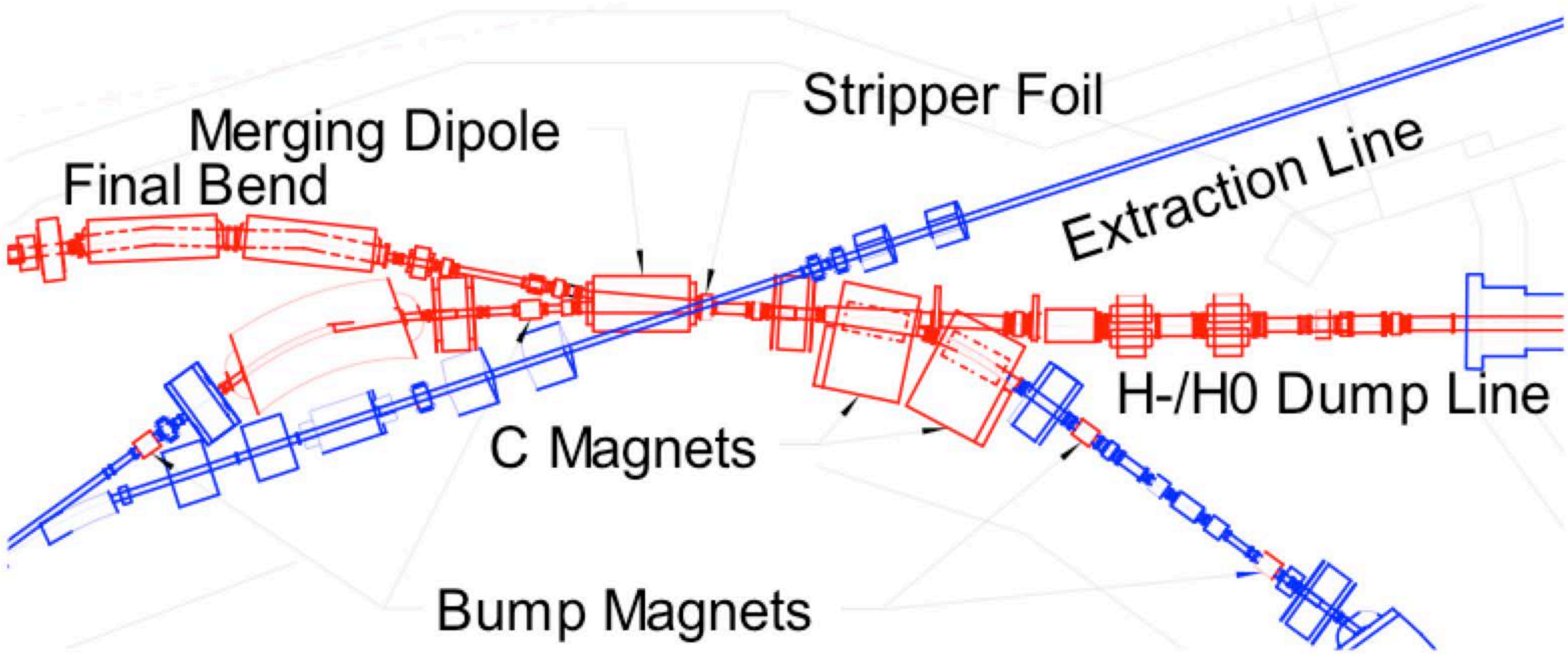

Injection of H^- beam into LANL Proton Storage Ring

H^- Beam Losses in Linac

Beam Loss Mechanisms Observed at Various H^- Linacs (M.Plum, IPAC2013)

Beam loss mechanism	SNS	J-PARC	ISIS	LANSCE
Intra-beam stripping	Yes, dominant loss in SCL linac	Not noted as significant	Not noted as significant	Yes, significant, 75% of loss in CCL
Residual gas stripping	Yes, moderate stripping in CCL and HEBT	Yes, significant, improved by adding pumping to S-DTL and future ACS section	Yes, not significant when vacuum is good, but can be significant if there are vacuum problems	Yes, significant, 25% of loss in CCL
H+ capture and acceleration	Possibly, but not significant concern	Yes, was significant, cured by chicane in MEBT	Not noted as significant	Yes, significant if there is a vacuum leak in the LEBT
Field stripping	Insignificant	Insignificant	Yes, <1% in 70 MeV transport line, some hot spots	Insignificant

H^- Beam Losses in Coupled Cavity Linac (100 MeV-800 MeV)

Energy (MeV)	100	800
Normalized rms beam emitttance (π mm mrad)	0.5	0.7

Beam losses in CCL: 0.1% - 0.2%

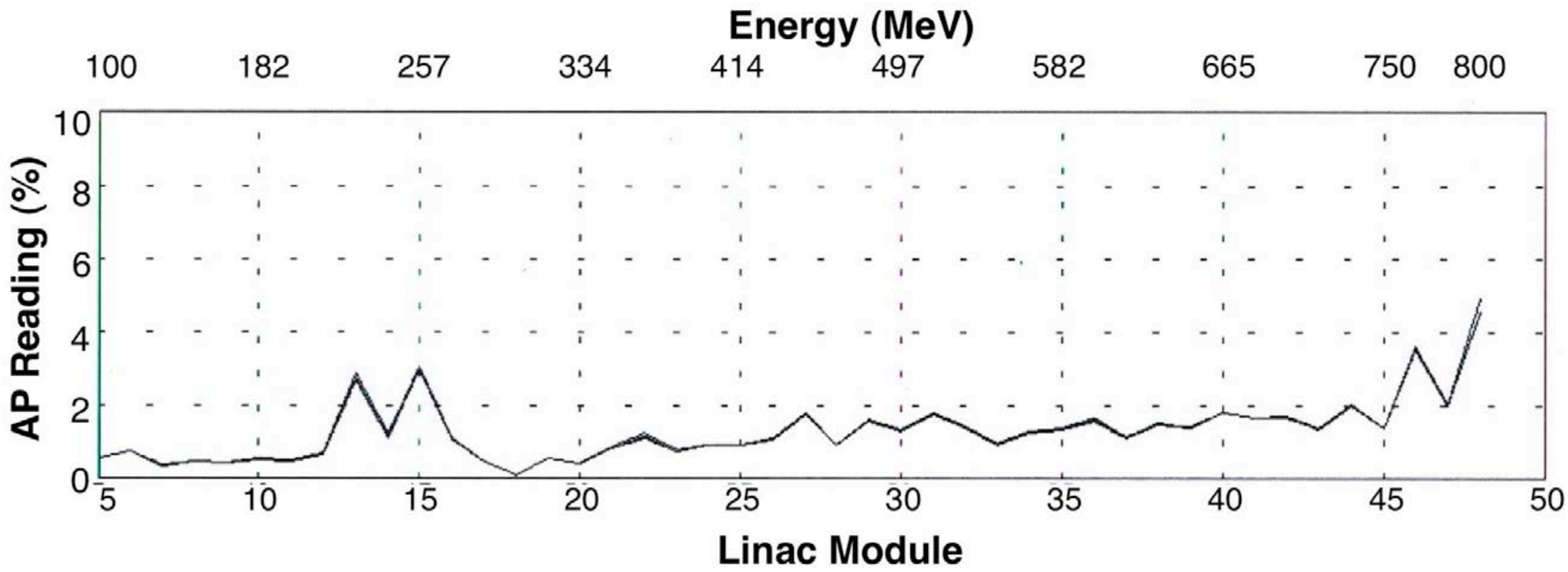

Distribution of H- beam losses along high-energy part of the linac.

H^- Beam Losses in Coupled Cavity Linac (cont.)

The study performed at LANL indicated significance of Intra Beam Stripping and Residual Gas Stripping on H^- beam losses in Coupled Cavity Linac (L.Rybarcyk, et al, IPAC12, THPPP067):

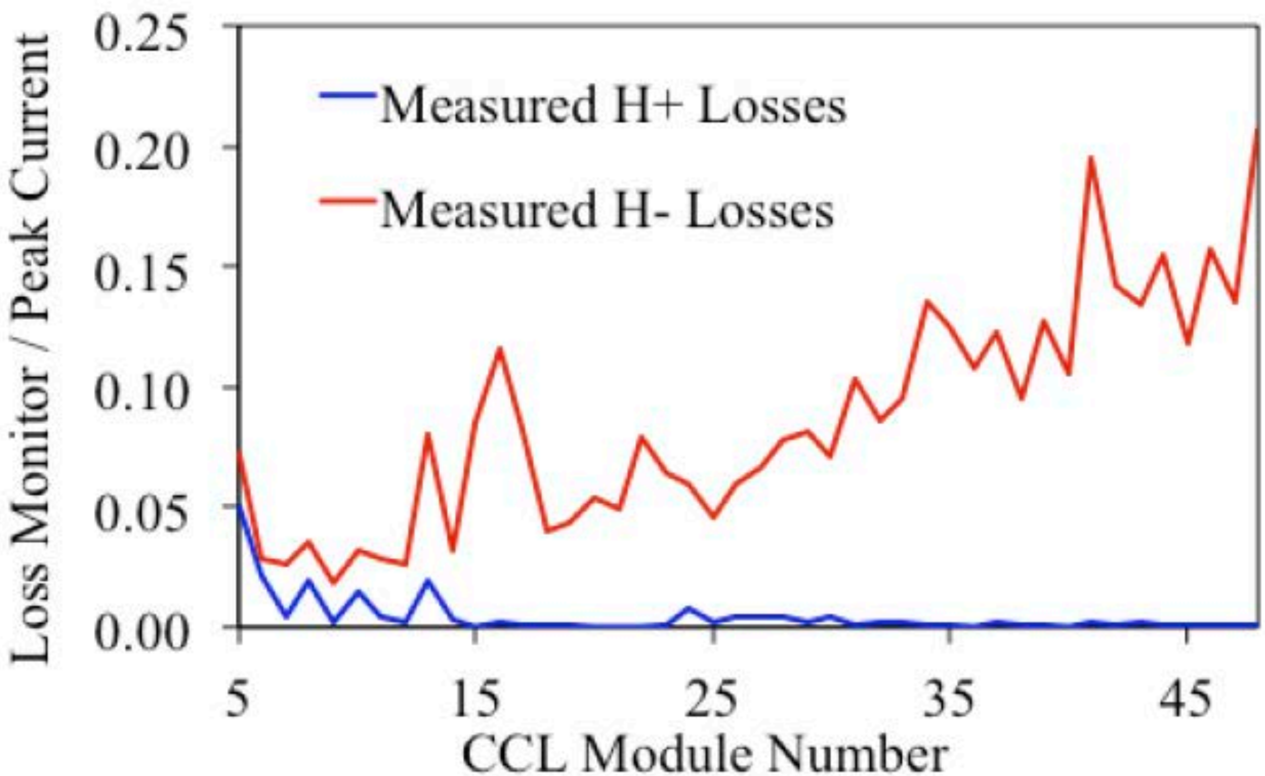

Stripping Mechanism	Beam Fractional Loss
Residual Gas Stripping	2×10^{-4}
Intrabeam Stripping	1.6×10^{-4}
Lorentz Field Stripping	4.5×10^{-11}

Residual Gas Stripping of H⁻ Beam

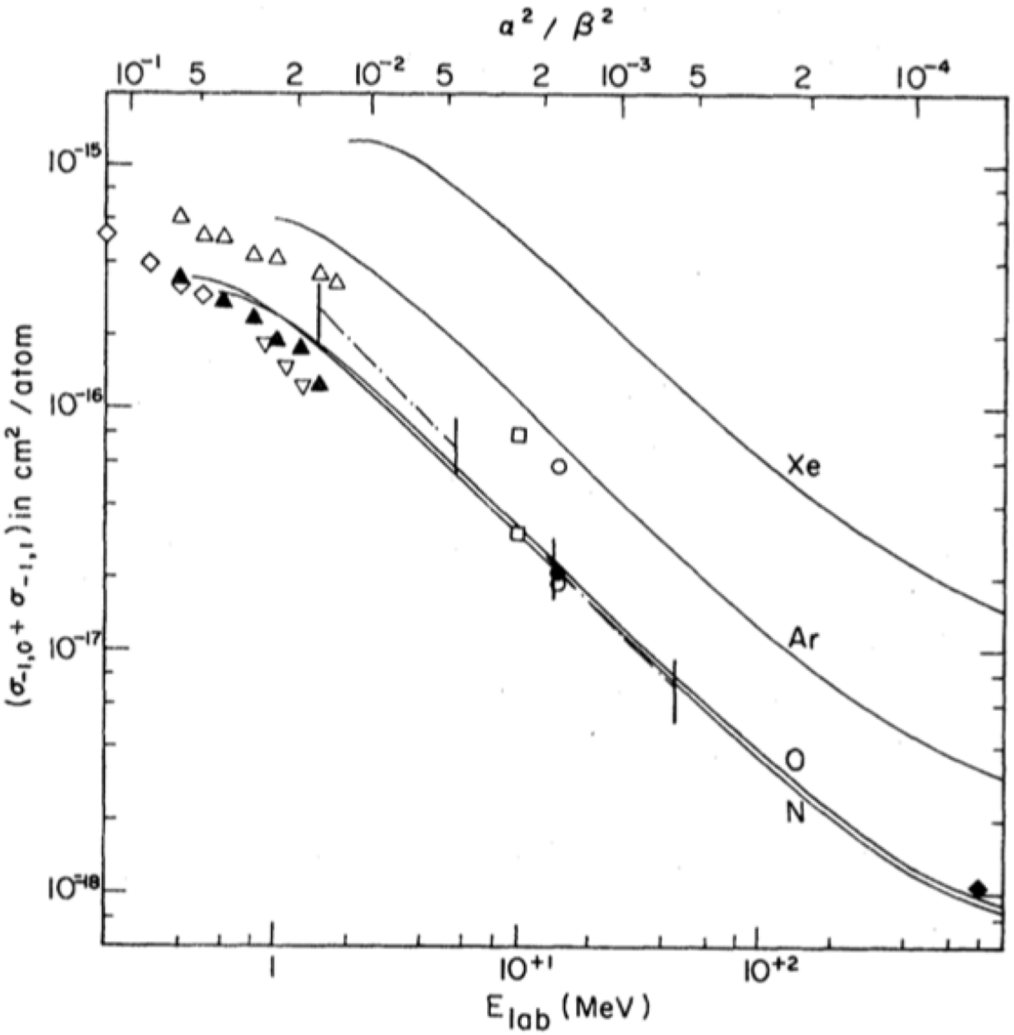

Gas stripping cross-section as a function of H⁻ beam energy, for various residual gases

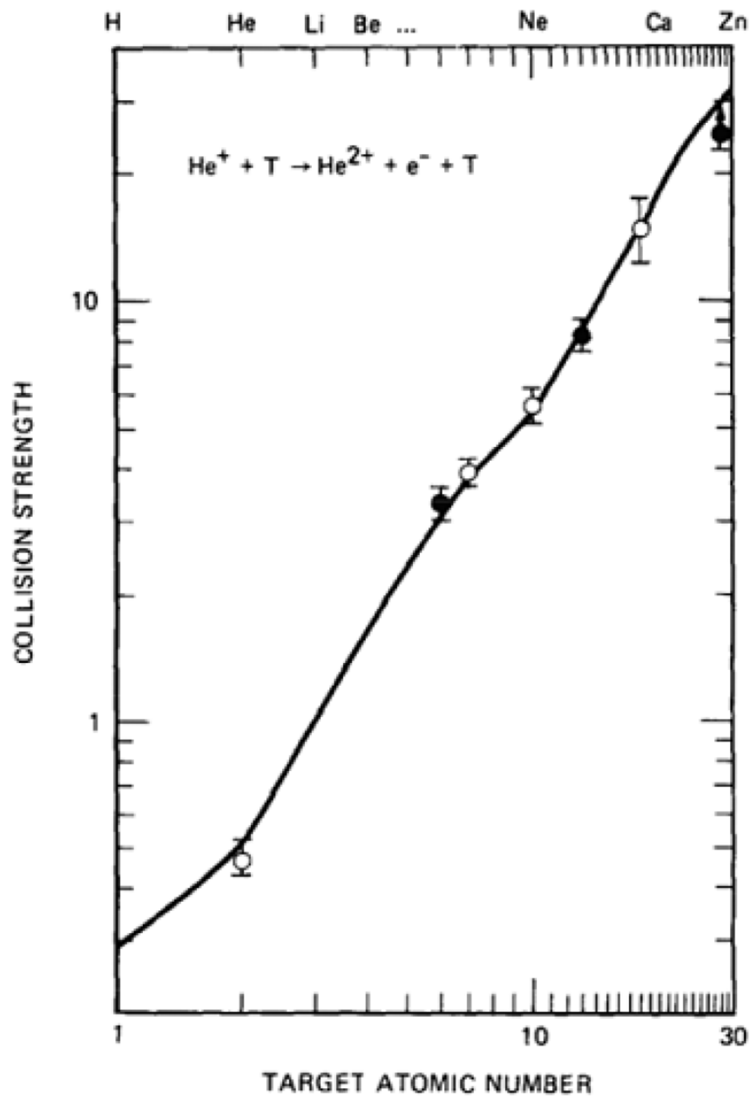

Gas stripping cross-section as a function of atomic number.

Residual Gas Stripping of H$^-$ Beam (cont.)

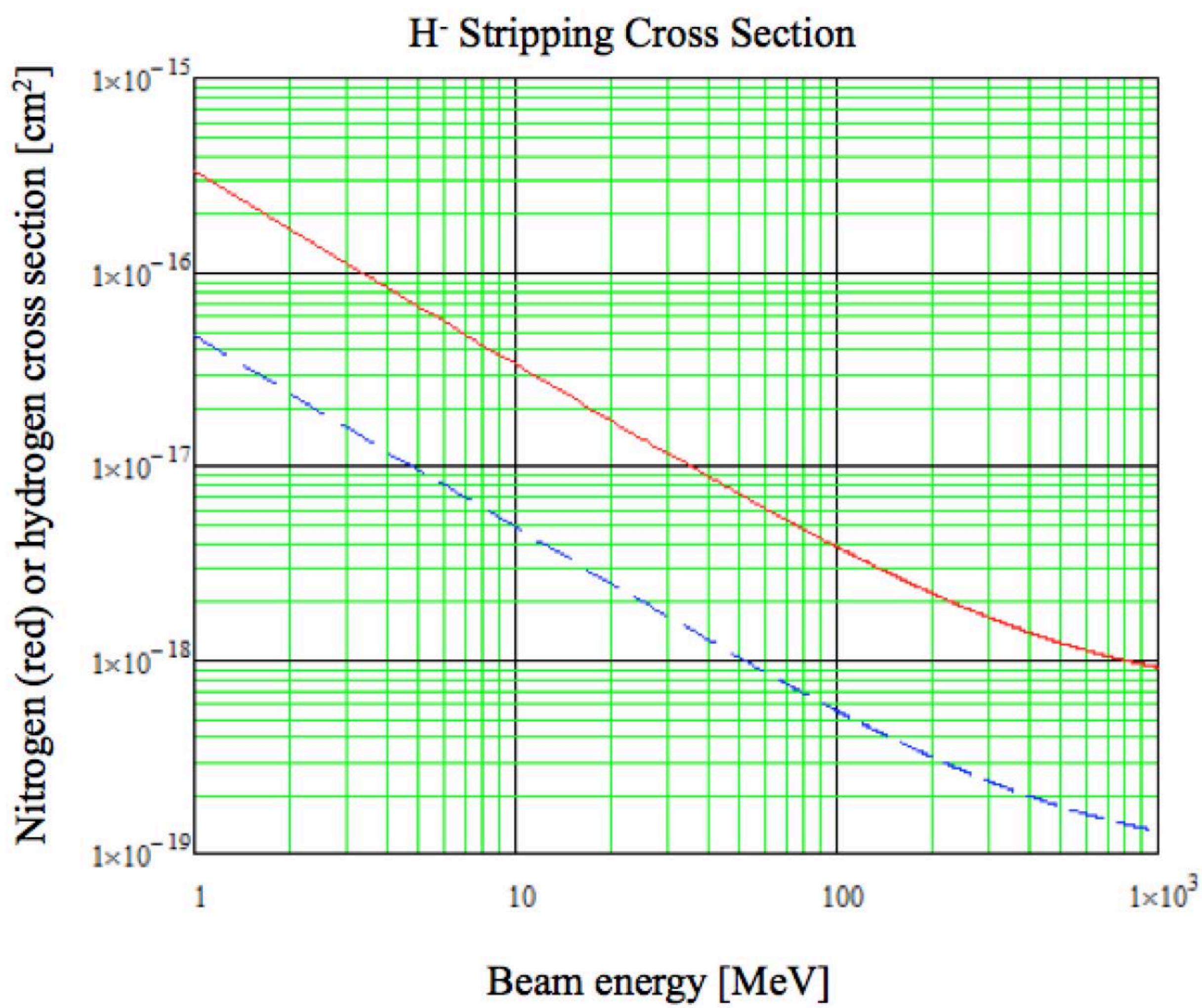

Gas stripping cross-sections for nitrogen or oxygen (solid red line) and hydrogen (blue dashed line) as a function of beam energy.

Residual Gas Stripping of H^- Beam (cont.)

The cross section for double stripping (H^- to H^+) is about 4% of the cross section for single stripping (H^- to H^o).

In a typical accelerator, the residual gases are mainly H_2 , H_2O, CO, CO_2 (low atomic numbers molecules).

With increasing of beam energy, the stripping cross section drops, but beam power increases. With the given gas pressure, residual gas stripping results in increase of beam loss with energy (increase of beam power dominates over dropping cross section).

Allowable gas pressure for acceleration of 1 mA continuous H^- beam current is between 10^{-7} Torr at 100 MeV to 10^{-8} Torr at 1 GeV.

H^+ Capture and Acceleration

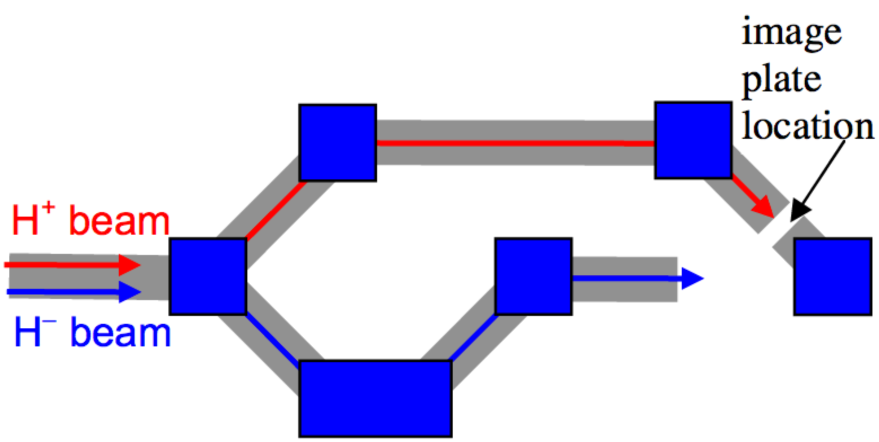

Figure 2: Layout of the beam switchyard showing the location of the image-plate used in detecting the protons that result from stripping of H^- ions. Downstream of this section H^- beam is bent out of the plane of the drawing for delivery to experiment areas.

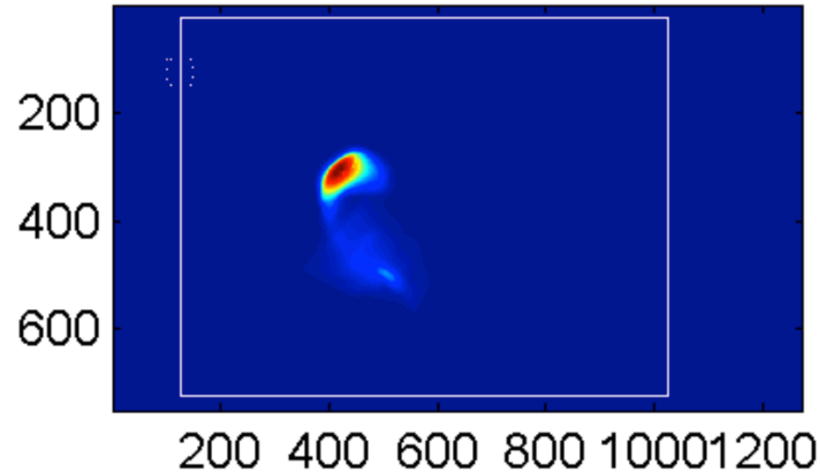

Figure 4: Image plate exposed to the contaminating proton beam with beam plug TRBL01 retracted, i.e. including protons that originate in the LEBT and DTL. The numbers on the axes are pixel numbers. The solid and dashed rectangles indicate the signal and background regions used in the analysis. The color axis has been scaled to show maximum detail in the image.

Detection of H+ beam after 800 MeV acceleration of H^- beam in LANSCE accelerator (R.McCrady, LINAC 2010).

Magnetic Field Stripping of H$^-$ Ions

Magnetic field is Lorentz transformed into electric field in the rest frame of the H$^-$ beam

$$E[MV/cm] = 0.3\,\beta\gamma\,B[kGs]$$

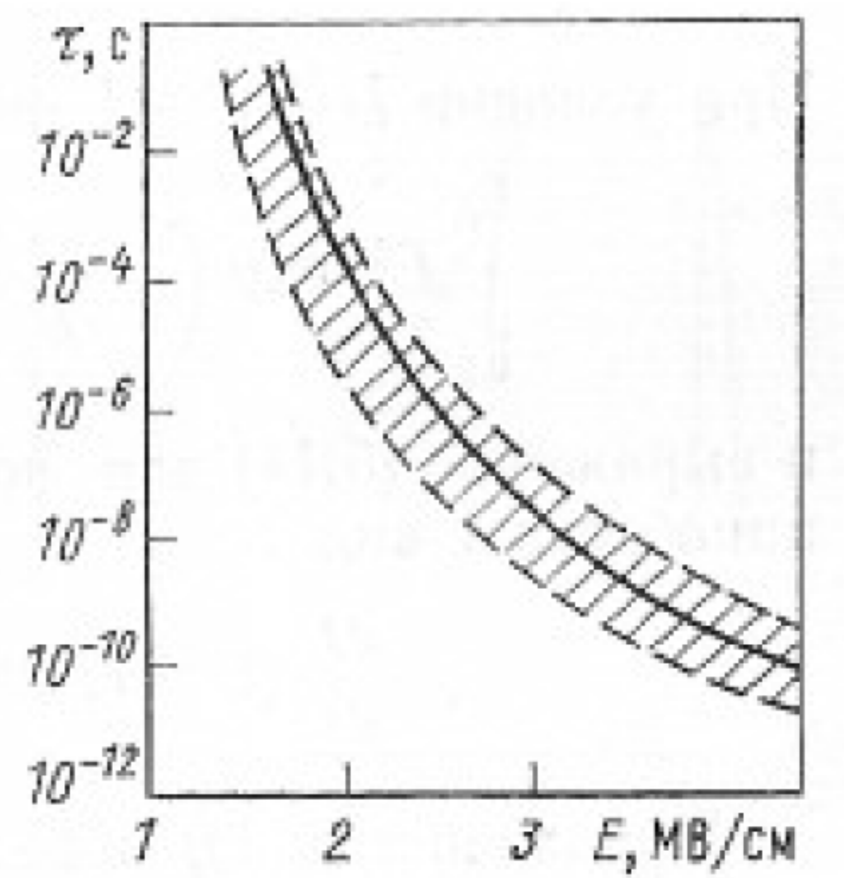

Life time of H$^-$ ion versus electric field E

$$\boxed{\tau(E) = \frac{A}{E}\exp\left(\frac{D}{E}\right)}$$

$$A = 1.05\cdot 10^{-14}\ \sec MV\,cm^{-1}$$

$$D = 49.25\,MV\,cm^{-1}$$

Life time of H$^-$ ion versus electric field

Magnetic Field Stripping of H^- Ions (cont.)

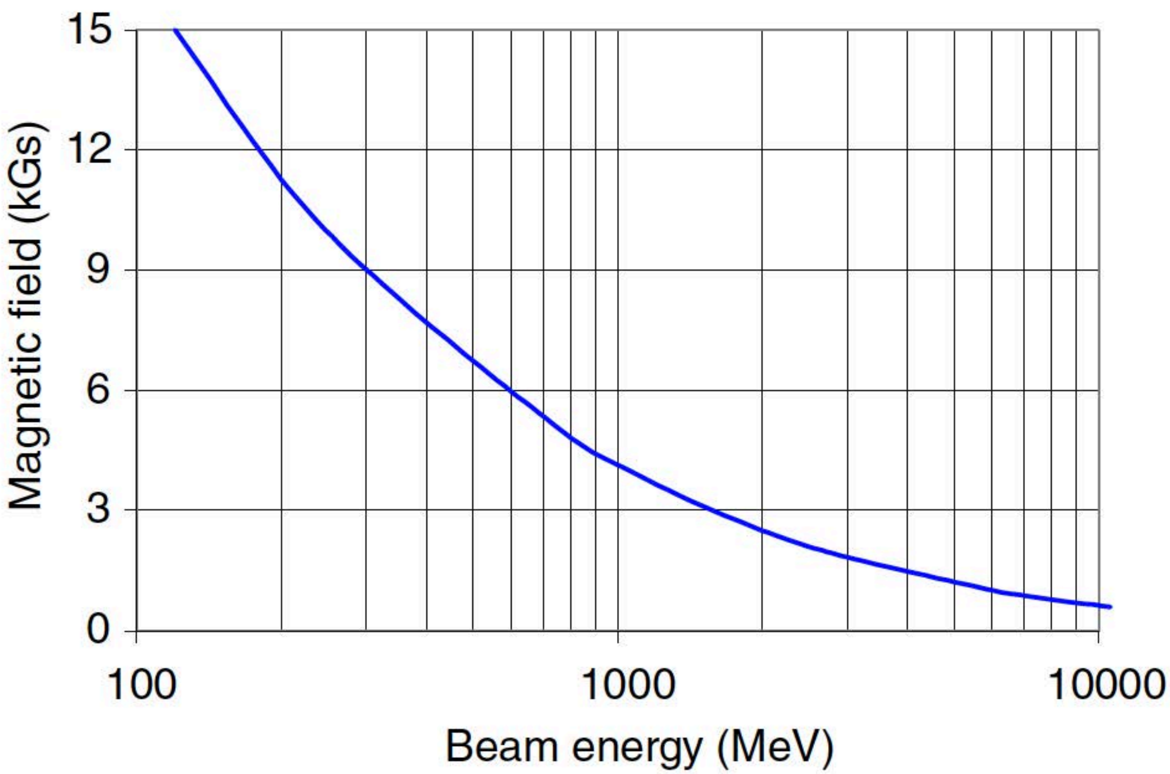

Tolerable magnetic field as a function of beam energy (P.Ostroumov, 2006).

The effect is greatest at high beam energies where the Lorentz transform has the greatest effect. The ISIS facility sees a small amount of field stripping in the 70 MeV transport line between the linac and the ring, at the level of <1%, just enough to create some minor hot spots. SNS, J-PARC and LANSCE have not reported any significant beam loss due to this mechanism (M.Plum, CERN-2016-002).

Intrabeam Stripping in H^- Linacs

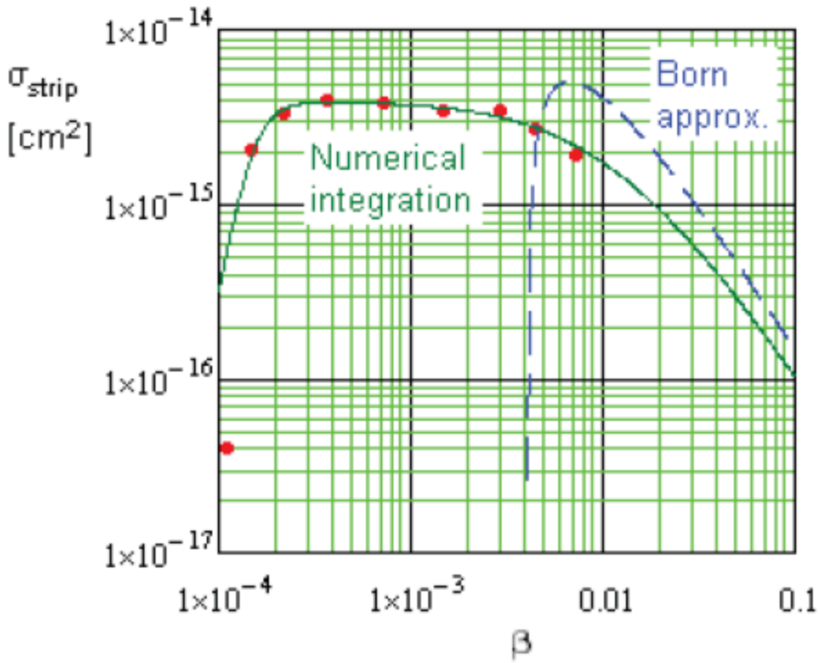

Figure 1: Comparison of Eq. (1) predictions (green solid line) to the numerical simulations of Ref. [5] (red dots), and to the results of Born approximation of Ref. [6] (dashed blue line).

(V.Lebedev et al, LINAC 2010)

Transforming Eq. (4) to the laboratory frame one obtains the relative intensity loss per unit length travelled by the bunch:

$$\frac{1}{N}\frac{dN}{ds}=\frac{N\sigma_{\max}\sqrt{\gamma^2\theta_x^{\,2}+\gamma^2\theta_y^{\,2}+\theta_s^{\,2}}}{8\pi^2\sigma_x\sigma_y\sigma_s\gamma^2}F\left(\gamma\theta_x,\gamma\theta_y,\theta_s\right), \qquad (7)$$

where γ is the relativistic factor, $\sigma_{x,y}=\sqrt{\varepsilon_{x,y}\beta_{x,y}}$ are the transverse rms bunch sizes, $\theta_{x,y}=\sqrt{\varepsilon_{x,y}/\beta_{x,y}}$ are the transverse local rms angular spreads, σ_s and θ_s are the rms bunch length and the relative rms momentum spread.

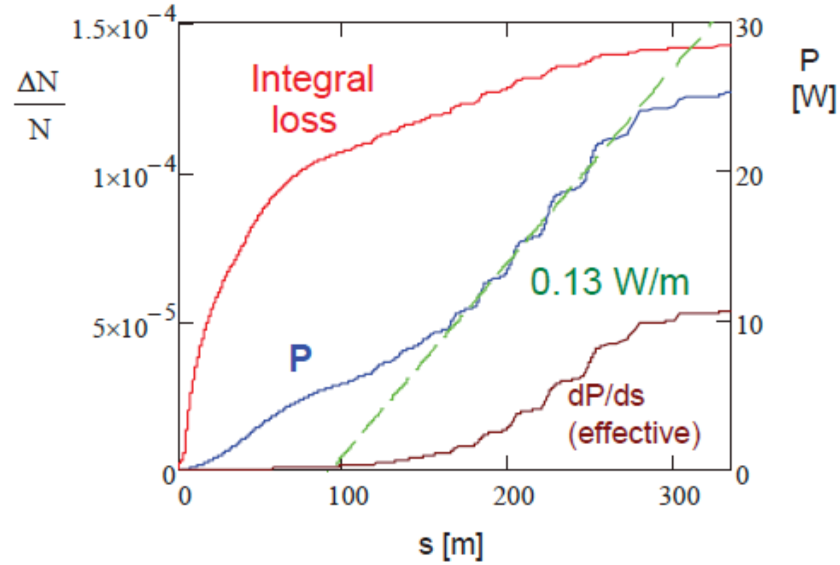

Figure 3: Integrals over linac length for the relative particle loss rate and the power density due to particle loss.

Intrabeam Stripping in H$^-$ Linacs (cont.)

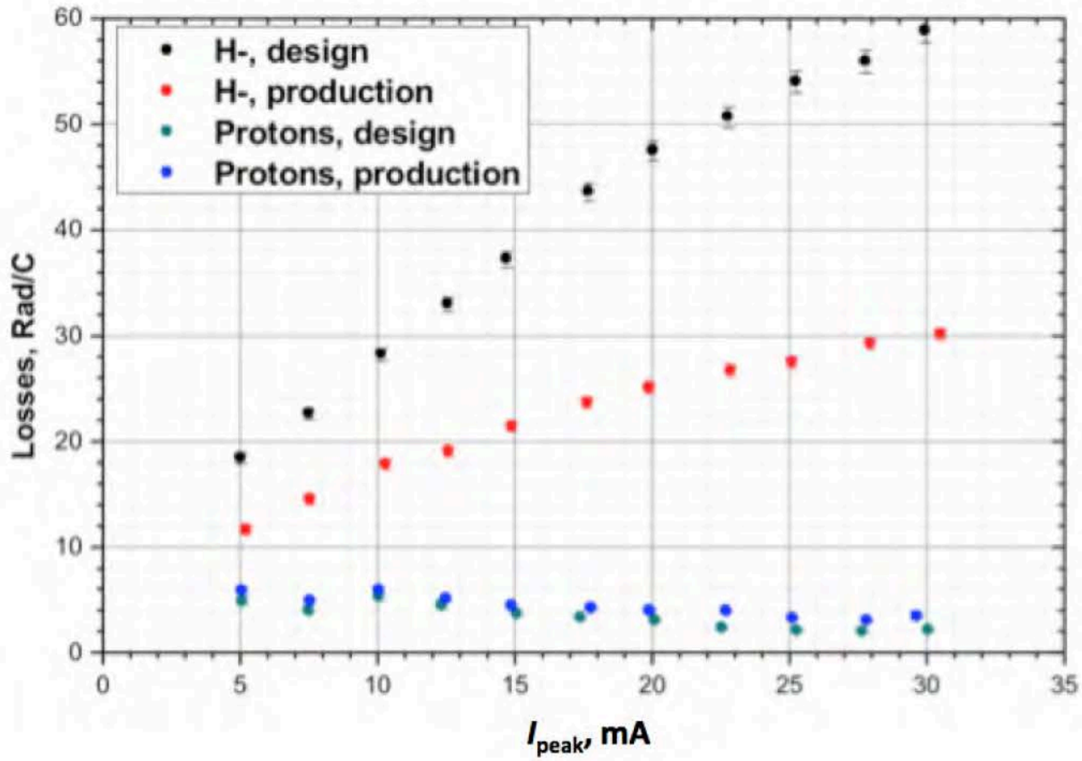

Fig. 10: Normalized beam loss (loss monitor signal divided by the peak beam current) in the SNS SCL for two different optics cases, as a function of ion source current, for both H$^+$ and H$^-$ beams. Black: H$^-$ beam with SCL quadrupole gradients set to design values. Green: H$^+$ beam with SCL quadrupole gradients set to design values. Red: H$^-$ beam with SCL quadrupole gradients lowered by up to 40% to minimize the beam loss. Blue: H$^+$ beam with SCL quadrupole gradients set to the same values as for the H$^-$ minimum loss case. Figure reproduced from Ref. [16].

A.Shishlo et al (IPAC 2012)

Black Body Radiation

Photodetachment of electron from H^- ions can be caused by black-body radiation. In this process, photons strip off the loosely bound electrons from H^- particles. Stripping rate is minimal for today's H^- beam energies. At 1 GeV the beam loss rate due to room-temperature blackbody radiation has been estimated to be just $3x10^{-9}$ per meter or about 100 times less than our maximum allowable loss rate. However, as the H^- beam energy increases, the Doppler-shifted black-body photon energies can increase enough to cause significant stripping rates. For example, at 8 GeV, which is a possible charge exchange injection energy for Fermilab's Project X, the stripping rate climbs to $8x10^{-7}$ per meter. At this level of beam loss photodetachment becomes a serious concern and mitigation methods such as cooling the beam pipe to cryogenic temperatures have been considered.

The probability of beam loss due to black-body photodetachment depends on the overlap of two distributions: the H^- photodetachment cross-section versus photon energy, which peaks at a photon energy of about 1.4 eV; and the black-body photon spectral density Doppler shifted to the rest frame of the H^- ions. For 300 K room-temperature black-body radiation, the probability of stripping is maximum for a beam energy of about 50 GeV.

Beam Loss Mitigation

Table 3: Some methods of beam loss mitigation

Cause of beam loss	Mitigation
Beam halo—both transverse and longitudinal	Scraping, collimation, better matching from one lattice to the next, magnet and RF adjustments
Intra-beam stripping	Increase beam size (both transverse and longitudinal)
Residual gas stripping	Improve vacuum
H^+ capture and acceleration	Improve vacuum, add chicane at low energy
Magnetic field stripping	Avoid by design
Dark current from ion source	Deflect at low energy, reverse (phase shift) RF cavity field when beam is turned off
Off-normal beams (sudden, occasional beam losses)	Turn off beam as fast as possible, track down troublesome equipment and modify to trip less often

(M.Plum, CERN-2016-002)

Space Charge Induced Beam Emittance Growth and Halo Formation

Table 9.1 Properties of space-charge-induced emittance growth.

	Charge redistribution	RMS mismatch	Emittance transfer	Structure resonance
Free- energy source	Nonlinear field energy	Oscillation energy of excited mode	Space-charge coupling resonances	Longitudinal energy
Approximate timescale	$\approx \frac{\tau_{\text{plasma}}}{4}$	Typically $\geq 10\tau_{\text{plasma}}$	Typically $\geq 10\tau_{\text{plasma}}$	$\approx 2\tau_{\text{betatron}}$
Distribution function sensitivity	Strongly dependent	Weakly dependent	Weakly dependent	Strongly dependent
For minimum growth	Avoid transitions toward stronger tune depression	RMS match	Avoid space-charge coupling resonances	Keep $\sigma_0 < 90^\circ$

Effect of Space Charge Aberration on Beam Emittance

Space charge density and space charge field of the beam with Gaussian distribution are given by

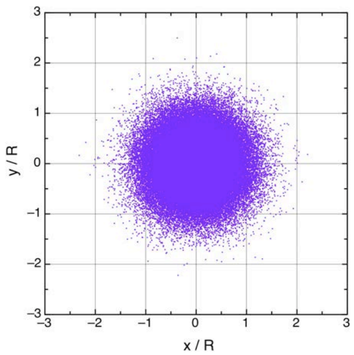

$$\rho(r_o) = \frac{2I}{\pi R_o^2 \beta c} \quad exp(-2\frac{r_o^2}{R_o^2})$$

$$E_b = \frac{I}{2\pi \varepsilon_o \beta c}\frac{1}{r_o}[1 - exp(-2\frac{r_o^2}{R_o^2})]$$

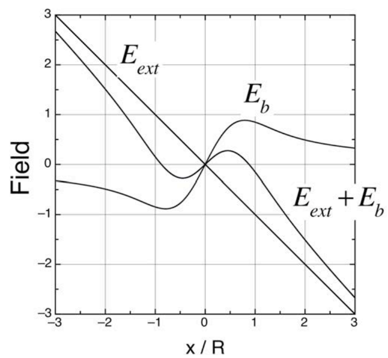

Nonlinear function in space charge field is expanded as

$$f(r_o) = 1 - exp(-2\frac{r_o^2}{R_o^2}) \approx 2\frac{r_o^2}{R_o^2} - 2\frac{r_o^4}{R_o^4} + \ldots$$

At the initial stage of beam emittance growth we can assume, that particle radius is unchanged, while the slope of the trajectory is changed. It gives us the nonlinear transformation:

$$r = r_o$$

$$r' = r_o' + \frac{2zP^2}{R_o^2} r_o - \frac{2zP^2}{R_o^4} r_o^3$$

where $P^2 = \dfrac{2I}{I_c \beta^3 \gamma^3}$ is the generalized perveance, $I_c = 4\pi\varepsilon_o mc^3 / q$ is the characteristic beam current.

Effect of Space Charge Aberration on Beam Emittance

Parameter υ , which determines effect of spherical abberation on beam emittance is

$$\frac{C_\alpha R_o^4}{f\epsilon} = \frac{4}{\beta^3\gamma^3}\frac{I}{I_c}\frac{z}{\epsilon}$$

Therefore, space charge induced beam emittance growth in free space is:

$$\frac{\epsilon_{eff}}{\epsilon} = \sqrt{1+\bar{K}\left(\frac{I}{I_c\beta^3\gamma^3}\frac{z}{\epsilon}\right)^2}$$

Parameter $\bar{K}$ was determined numerically for different distributins. Results are summarized in Table. As follows from above equation, initial emittance growth does not depend on initial beam radius.

Distribution	Coeff. $\bar{K}$
KV	0
Water Bag	0.094
Parabolic	0.187
Gaussian	0.55

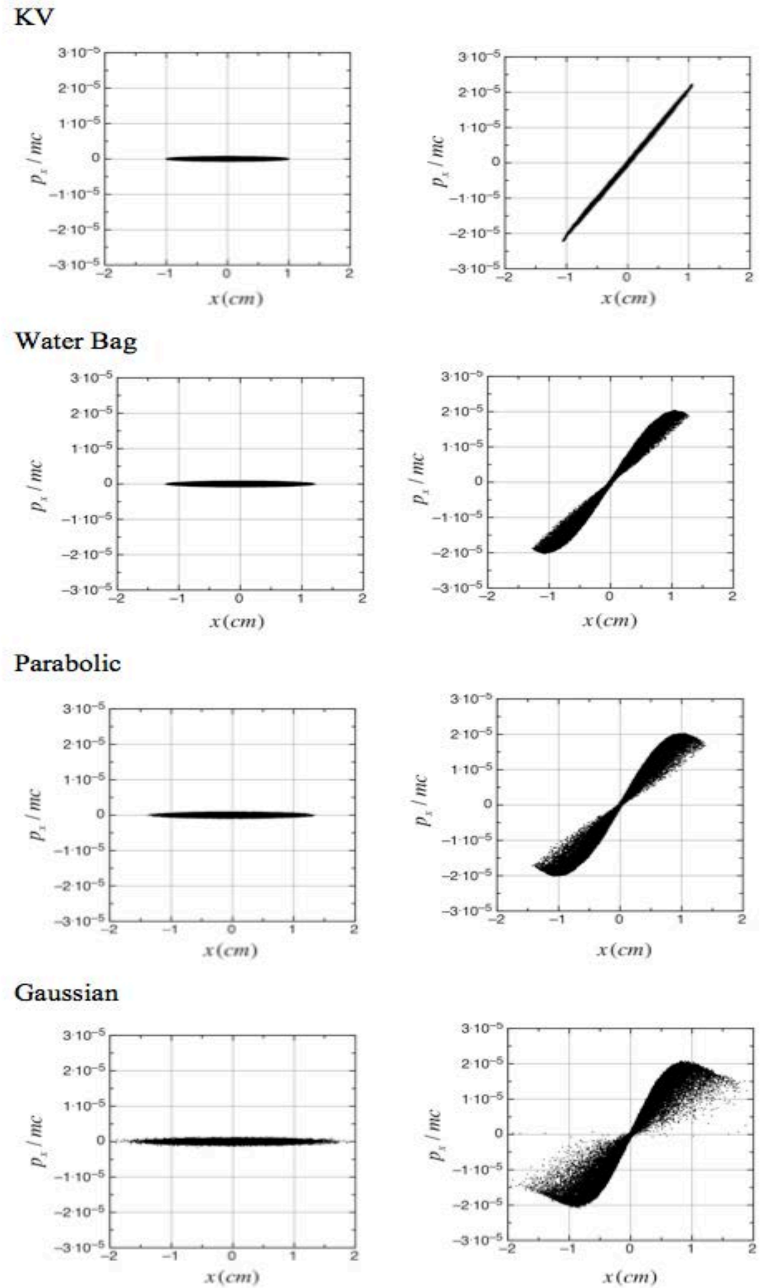

Effect of Space Charge Aberration on Beam Emittance

Drift

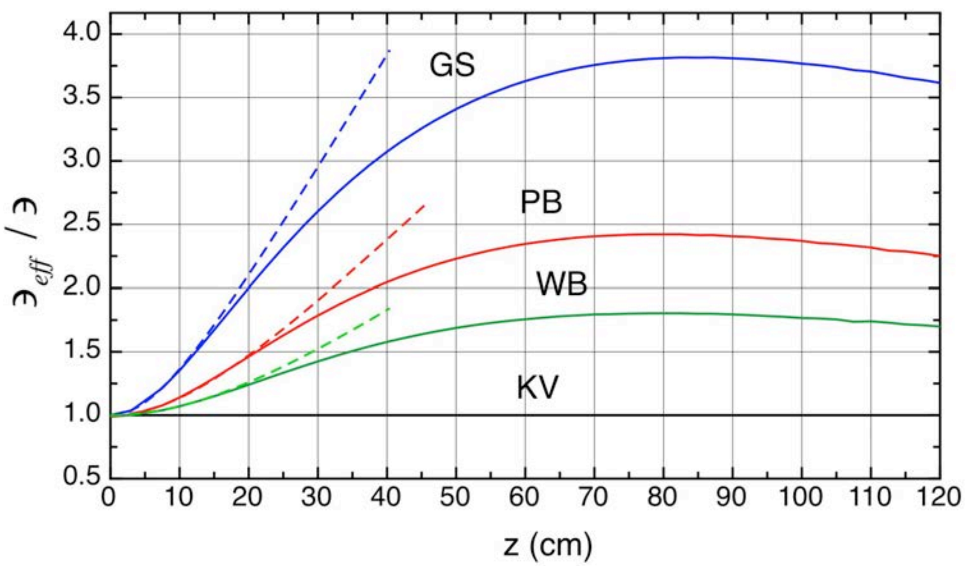

FODO Channel

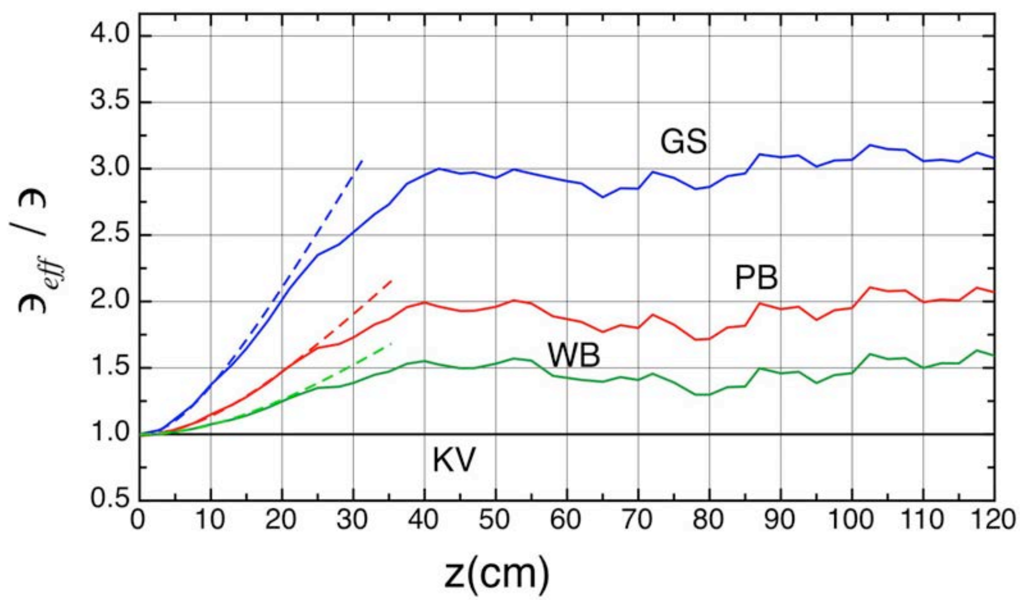

Emittance growth of a 50 keV proton beam with current *I* = 20 mA and unnormalized emittance 4.64 π cm mrad in drift space and in FODO focusing channel for different beam distributions.

Experimental Observation of Effect of Nonlinear Space Charge Forces on Beam Emittance

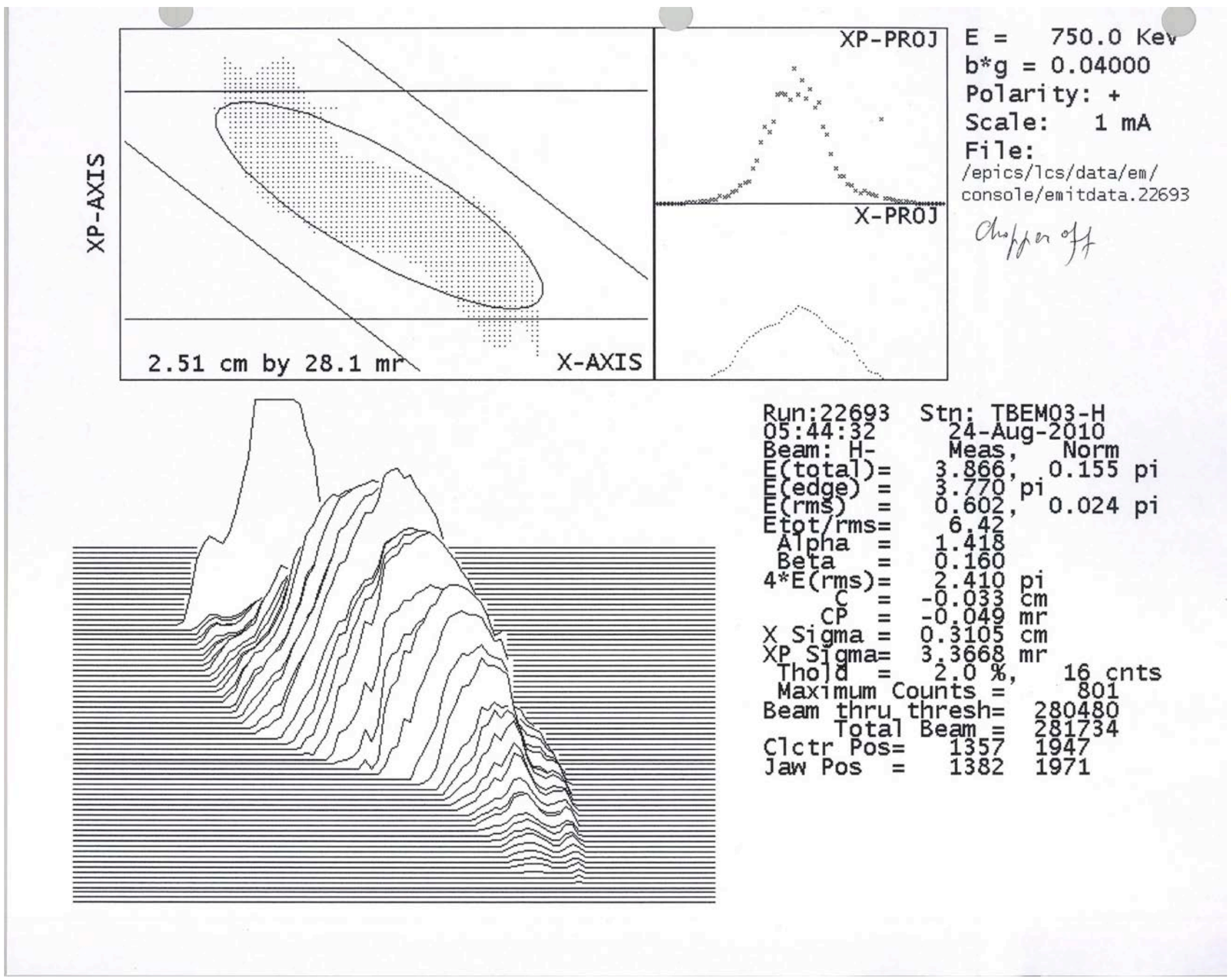

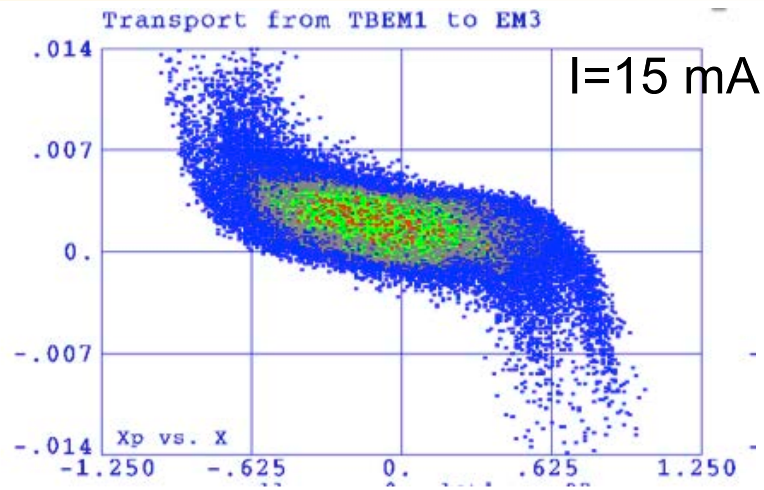

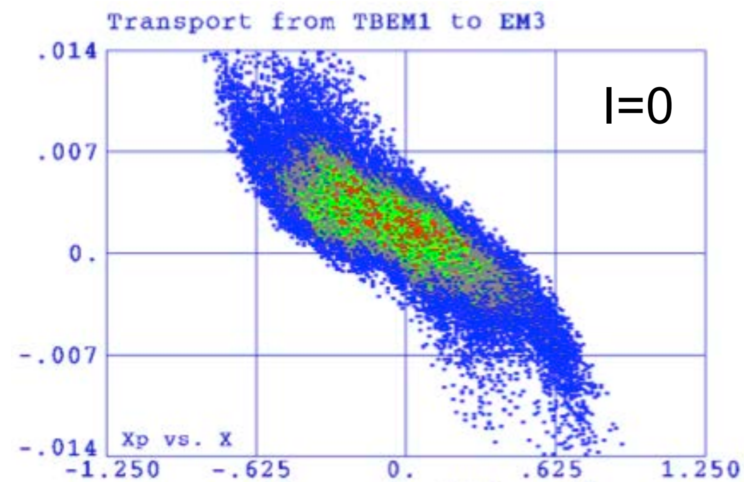

(Y.B. et al, Proc. of PAC2011, p. 64)

Effect of Elliptical Cross Section on Beam Emittance Growth

Suppose that the density is parabolic, given by

$$n(x,y) = \frac{2N_1}{\pi ab}\left[1 - \frac{x^2}{a^2} - \frac{y^2}{b^2}\right],$$

within the boundary of the ellipse defined by

$$\frac{x^2}{a^2} + \frac{y^2}{b^2} = 1 .$$

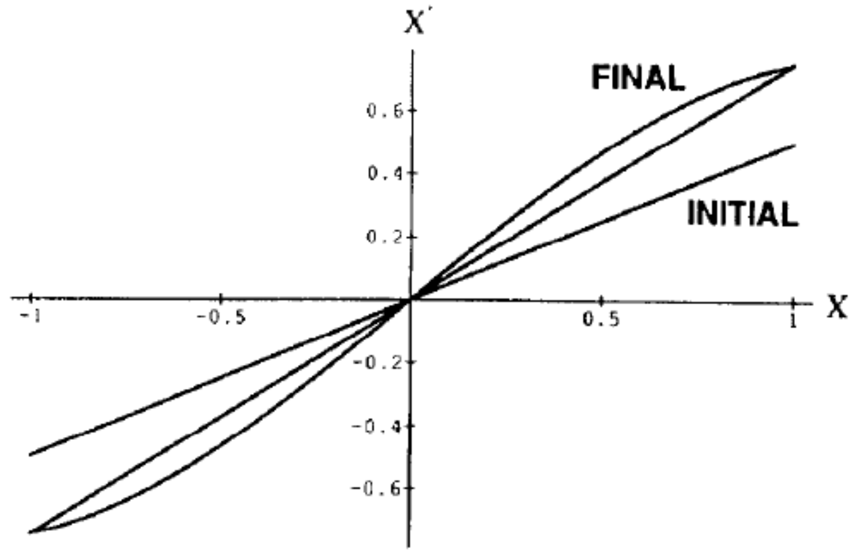

Figure 3. Effect of space charge from a parabolic density on an initial zero-emittance beam. The initial and final phase-space distributions are shown.

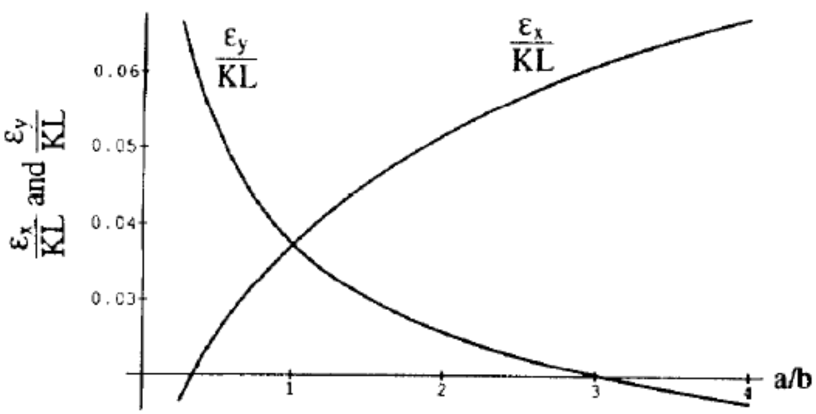

Figure 4. Final rms emittance values versus ellipse-aspect ratio a/b for a beam with parabolic density.

$$\varepsilon_x = KL\frac{a}{b}\sqrt{\frac{1}{432}\frac{\left(\frac{2a}{b}+1\right)^2}{\left\{1+\frac{a}{b}\right\}^4} + \frac{7}{720}\frac{1}{\left\{1+\frac{a}{b}\right\}^4} - \frac{1}{360}\frac{\left(\frac{2a}{b}+1\right)}{\left\{1+\frac{a}{b}\right\}^4}} .$$

(T.Wangler, P.Lapostolle, A.Lombardi, PAC 1993, p.3606)

Space Charge Induced Beam Emittance Growth in a Focusing Channel (Free Energy Effect)

z = 0

z = 30 cm

z = 104 cm

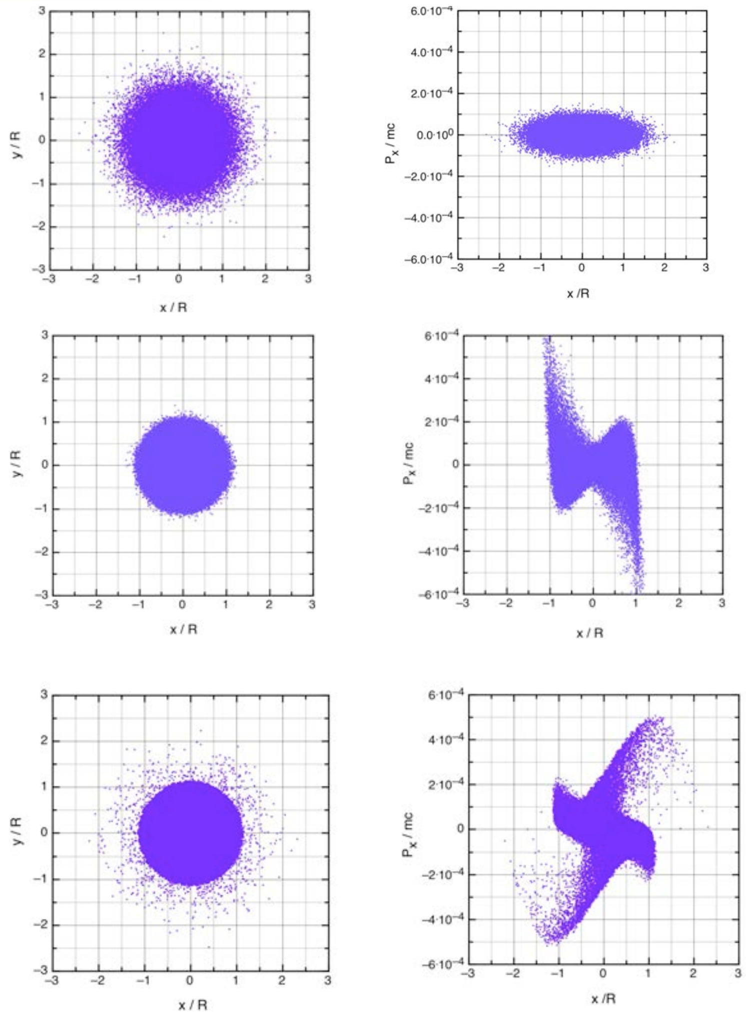

Fig. 3.7. Injection of 135 keV, 100 mA, 0.07 π cm mrad proton beam with Gaussian distribution in a focusing channel with linear field. It results in (a) beam uniforming
(b) beam emittance growth
(c) halo formation.

Application of Poynting's Theorem

Conservation of energy for electromagnetic field (Umov-Poynting's theorem)

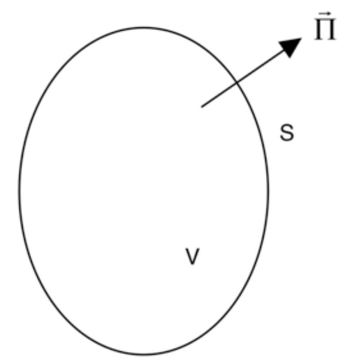

$$\oint_S [\vec{E},\vec{H}]\, d\vec{S} = -\frac{d}{dt}\int_V \left(\frac{\mu_o H^2}{2} + \frac{\varepsilon_o E^2}{2}\right) dV - \int_V \vec{j}\vec{E}\, dV \qquad (3.52)$$

Expression on the left side is an integral of Poynting's vector

$$\vec{\Pi} = [\vec{E},\vec{H}] \qquad (3.53)$$

over surface *S* surrounding volume *V* and is equal to the power of electromagnetic irradiation, or energy of electromagnetic field coming through the surface *S* per second. The first integral in right side of Eq. (3.52) is a change of energy of electromagnetic field per second:

$$\frac{dW}{dt} = \frac{d}{dt}\int_V \left(\frac{\mu_o H^2}{2} + \frac{\varepsilon_o E^2}{2}\right) dV \qquad (3.54)$$

where electromagnetic energy in volume *V* is

$$W = \frac{1}{2}\int_V (\mu_o H^2 + \varepsilon_o E^2) dV \qquad (3.55)$$

Emittance Growth due to Charge Redistribution

Second term in right side of Eq. (3.52) can be expressed as a sum over all charges in the beam

$$\int_V \vec{j}\vec{E}\, dV = \int_V \rho\vec{v}\vec{E}\, dV = \sum q\vec{v}\vec{E} \qquad (3.56)$$

Change of kinetic energy $W_{kin} = mc^2(\gamma - 1)$ of particle in time is

$$\frac{dW_{kin}}{dt} = mc^2 \frac{d\gamma}{dt} \qquad (3.57)$$

where derivative of reduced particle energy $\gamma = \sqrt{1 + (p / mc)^2}$ over time is

$$\frac{d\gamma}{dt} = \frac{1}{\gamma(mc)^2}\vec{p}\frac{d\vec{p}}{dt} = \frac{1}{mc^2}\vec{v}\frac{d\vec{p}}{dt} = \frac{1}{mc^2}q\vec{v}\vec{E} \qquad (3.58)$$

Emittance Growth due to Charge Redistribution (cont.)

Therefore,

$$q\vec{v}\vec{E} = \frac{dW_{kin}}{dt} \tag{3.59}$$

and second term, Eq. (3.52), is the change of kinetic energy of the beam in time:

$$\sum q\vec{v}\vec{E} = \sum \frac{dW_{kin}}{dt} \tag{3.60}$$

Consider non-relativistic case (no magnetic field):

$$\frac{d}{dt}\left(\frac{\varepsilon_o}{2}\int E^2\,dV + \sum_{i=1}^{N} W_{kin}\right) = 0 \tag{3.61}$$

Emittance Growth due to Charge Redistribution (cont.)

where E is the total electrostatic field in the structure, and W_{kin} is the kinetic energy of particle:

$$W_{kin} = mc^2\sqrt{1+\frac{p_x^2+p_y^2+p_z^2}{(mc)^2}} \approx mc^2\gamma + \frac{p_x^2+p_y^2}{2m\gamma} \qquad (3.62)$$

and summation in Eq. (3.61) is performed over all particles of the beam. Assume that energy is the same for all particles, and is not changed during beam transport. Below consider only transverse particle motion and kinetic energy, associated with this motion. According to definition of rms beam values, kinetic energy of particles is:

$$\sum_{i=1}^{N} W_{kin} = \frac{N}{2m\gamma}[<p_x^2> + <p_y^2>] . \qquad (3.63)$$

where rms value of transverse momentum is $$<p_x^2> = (\frac{mc\varepsilon}{2R})^2 . \qquad (3.64)$$

In a round beam rms values in both transverse directions are the same, $<p_x^2> = <p_y^2>$, therefore

$$\sum_{i=1}^{N} W_{kin} = N\frac{mc^2}{\gamma}(\frac{\varepsilon}{2R})^2 . \qquad (3.65)$$

Emittance Growth due to Charge Redistribution (cont.)

We consider continuous beam, therefore Eq. (3.61) can be rewritten as

$$L_b \frac{\varepsilon_o}{2} \int_o^\infty E^2\, dS + N \frac{mc^2}{\gamma} \left(\frac{\varepsilon}{2R}\right)^2 = const \quad , \tag{3.66}$$

where L_b is an arbitrary length along the beam, containing N particles. Using beam current $I = q\beta c N / L_b$, Eq. (3.66) becomes:

$$\frac{4q\gamma\beta c}{mc^2 I}\left(\frac{\varepsilon_o}{2}\int_0^\infty E^2 dS\right) + \left(\frac{\varepsilon}{R}\right)^2 = const \tag{3.67}$$

Applying the last equation to the initial and final beam, one has,

$$\frac{\varepsilon_f^2}{\varepsilon_i^2} = \frac{R_f^2}{R_o^2} + \frac{4q\gamma\beta c R_f^2}{mc^2 I \varepsilon_i^2}\left(\frac{\varepsilon_o}{2}\int_o^\infty E_i^2\, dS - \frac{\varepsilon_o}{2}\int_o^\infty E_f^2\, dS\right) \quad . \tag{3.68}$$

Emittance Growth due to Charge Redistribution (cont.)

Eq. (3.68) can be rewritten as $$\frac{\varepsilon_f^2}{\varepsilon_i^2}=\frac{R_f^2}{R_o^2}\left(1+b\frac{W_i-W_f}{W_o}\right), \qquad (3.69)$$

where initial, W_i, and final, W_f, energy stored in electrostatic field are

$$W_i=\frac{\varepsilon_o}{2}\int_o^\infty E_i^2\,dS \qquad W_f=\frac{\varepsilon_o}{2}\int_o^\infty E_f^2\,dS, \qquad (3.70)$$

and normalization constant is $$W_o=2\pi\varepsilon_o\left(\frac{I}{I_c}\frac{mc^2}{q\beta\gamma}\right)^2 \qquad (3.71)$$

If the beam is initially rms-matched, then the rms beam radius is changing insignificantly, so we can put $R_f \approx R_o$. Additionally, taking into account expression

$$b=\frac{\mu_o^2}{\mu^2}-1$$

one can write:

$$\frac{\varepsilon_f}{\varepsilon_i}=\sqrt{1+\left(\frac{\mu_o^2}{\mu^2}-1\right)\left(\frac{W_i-W_f}{W_o}\right)}. \qquad (3.72)$$

Emittance Growth due to Charge Redistribution (cont.)

In emittance-dominated regime $\mu \approx \mu_o$, and Eq. (3.72) gives us conservation of beam emittance. Consider space charge dominated regime. Initial total field E_i is given by:

$$E_i = \frac{mc^2}{qR\gamma}\frac{2I}{\beta\gamma I_c}\{-\frac{r}{R}+\frac{R}{r}[1-exp(-\frac{2r^2}{R^2})\}\,. \qquad (3.73)$$

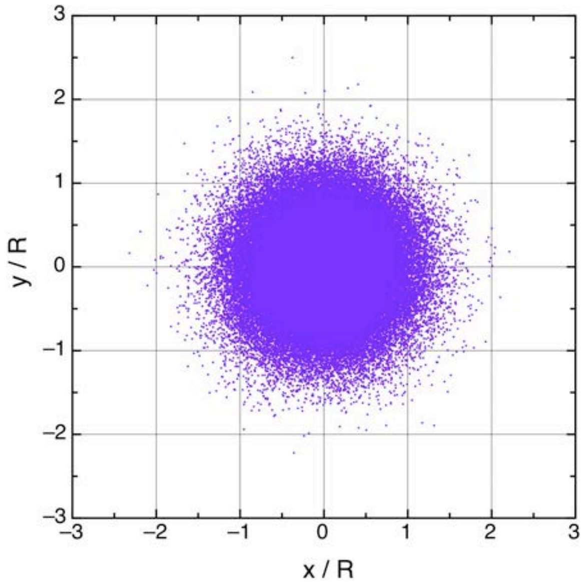

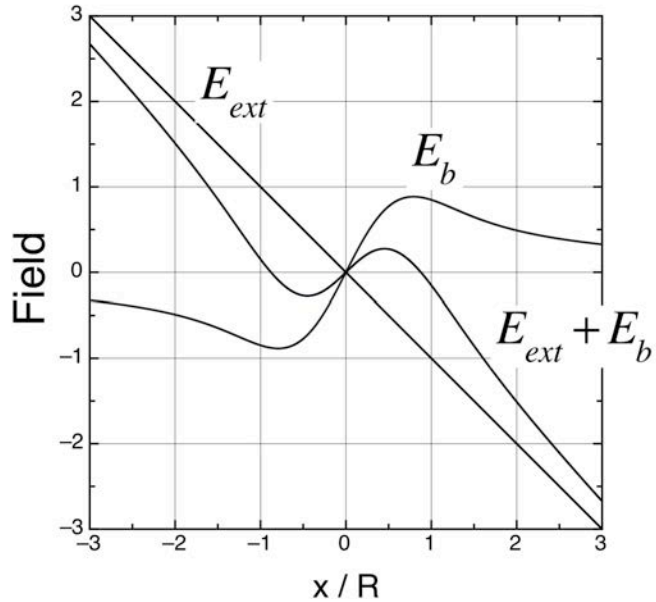

External focusing field E_{ext}, space charge field of Gaussian beam E_b, and total field E_{ext} + E_b at initial moment of time.

Emittance Growth due to Charge Redistribution (cont.)

Final beam distribution is close to uniform with the same value of beam radius *R*. It is a general property of space-charge dominated regime, that self-field of the beam almost compensates for external field within the beam. We can put $E_f \approx 0$ within the beam and $E_f = E_{ext} + E_b$ outside the beam

$$E_f = \begin{cases} 0, & r \le R \\ \dfrac{mc^2}{qR}\dfrac{2I}{\beta\gamma^2 I_c}\left(-\dfrac{r}{R}+\dfrac{R}{r}\right), & r > R \end{cases} \quad . \tag{3.74}$$

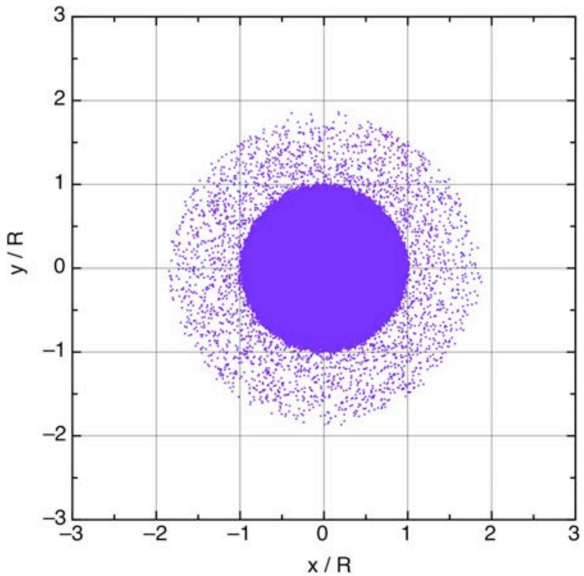

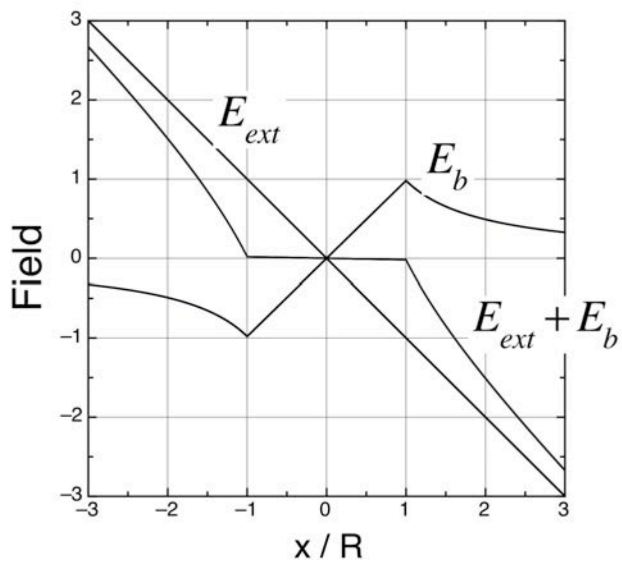

External focusing field E_{ext}, space charge field E_b, and total field $E_{ext} + E_b$ after beam uniforming.

Emittance Growth due to Charge Redistribution (cont.)

Substitution of E_f and E_i into Eq.(3.70) gives for

$$\frac{W_i - W_f}{W_o} = \int_o^{\xi_{max}} [-\xi + \frac{1}{\xi}(1 - e^{-2\xi^2})]^2 \xi d\xi - \int_1^{\xi_{max}} (-\xi + \frac{1}{\xi})^2 \xi d\xi \approx 0.077 \qquad (3.75)$$

where $x = r / R$. In Eq. (3.75) the upper limit of integration is arbitrary and usually is determined by the aperture of the channel, $x_{max} = a / R$.

Free energy parameter for different beam distributions

4D Distribution	2D Projection	$\frac{W_i - W_f}{W_o}$
KV	ρ_o	0
Water Bag	$\rho_o(1 - \frac{r^2}{R^2})$	0.01126
Parabolic	$\rho_o(1 - \frac{r^2}{R^2})^2$	0.02366
Gaussian	$\rho_o \exp(-\frac{r^2}{R^2})$	0.077

Instability of Anisotropic KV Beam (I.Hofmann, 1998)

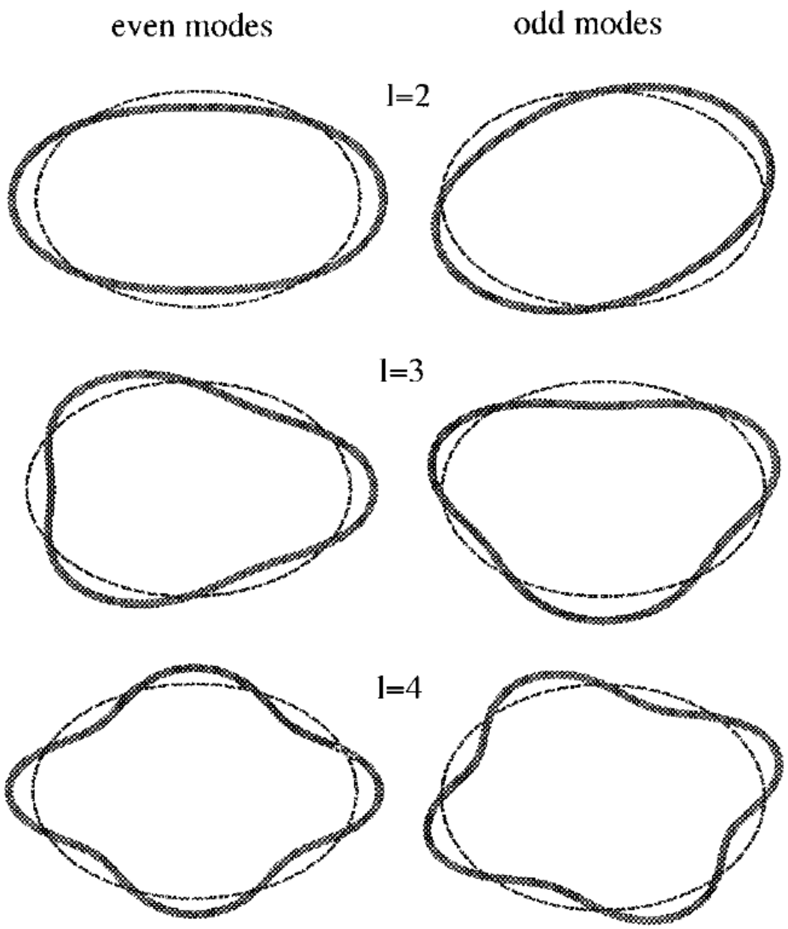

KV Beam with unequal emittances in a focusing channel with different focusing strength in x- and y- directions

$$f_0(x, y, p_x, p_y) = \frac{NT\nu_y/\nu_x}{2\pi^2 m\gamma a^2}\delta(H_{0x} + TH_{0y} - m\gamma\nu_x^2 a^2/2)$$

Ratio of beam emittances:

$$\frac{\epsilon_x}{\epsilon_y} = \frac{a^2\nu_x}{b^2\nu_y}$$

Beam cross sections for second, third and fourth order even and odd modes ~schematic, with x horizontal and y vertical coordinates.

Instability of Anisotropic KV Beam (cont.)

Perturbed distribution function

$$f \equiv f_0(H_{0x}, H_{0y}) + f_1(x, y, p_x, p_y, t)$$

Vlasov's equation for perturbed beam distribution function

$$\frac{df_1}{dt} \equiv \frac{\partial f_1}{\partial t} + \frac{p_x}{m\gamma}\frac{\partial f_1}{\partial x} + \frac{p_y}{m\gamma}\frac{\partial f_1}{\partial y} - m\gamma\nu_x^2 x\frac{\partial f_1}{\partial p_x} - m\gamma\nu_y^2 y\frac{\partial f_1}{\partial p_y}$$

$$= \frac{NTq\nu_y/\nu_x}{2\pi^2 m^2\gamma^4 a^2}\left(p_x\frac{\partial\Phi}{\partial x} + Tp_y\frac{\partial\Phi}{\partial y}\right)$$

$$\times \delta'[p_x^2 + \nu_x^2 x^2 + T(p_y^2 + \nu_y^2 y^2) - \nu_x^2 a^2]. \tag{11}$$

Poisson's equation for perturbed electrostatic potential created by perturbed space charge density

$$\nabla^2\Phi = -\frac{q}{\epsilon_0}n_1 = -\frac{q}{\epsilon_0}\int f_1 dp_x dp_y.$$

Instability of Anisotropic KV Beam

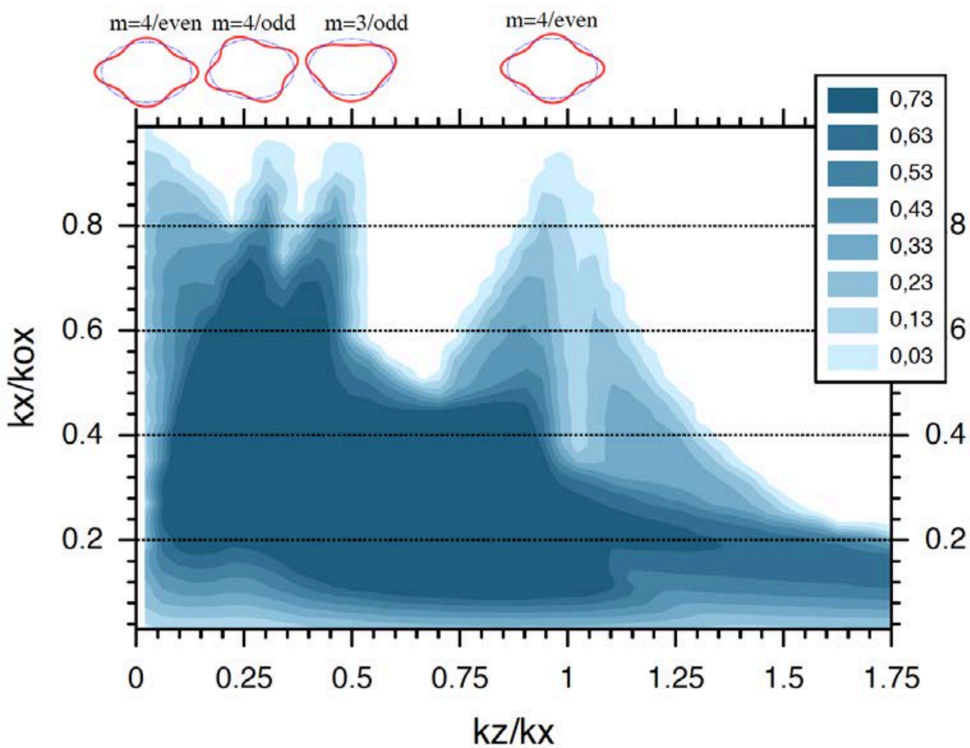

Stability chart for $\varepsilon_z/\varepsilon_x$=0.5.

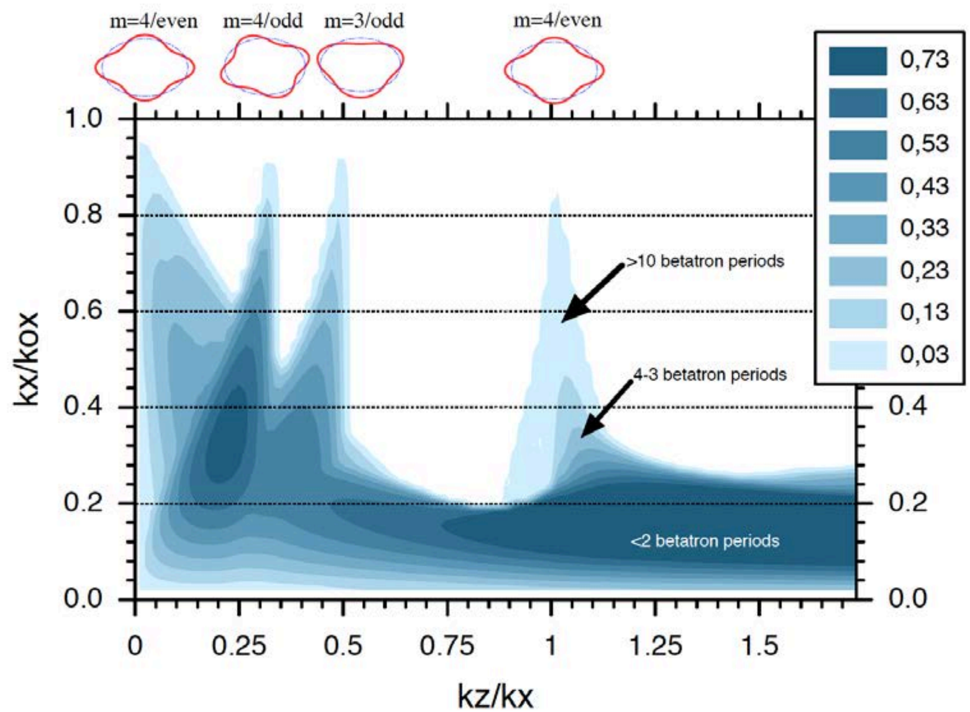

Stability chart for $\varepsilon_z/\varepsilon_x$=1.2.

Stability charts derived for KV beam with different transverse emittances in focusing channels with different focusing strengths in two transverse directions. Charts are applied to motion in RF field assuming one direction (x-) in transverse and another (z-) is longitudinal.

Instability of Anisotropic KV Beam

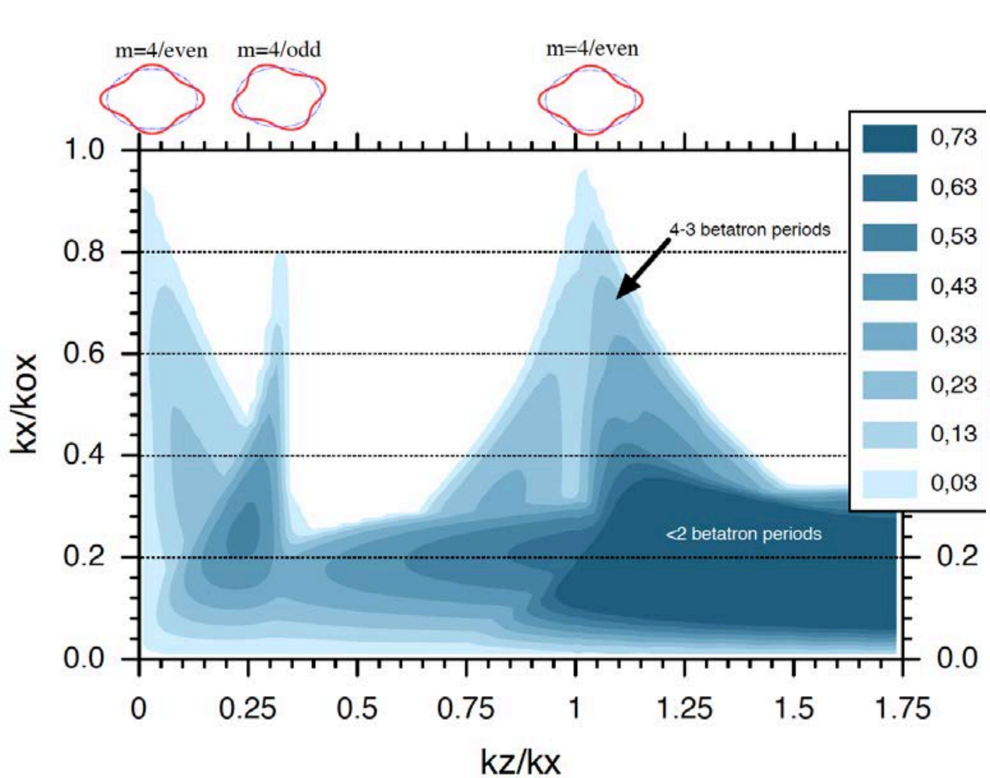

Stability chart for $\varepsilon_z/\varepsilon_x$=2.0.

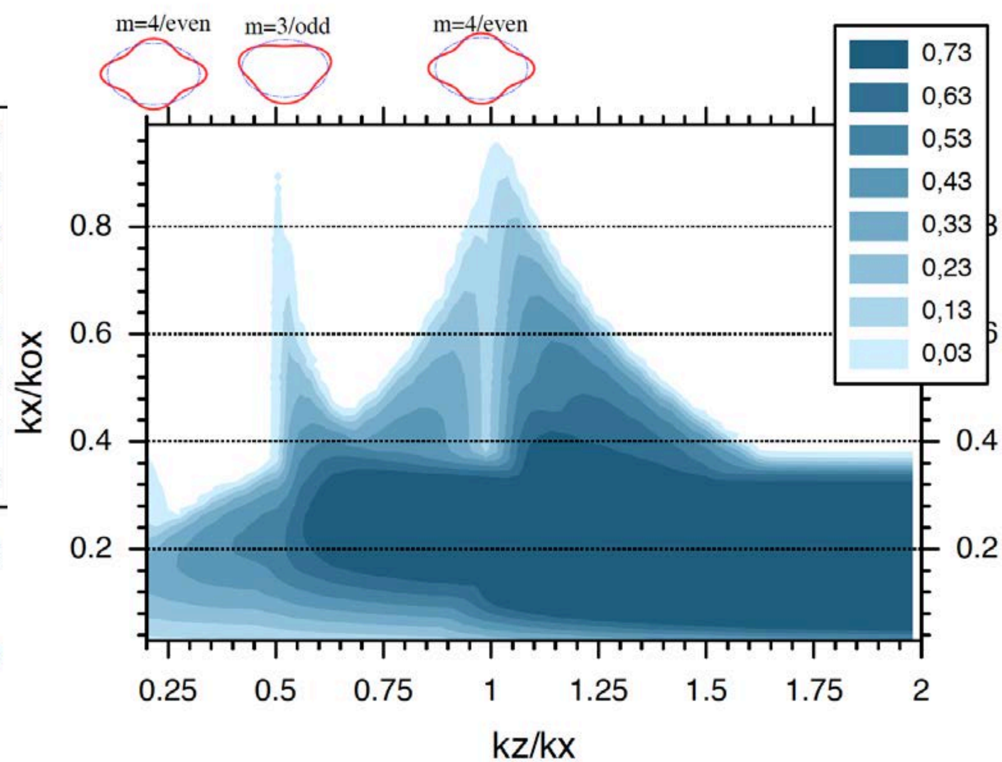

Stability chart for $\varepsilon_z/\varepsilon_x$=3.0.

Instability of Anisotropic KV Beam

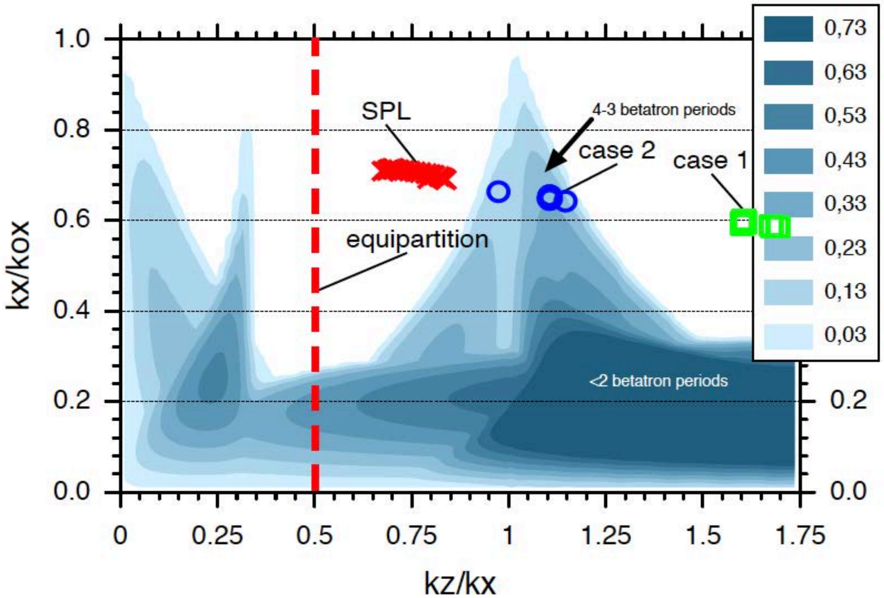

Stability chart for $\varepsilon_z/\varepsilon_x=2.0$.

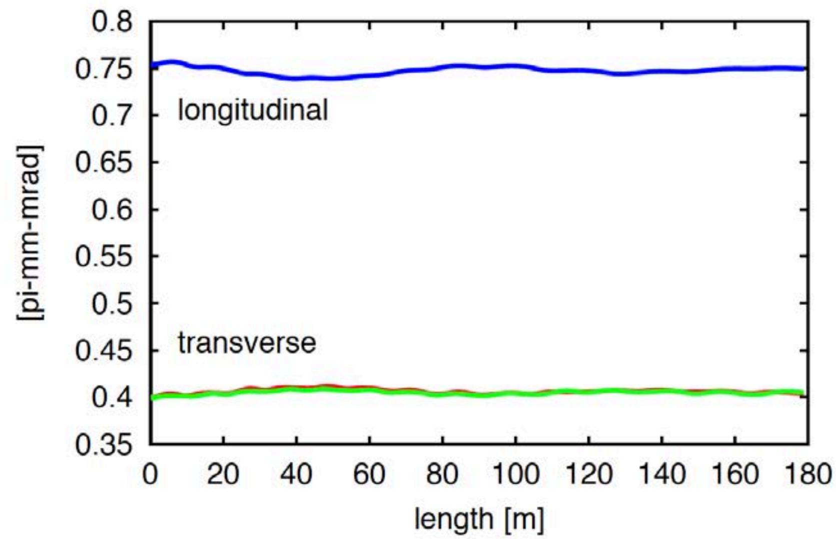

Rms emittance evolution for SPL lattice.

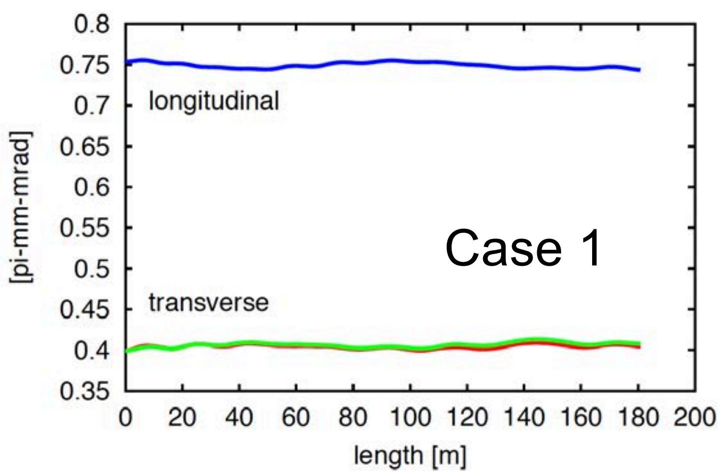

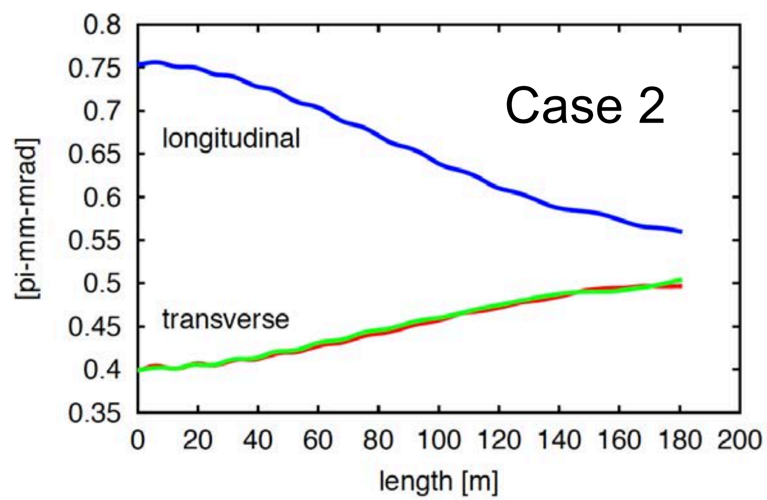

Rms emittance evolution

Halo Development in Particle-Core Interaction

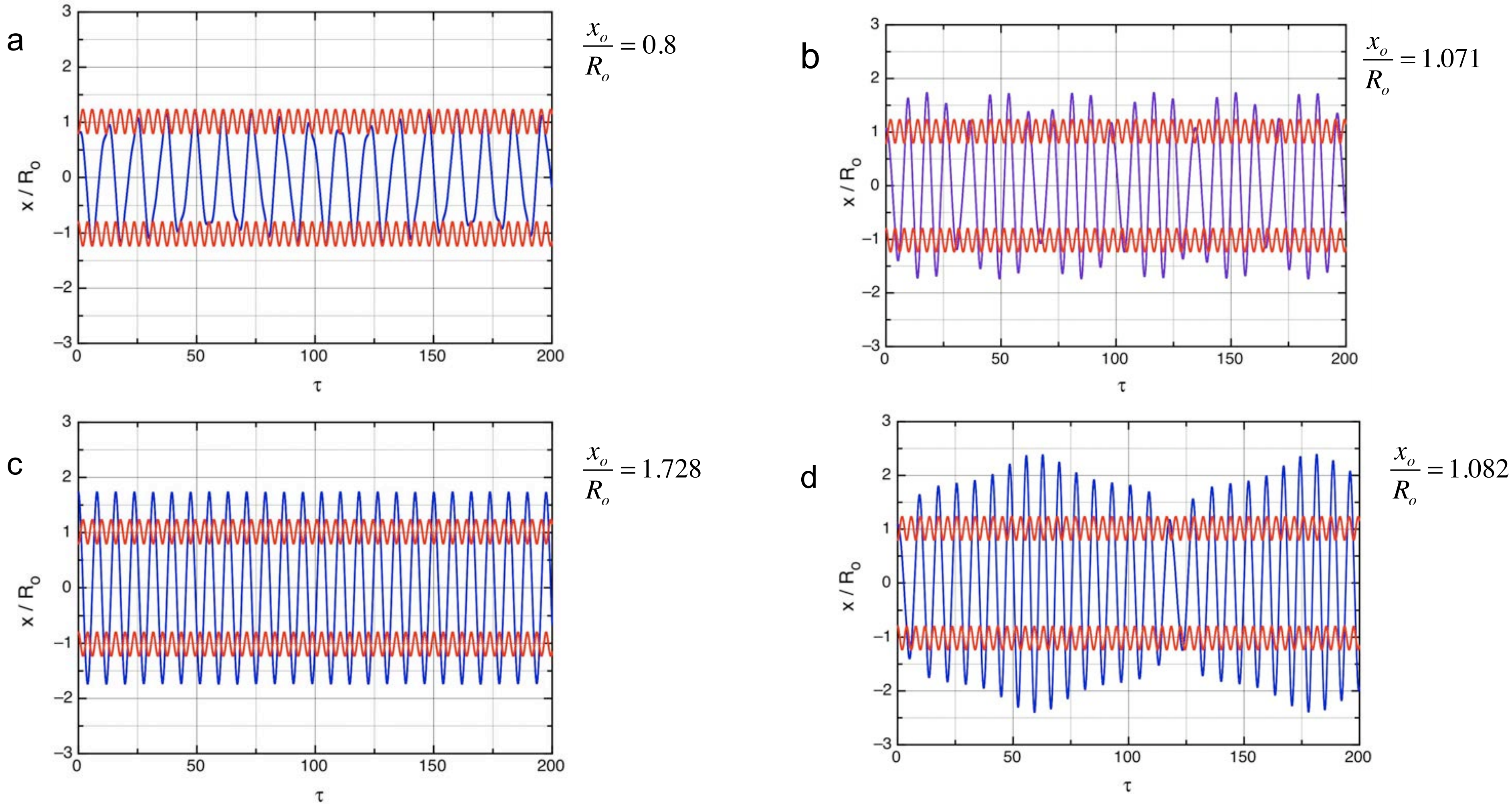

Envelope oscillations of the beam with space charge parameter b=3, amplitude Δ= 0.2 and single particle trajectories with initial conditions (a) x_o/R_o=0.8, (b) x_o/R_o =1.071, (c) x_o/R_o =1.728, (d) x_o/R_o =1.082.

Stroboscopic Particle Motion

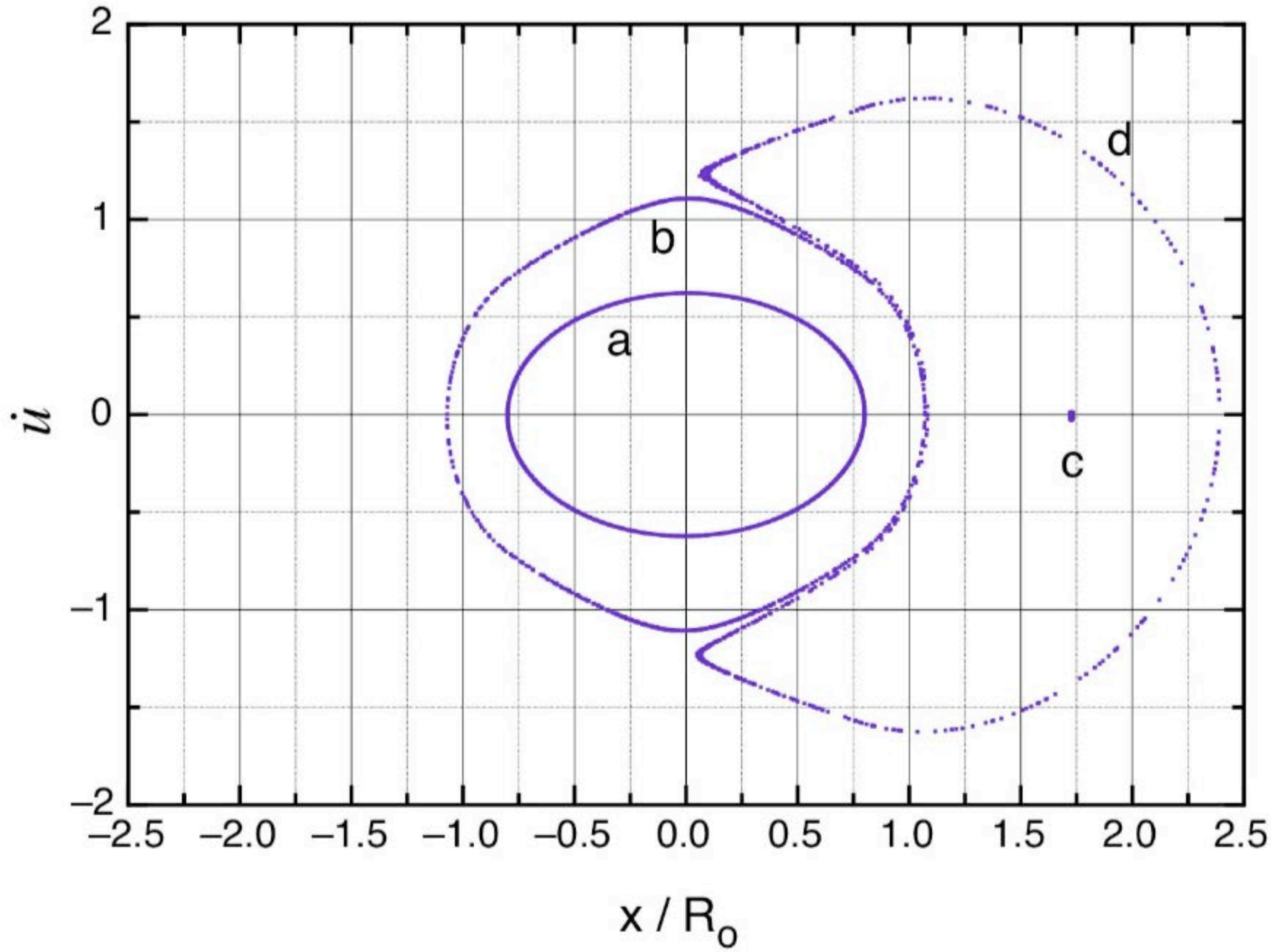

Stroboscopic particle trajectories at phase plane $(u, du / d\tau)$ taken after each two envelope oscillation periods: (a) x_o/R_o=0.8, (b) x_o/R_o =1.071, (c) x_o/R_o=1.728, (d) x_o/R_o =1.082.

Particle – Core Model

Dimensionless $r = \frac{R}{R_e}$ beam envelope (core) equation: $\frac{d^2 r}{d\tau^2} + r - \frac{1}{(1+b)r^3} - \frac{b}{(1+b)r} = 0$

Single particle equation of motion $u = \frac{x}{R_e}$:

$$\frac{d^2 u}{d\tau^2} + u = \begin{cases} \frac{b}{(1+b)} \frac{u}{r^2}, & |u| \le r \\ \frac{b}{(1+b)u}, & |u| > r \end{cases}$$

Space charge parameter

$$\boxed{b = \frac{2}{\beta\gamma} \frac{I}{I_c} \frac{R_e^2}{\varepsilon^2}}$$

I beam current

$I_c = 4\pi\varepsilon_o mc^3 / q$ characteristic beam current

ε normalized beam emittance

β particles velocity,

γ particle energy

R_e radius of the equilibrium envelope

Small intensity beam $b \approx 0$

High intensity beam b >> 1

Approximation of Space Charge Field

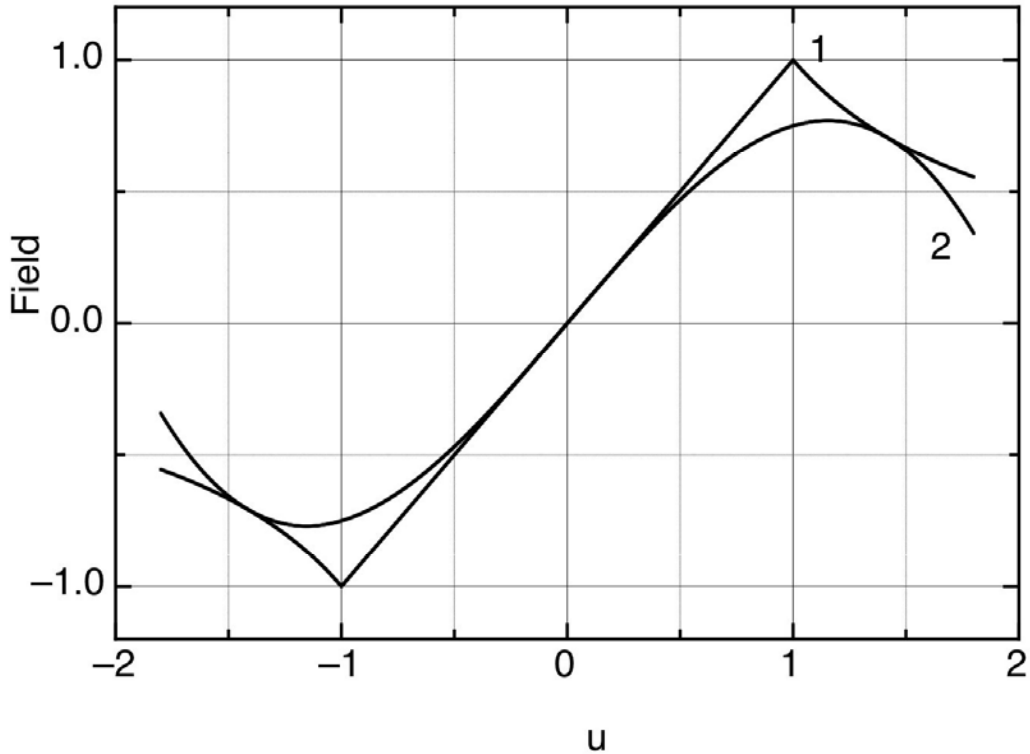

(1) Field of uniformly charged beam

$$F = \frac{b}{(1+b)}\begin{cases} \dfrac{u}{r^2}, & |u| \le r \\ \dfrac{1}{u}, & |u| > r \end{cases}$$

(2) Field approximation:

$$F = \frac{b}{(1+b)}\left(-\frac{u}{r^2} + \frac{u^3}{4}\right)$$

Mismatched Envelope Oscillation

Envelope equation $$\frac{d^2r}{d\tau^2}+r-\frac{1}{(1+b)r^3}-\frac{b}{(1+b)r}=0$$

Expansions $r=1+\vartheta$ $\quad \frac{1}{r}\approx 1-\vartheta$ $\quad \frac{1}{r^3}\approx 1-3\vartheta$ $$\frac{d^2\vartheta}{d\tau^2}+2(\frac{2+b}{1+b})\vartheta=0$$

Equation for small deviation from equilibrium

$$r=1+\Delta\cos(2\Omega\tau)$$

Envelope oscillation frequency

$$2\Omega=\sqrt{2(\frac{2+b}{1+b})}$$

For small intensity beam $b\approx 0$ $\quad r=1+\Delta\cos 2\tau$

For high intensity beam b >>1 $\quad r=1+\Delta\cos\sqrt{2}\tau$

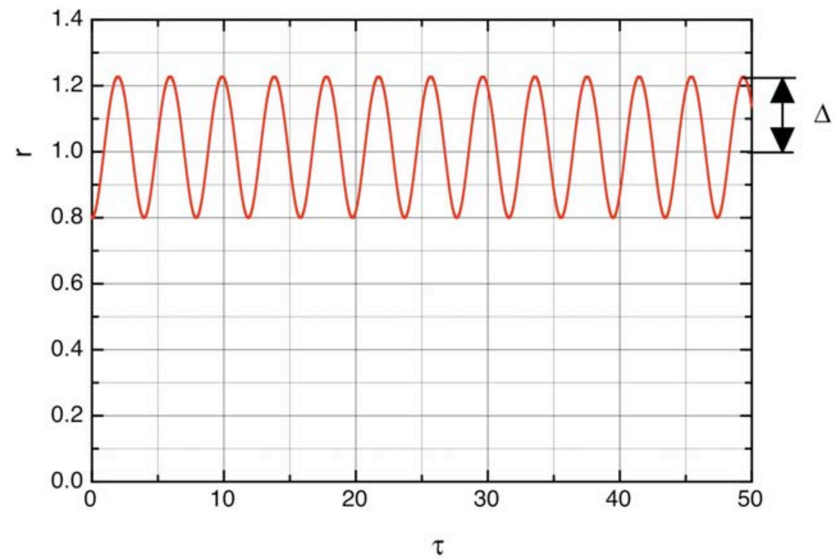

A Harmonic Oscillator with Parametric Excitation for Single Particle Motion

With field approximation, equation of particle motion is

$$\frac{d^2u}{d\tau^2}+u-\left(\frac{b}{1+b}\right)\left[\frac{u}{(1+\Delta\cos 2\Omega\tau)^2}-\frac{u^3}{4}\right]=0$$

Using expansion

$$\frac{1}{(1+\Delta\cos 2\Omega\tau)^2}\approx 1-2\Delta\cos 2\Omega\tau$$

Equation of particle motion

$$\frac{d^2u}{d\tau^2}+u\left(\frac{1}{1+b}\right)(1+2b\Delta\cos 2\Omega\tau)+\left(\frac{b}{1+b}\right)\frac{u^3}{4}=0$$

Equation corresponds to Hamiltonian

$$\boxed{H=\frac{\dot{u}^2}{2}+\varpi^2\frac{u^2}{2}(1-h\cos 2\Omega\tau)+\alpha\frac{u^4}{4}}$$

with the following notations

$$\varpi^2=\frac{1}{1+b}\qquad h=-2b\Delta\qquad \alpha=\frac{b}{4\,(1+b)}$$

Canonical Transformation of Hamiltonian

Change the variables ($\dot{u}$, u) to new variables (Q, P) using a generating function

$$F_2(u,P,\tau) = \frac{uP}{\cos\Omega\tau} - \left(\frac{P^2}{2\varpi} + \varpi\frac{u^2}{2}\right)tg\Omega\tau$$

Relationships between variables are given by:

$$\begin{cases} Q = \dfrac{\partial F_2}{\partial P} = \dfrac{u}{\cos\,\Omega\,\tau} + \dfrac{P}{\varpi}\,tg\Omega\,\tau \\ \dot{u} = \dfrac{\partial F_2}{\partial u} = \dfrac{P}{\cos\,\Omega\,\tau} - \varpi\,u\,tg\Omega\,\tau \end{cases}$$

or

$$\begin{cases} u = Q\cos\Omega\,\tau + \dfrac{P}{\varpi}\sin\Omega\,\tau \\ \dot{u} = -\varpi\,Q\sin\Omega\,\tau + P\cos\,\Omega\,\tau \end{cases}$$

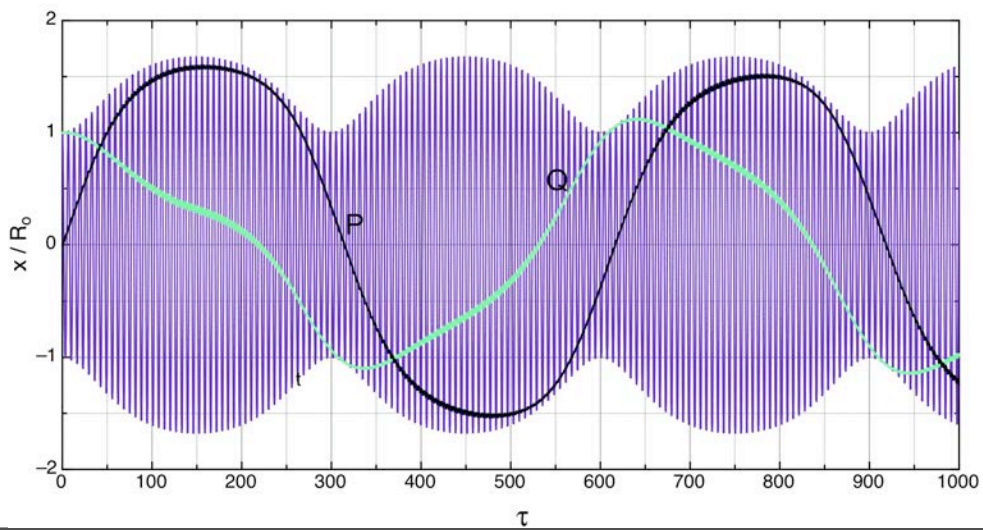

Averaged Hamiltonian

New Hamiltonian $$K = H + \frac{\partial F_2}{\partial \tau}$$

$$K = \frac{P^2}{2} + \varpi^2 \frac{Q^2}{2} - \frac{\varpi^2 h}{2}(Q\cos\Omega\tau + \frac{P}{\varpi}\sin\Omega\tau)^2 \cos 2\Omega\tau + \frac{\alpha}{4}(Q\cos\Omega\tau + \frac{P}{\varpi}\sin\Omega\tau)^4 - \frac{P^2\Omega}{2\varpi} - \frac{\Omega\varpi}{2}Q^2$$

After averaging all time-dependent terms over period of $2\pi/\Omega$

$$\bar{K} = \frac{\varpi^2 \bar{Q}^2}{2}(1 - \frac{\Omega}{\varpi} - \frac{h}{4}) + \frac{\bar{P}^2}{2}(1 - \frac{\Omega}{\varpi} + \frac{h}{4}) + \frac{3}{32}\alpha(\bar{Q}^2 + \frac{\bar{P}^2}{\varpi^2})^2$$

Second Canonical Transformation

Change variables $(\bar{Q},\bar{P})$ to action-angle variables *(J, ψ)* using generating function

$$F_1(\bar{Q},\psi) = \frac{\varpi\,\bar{Q}^2}{2tg\psi}$$

Transformation is given by

$$\begin{cases} \bar{Q} = \sqrt{\dfrac{2J}{\varpi}}\sin\psi \\ \bar{P} = \sqrt{2J\varpi}\cos\psi \end{cases}$$

New Hamiltonian

$$\boxed{\bar{K} = \upsilon J + \kappa J^2 + 2\chi J\cos 2\psi}$$

with the following notations

$$\upsilon = \varpi - \Omega = \frac{\sqrt{2}-\sqrt{2+b}}{\sqrt{2(1+b)}} \qquad \kappa = \frac{3}{32}b \qquad \chi = -\frac{1}{4}\frac{b\Delta}{\sqrt{1+b}}$$

Nonlinear Parametric Resonance

Hamiltonian of averaged motion:

$$\boxed{\bar{K} = \upsilon J + \kappa J^2 + 2\chi J \cos 2\psi}$$

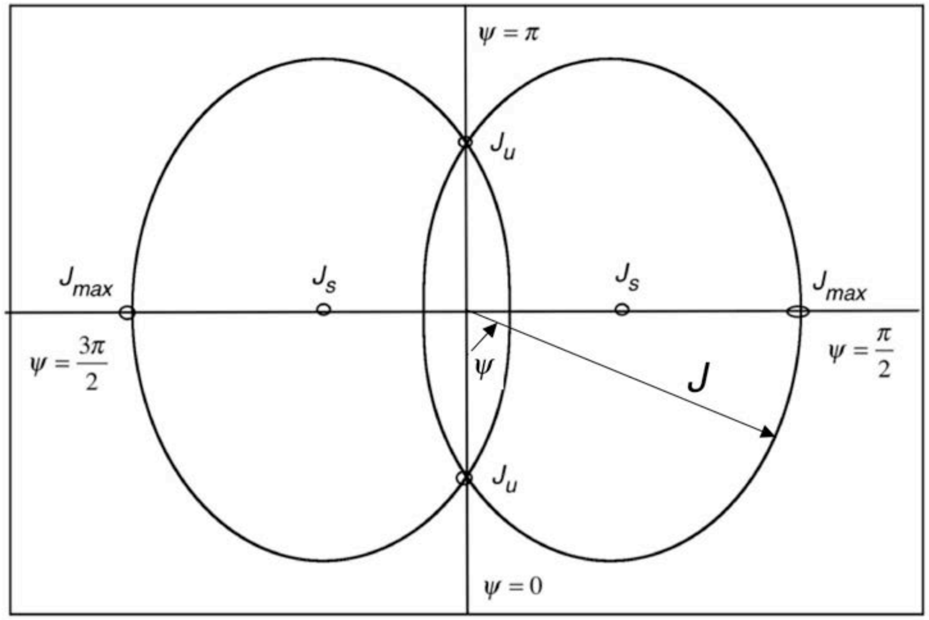

Maximum deviation of particle from the axis $\frac{x_{max}}{R_e} = \sqrt{\frac{2J_{max}}{\varpi}}$

$$\boxed{J_{max} = \frac{(-\upsilon + 2\chi) + \sqrt{8|\upsilon\chi|}}{2\kappa}}$$

$$\boxed{\frac{x_{max}}{R_e} = \sqrt{\frac{32}{3}\frac{\sqrt{1+\frac{b}{2}} - 1 + \frac{b|\Delta|}{2} + \sqrt{2b|\Delta|(\sqrt{1+\frac{b}{2}} - 1)}}{b}}}$$

Nonlinear Parametric Resonance

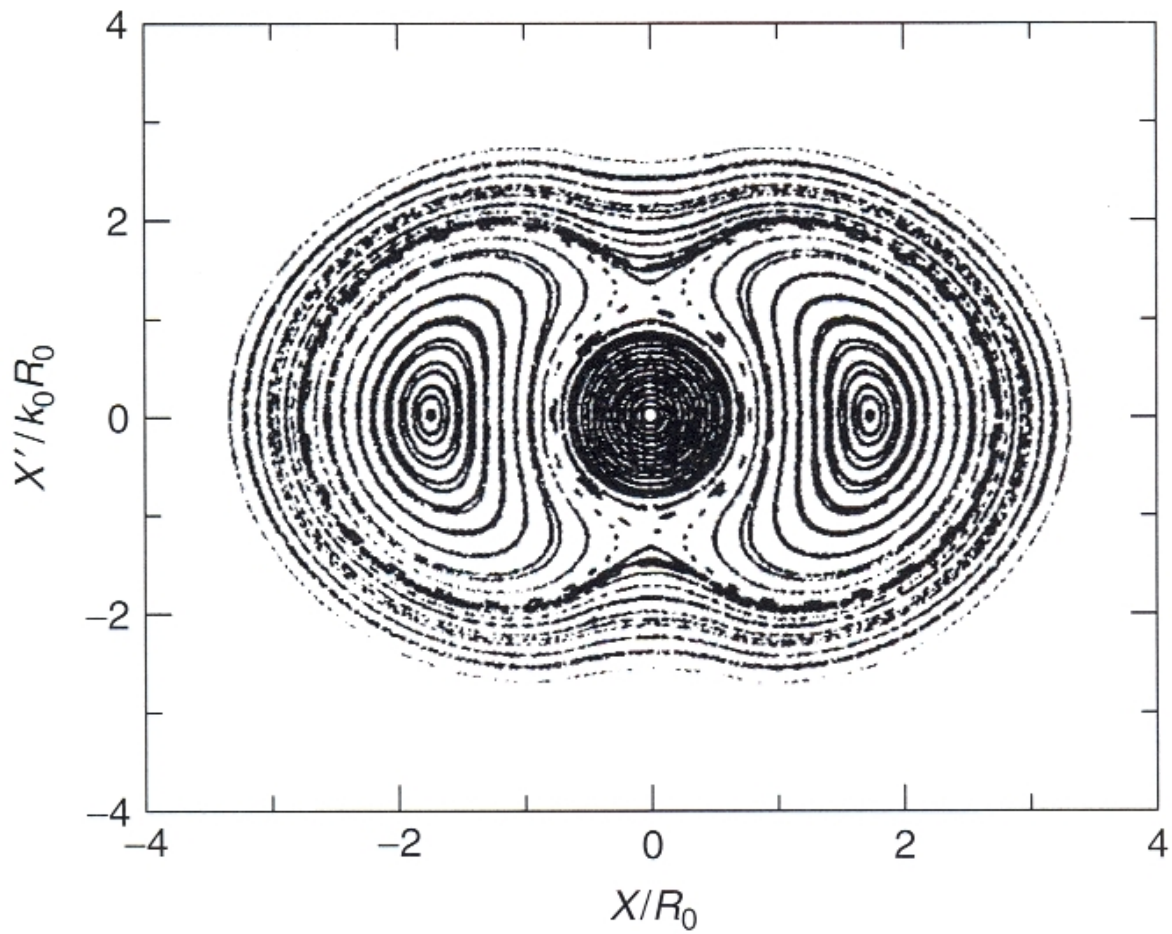

Figure 9.12 Stroboscopic plot obtained by taking snapshots of many independent particle trajectories, once per core-oscillation cycle at the phase of the core oscillation that gives the minimum core radius. Initial particle coordinates were defined on the x and x' axes.

Comparison of Analytical and Numerical Results

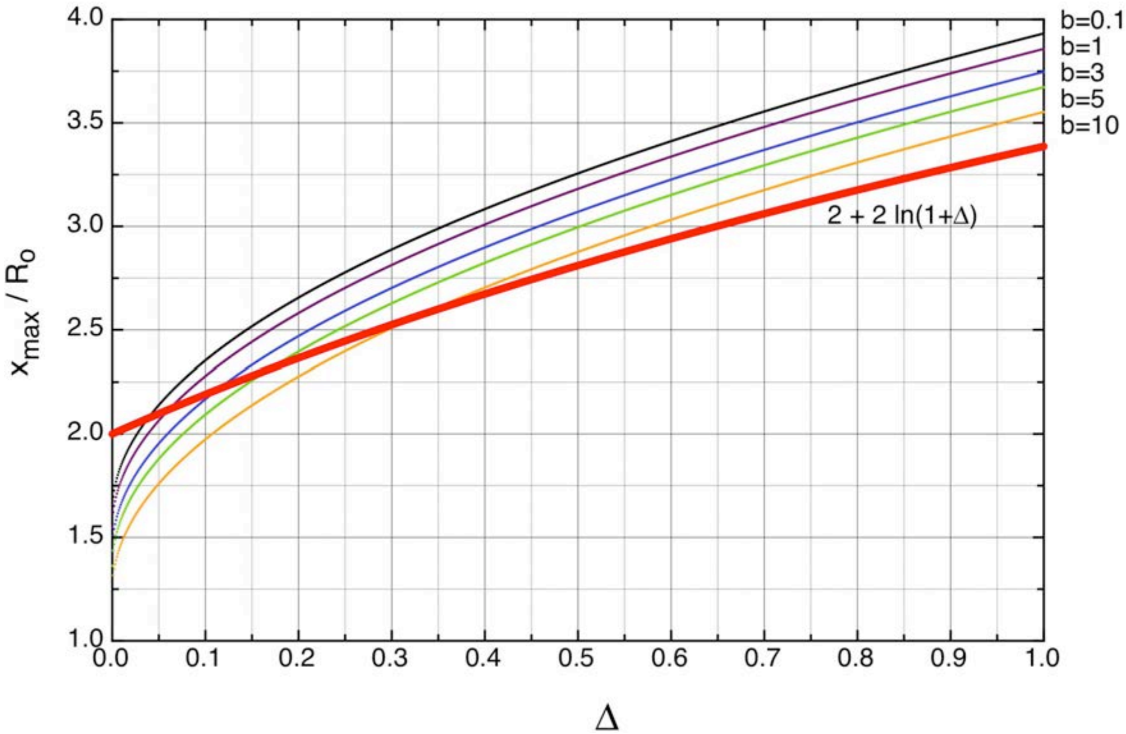

Maximum values of particle deviation from the axis as a function of amplitude of core oscillations (Y.B. NIM-A 618, 2010, p.37). (Red) model of Tom Wangler (*RF Linear Accelerators*, Wiley, 1998)

$$\frac{x_{\max}}{R_o/2} = A + B\ln(\mu)$$

where $A = B = 4$, $\mu = 1 + \Delta$.

LANL Beam Halo Experiment (2002)

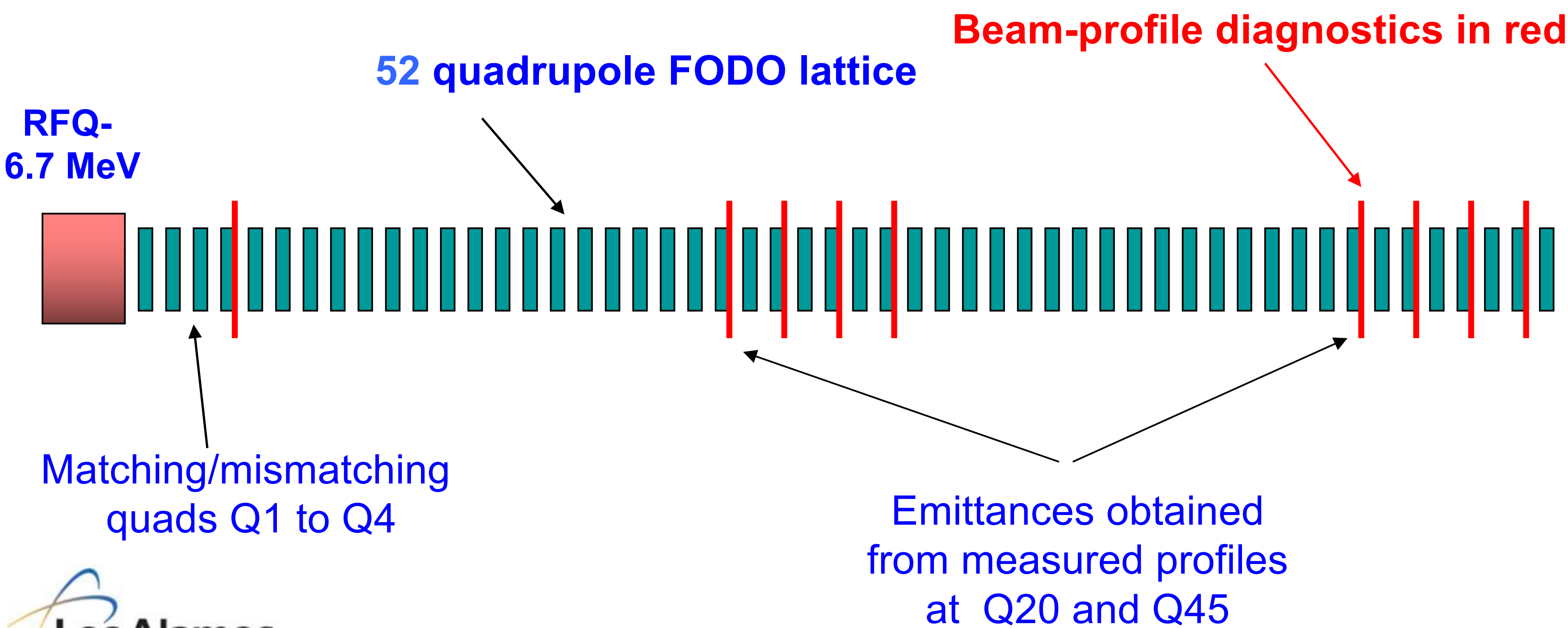

LANL Beam Halo Experiment Lattice

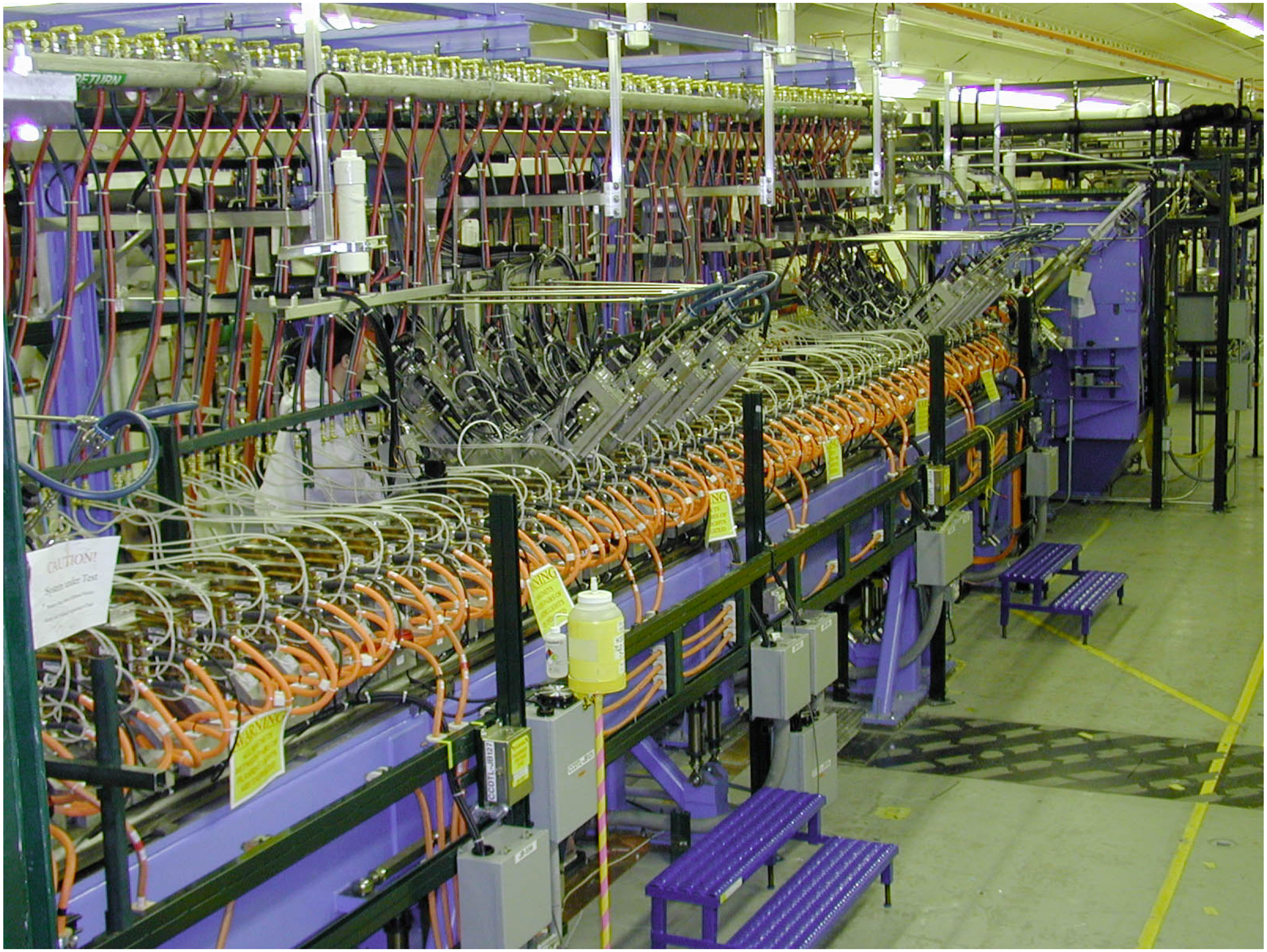

Wire and Scraper Beam-Profile Diagnostic to Measure Beam Profile

- 33-micron carbon wire (too thin to be visible in picture) measures density in beam core above 10^{-3} level.
- Proton range=300 microns so protons pass through wire and make secondary electrons to measure high density in beam core.
- Pair of 1.5mm graphite scraper plates in which protons stop. Can measure proton density outside beam core from 10^{-3} to 10^{-5}.
- Data from wire and scraper plates were combined to produce a single distribution.

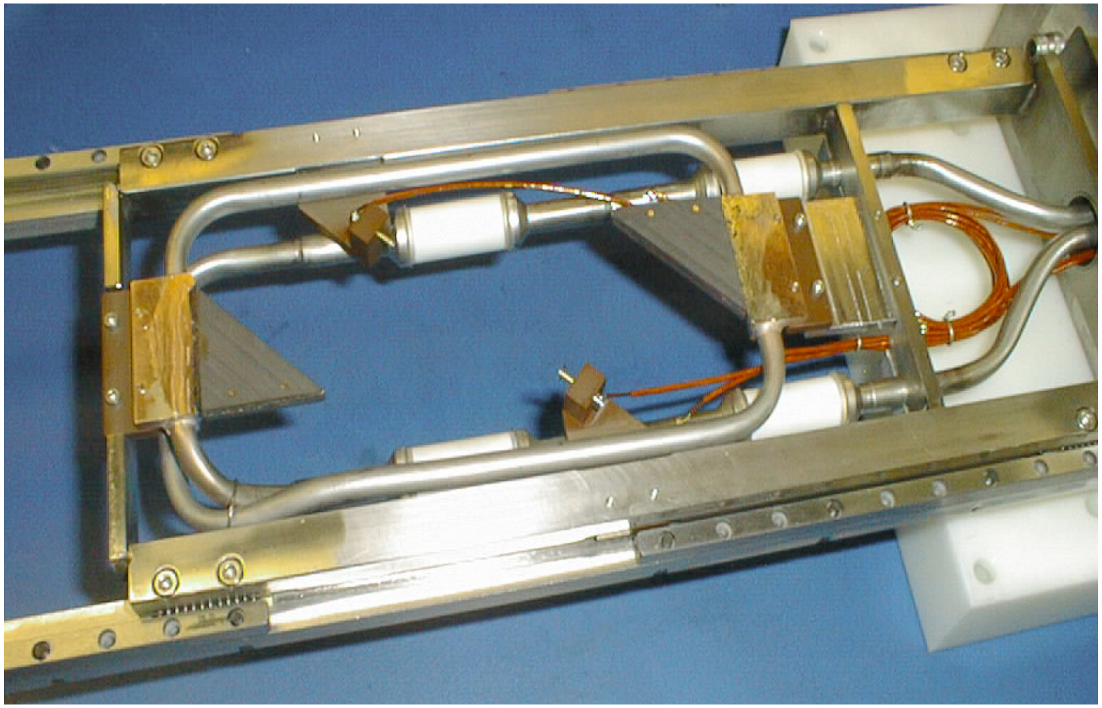

Measured Beam Profile

Typical matched beam profile for 75 mA. (μ=1,matched)

Shows Gaussian-like core plus low-density halo input beam, observed out to 9 rms.

Linear Plot

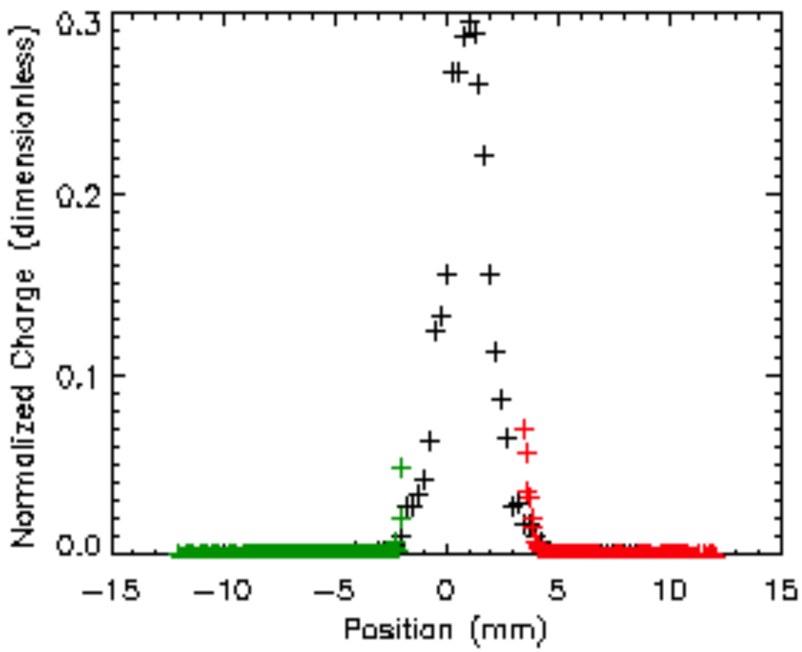

Semilog Plot

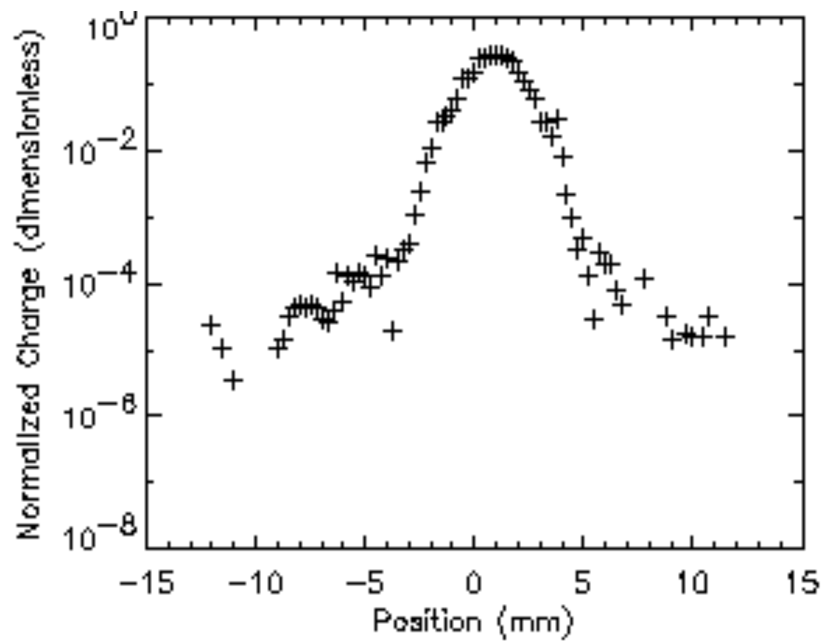

Beam Emittance Growth

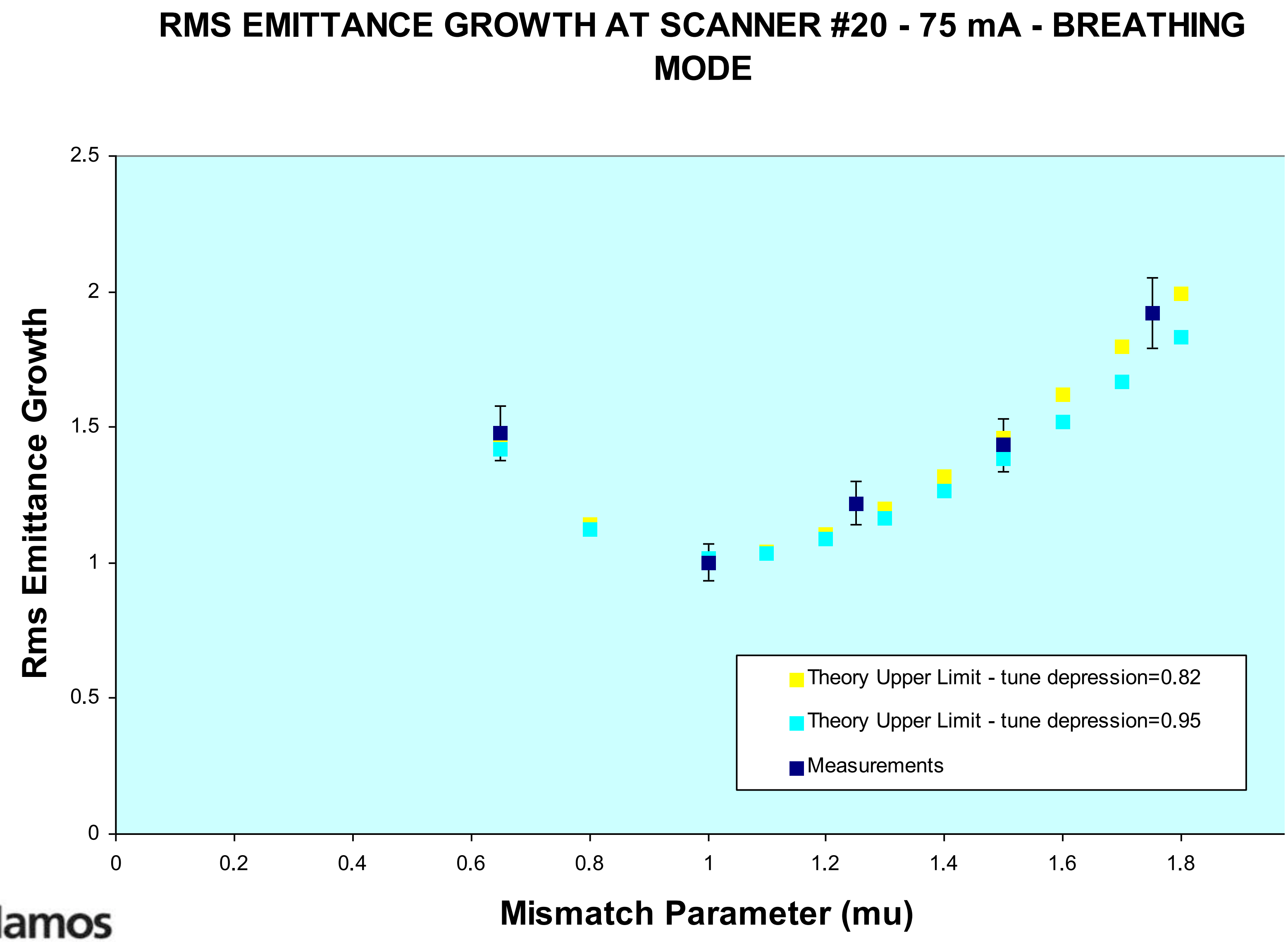

Test of Particle-Core Model Measurements at Different Fractional Intensity Levels (10%, 1%, 0.1%)

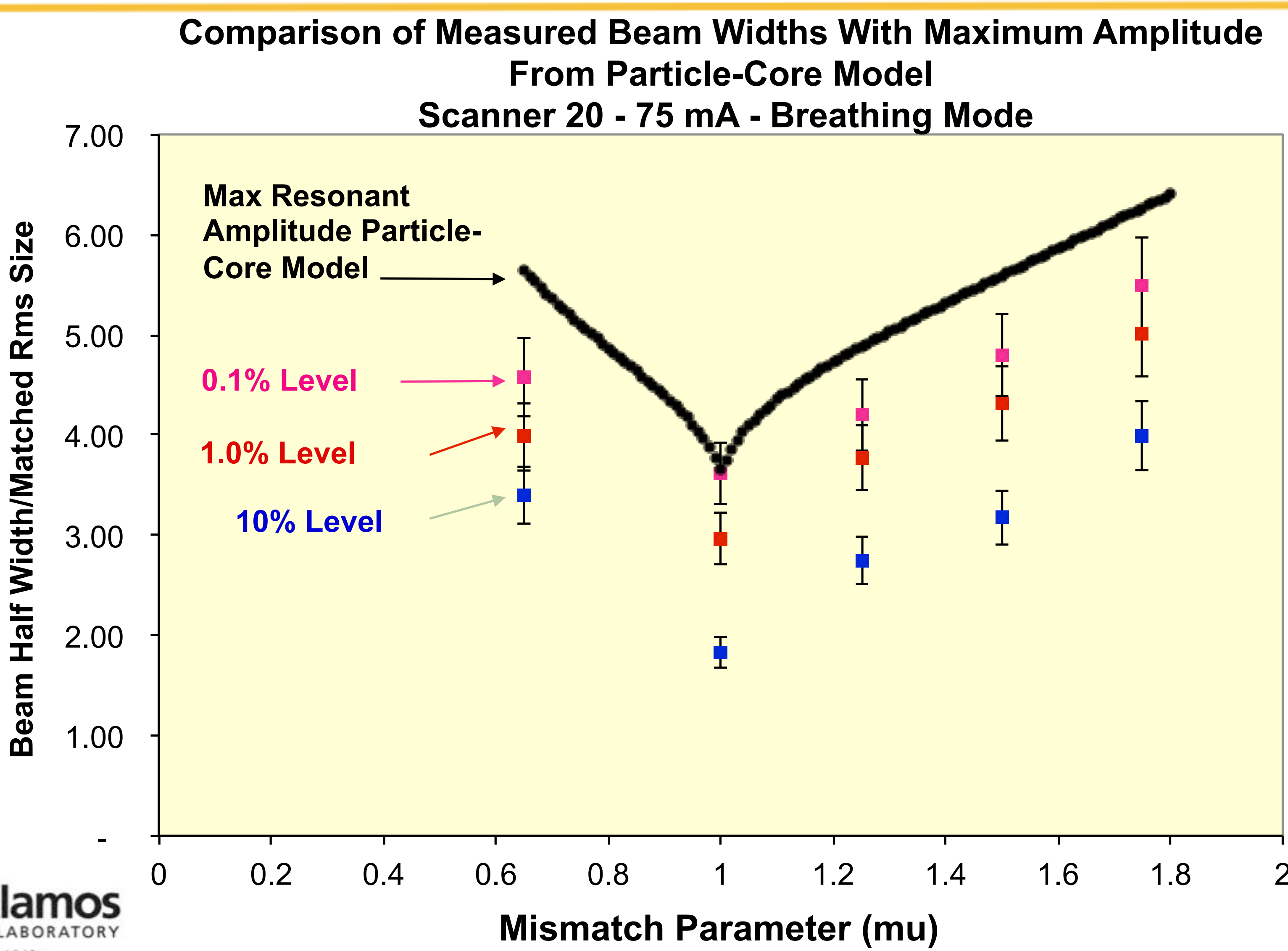

Experimental Observation of Space-Charge Driven Resonances in Linac (L.Groening et al, LINAC2010)

Matched beam envelope

$$R(s, \sigma_{env}) = R_o(\sigma_{env}) + \Delta R(\sigma_{env}) \cdot cos(\sigma_{env} s)$$

Radial electric field

$$E_r = \frac{18 \cdot I}{\pi \epsilon_o \cdot R(s)^2 \beta c} \left[r - \frac{r^3}{2R(s)^2} + O(r) \right]$$

Single-particle trajectory

$$r'' = -\sigma^2_{\perp,o} r + \frac{e \cdot q}{A \cdot m_u} \cdot E_r$$

or

Disturbed oscillator with $\sigma_\perp$ *as* depressed phase advance

$$r'' + \sigma_\perp^2 r \sim r^3 \cdot e^{i \sigma_{env} s}$$

Resonance condition:

$$\sigma_{env} = 4\sigma_\perp.$$

Phase advance of the matched envelope is 360°, the resonance occurs at $\sigma_\perp$ = 90°

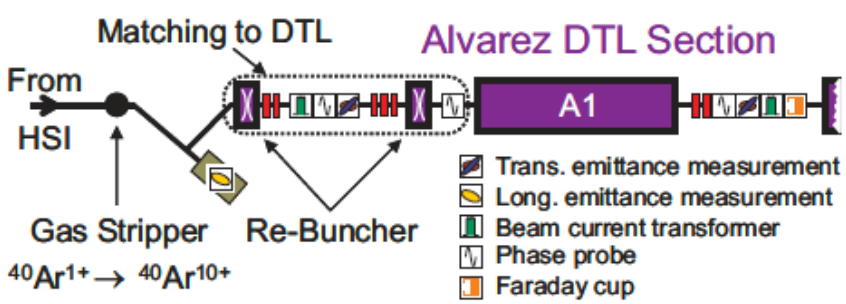

Figure 3: Schematic set-up of the experiments (not to scale).

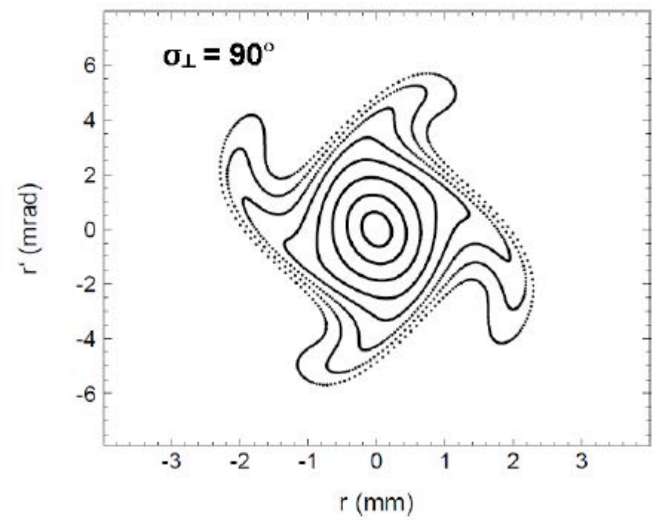

Figure 1: Distribution of particles at the exit of the periodic channel according to the radial particle-core model of the space charge driven transverse 4th-order resonance.

Experimental Observation of Space-Charge Driven Resonances (cont.)

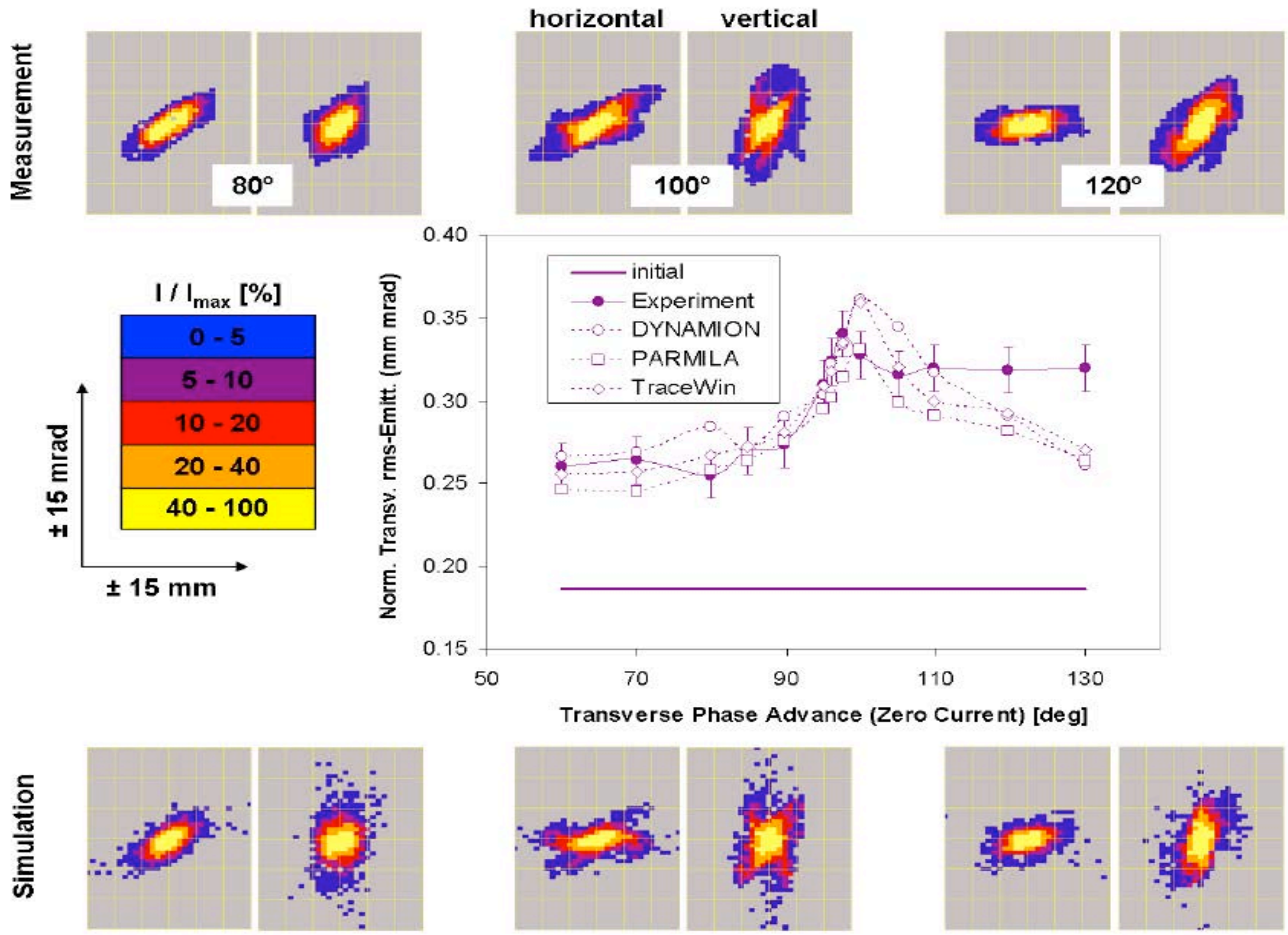

Figure 7: Upper and lower: phase space distributions at the exit of the first DTL tank as obtained from measurements and from the DYNAMION code for phase advances $\sigma_{\perp,o}$ of 80°, 100°, and 120°. Left (right) side distributions refer the horizontal (vertical) plane. The scale is ±15 mm and ±15 mrad. Fractional intensities refer to the phase space element including the highest intensity. Center: Mean of horizontal and vertical normalized rms emittance behind the first DTL tank as a function of the transverse zero current phase advance.

Non-Uniform Beam Equilibrium

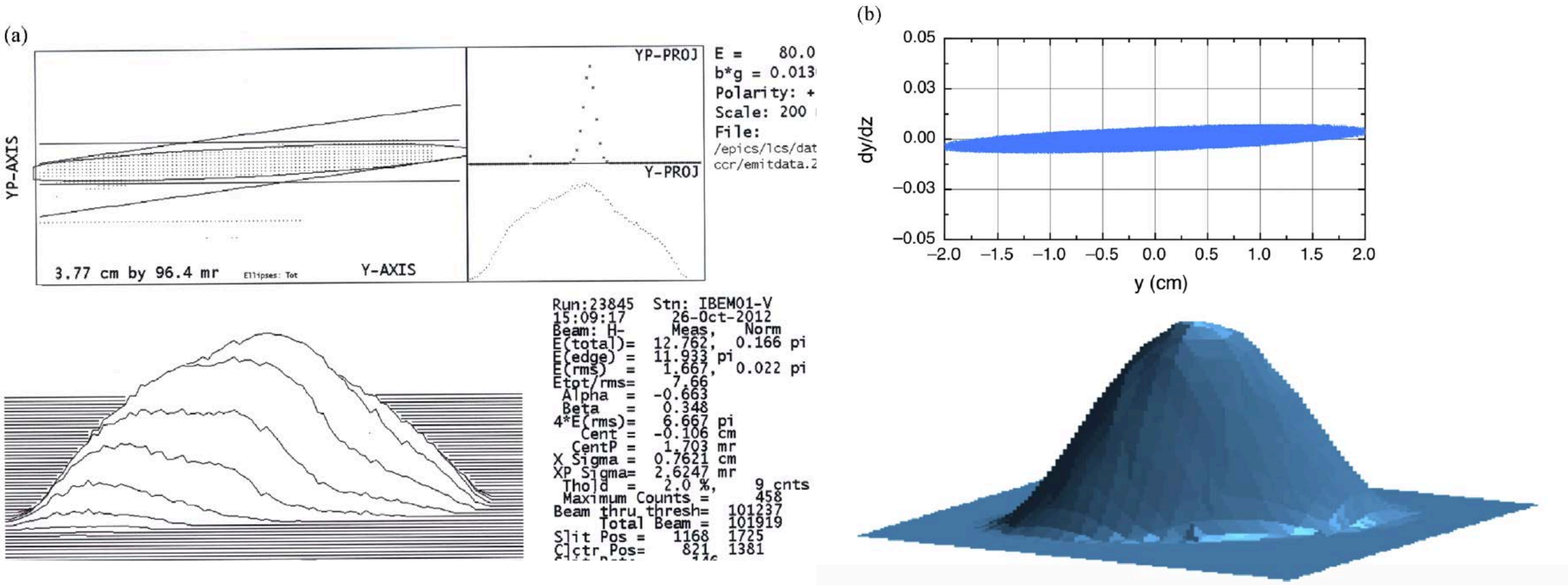

(a) Experimentally observed distribution of 80 keV H$^-$ beam, extracted from LANL ion source,

(b) modeling of the same beam with parabolic distribution function in 4D phase space:

$$\boxed{f = f_o\left(1 - \frac{x^2 + y^2}{2R_b^2} - \frac{p_x^2 + p_y^2}{2p_o^2}\right)}$$

Non-Uniform Beam Matching in Transport Channel

Beam is matched with continuous (z-independent) focusing channel, if beam distribution function *f* (x,p_x,y,p_y) is constant.

Self-consistent problem:

Vlasov's Equation

$$\frac{df}{dt} = \frac{\partial f}{\partial t} + \frac{\partial f}{\partial \vec{x}}\frac{d\vec{x}}{dt} + \frac{\partial f}{\partial \vec{P}}\frac{d\vec{P}}{dt} = 0$$

Poisson's Equation

$$\Delta U = -\frac{\rho}{\varepsilon_o}$$

Solution:

1.Express distribution function as a function of constant of motion (Hamiltonian) $f = f\,(H)$. Distribution function automatically obeys Vlasov's equation:

$$\frac{df}{dt} = \frac{\partial f}{\partial H}\frac{\partial H}{\partial t} = 0$$

2. Substitute distribution function into Poisson's equation and solve it.

Non-Uniform Beam Matching in Transport Channel (cont.)

Two formulations of the self-consistent beam matching problem:

1. The beam distribution function is known (for example, of the beam extracted from the source). The problem is to find focusing potential, which maintains this distribution in the channel:

$$f\,(x, p_x,\; y, p_y) \rightarrow U_{ext}\;(x,y)$$

2. Potential of the focusing structure is given. The problem is to find the beam distribution function, which is maintained in focusing structure:

$$U_{ext}\;(x,y) \rightarrow f\,(x, p_x,\; y, p_y)$$

More info:
Y.B. Phys. Rev. E Vol. 53, No. 5, 5358, 1996;
Y.B. Phys. Rev. E Vol. 57, No. 5, 6020, 1998

Equilibrium of a Gaussian Beam

Beam with Gaussian distribution function

$$f = f_o \exp\left(-2\frac{x^2+y^2}{R^2} - 2\frac{p_x^2+p_y^2}{p_o^2}\right)$$

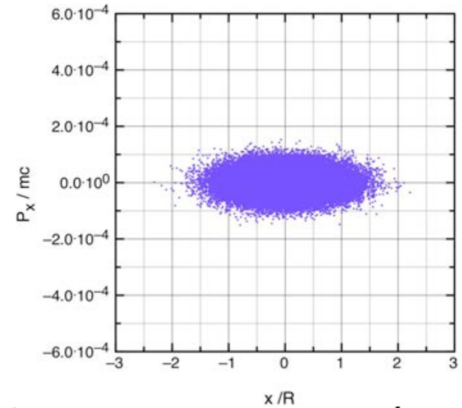

Time-independent Vlasov's equation

$$\frac{mc^2}{q}\frac{1}{\gamma}(x p_x + y p_y) = \frac{R^4}{\varepsilon^2}\left(p_x\frac{\partial U}{\partial x} + p_y\frac{\partial U}{\partial y}\right)$$

Total potential

$$U(x,y) = \frac{mc^2}{q}\frac{1}{\gamma}\frac{\varepsilon^2}{R^4}\left(\frac{x^2+y^2}{2}\right)$$

Total field

$$E_{tot} = -\frac{mc^2}{q}\frac{1}{\gamma}\frac{\varepsilon^2}{R^4}\, r$$

Space-charge field

$$E_b = -\frac{\partial U_b}{\partial r} = \frac{I}{2\pi\,\varepsilon_o\,\beta c}\frac{1}{r}\left[1 - \exp\left(-2\frac{r^2}{R^2}\right)\right]$$

Required focusing field

$$E_{ext} = -\frac{mc^2}{qR\gamma}\left[\frac{\varepsilon^2 r}{R^3} + 2\frac{I}{I_c\,\beta\gamma}\frac{R}{r}\left(1 - \exp\left(-2\frac{r^2}{R^2}\right)\right)\right]$$

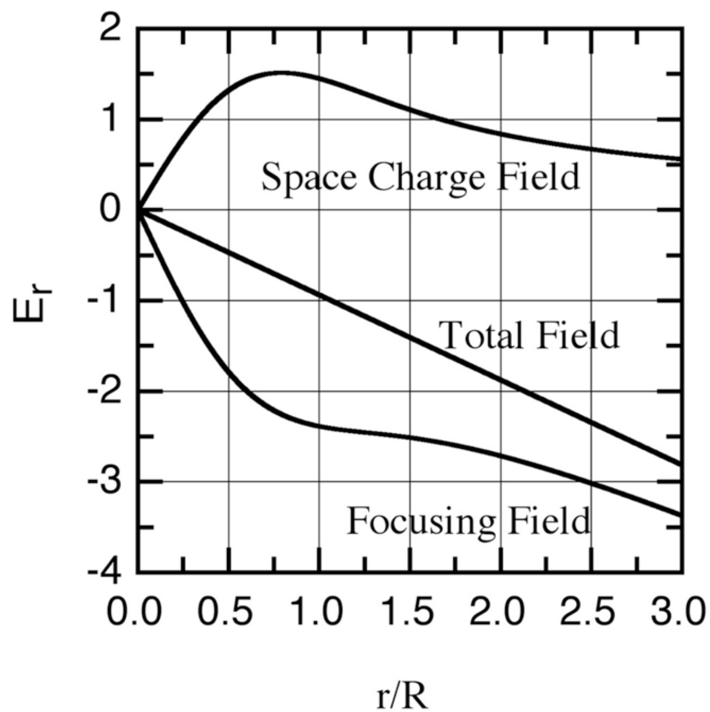

On Equilibrium of a Gaussian Beam

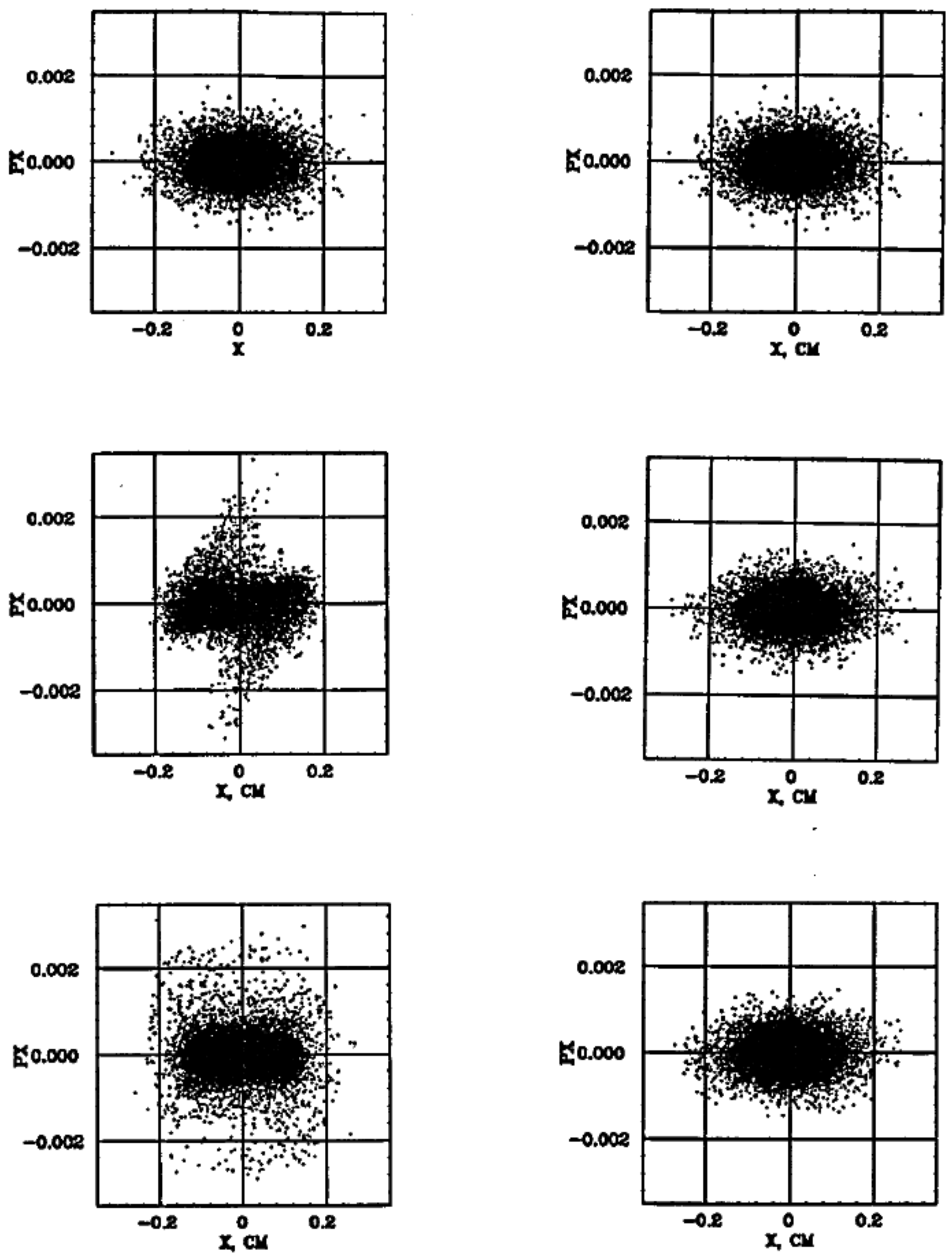

FIG. 7. Mismatching of the Gaussian beam in the linear focusing channel (left column) and matching of the same beam with the nonlinear focusing channel (right column).

Equilibrium of the Beam with "Water Bag" and Parabolic Distributions

WB distribution in phase space

$$f = f_0, \quad \frac{2}{3}\left(\frac{x^2+y^2}{R^2} + \frac{p_x^2+p_y^2}{p_0^2}\right) \leqslant 1,$$

$$f = 0, \quad \frac{2}{3}\left(\frac{x^2+y^2}{R^2} + \frac{p_x^2+p_y^2}{p_0^2}\right) > 1.$$

Parabolic distribution in phase space

$$f = f_0\left(1 - \frac{x^2+y^2}{2R^2} - \frac{p_x^2+p_y^2}{2p_0^2}\right)$$

Space charge density

$$\rho(r) = \frac{4I}{3\pi\beta c R^2}\left(1 - \frac{2r^2}{3R^2}\right)$$

Space charge density

$$\rho_b = \frac{3I}{2\pi c\beta R^2}\left(1 - \frac{r^2}{2R^2}\right)^2$$

Equilibrium of the Beam with "Water Bag" and Parabolic Distributions

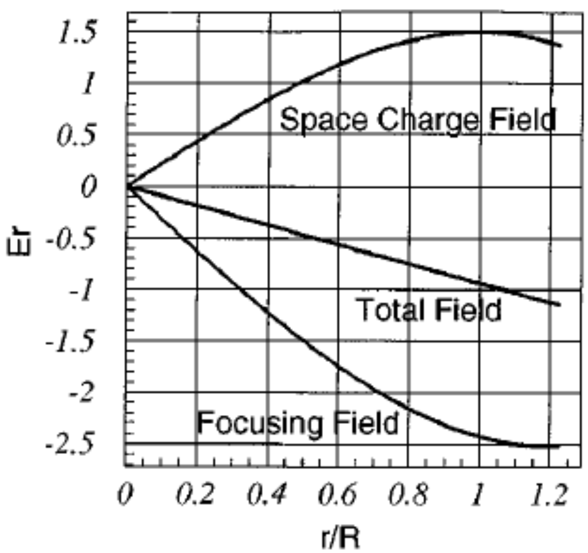

FIG. 4. Total field of the structure E_{tot} [Eq. (12)], required external focusing field E_{ext} [Eq. (21)] and space-charge field E_b [Eq. (20)] of the beam with ''water bag'' distribution.

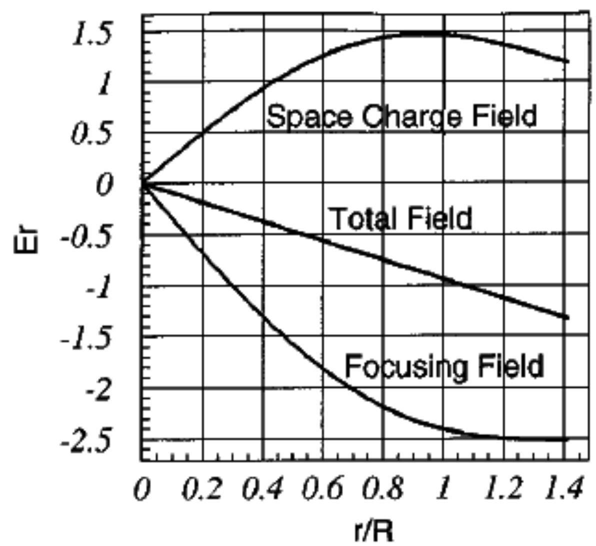

FIG. 5. Total field of the structure E_{tot} [Eq. (12)], required external focusing field E_{ext} [Eq. (25)] and space-charge field E_b [Eq. (24)] of the beam with parabolic distribution.

Focusing by Opposite Charged Particles (Plasma Lens)

Required potential distribution can be created by introducing inside the transport channel an opposite charged cloud of particles (plasma lens) with the space charge density:

$$\rho_{ext} = \rho_o \, exp(-2\frac{r^2}{R^2}) + \frac{I_c \, \varepsilon^2}{2\pi c \, R^4}$$

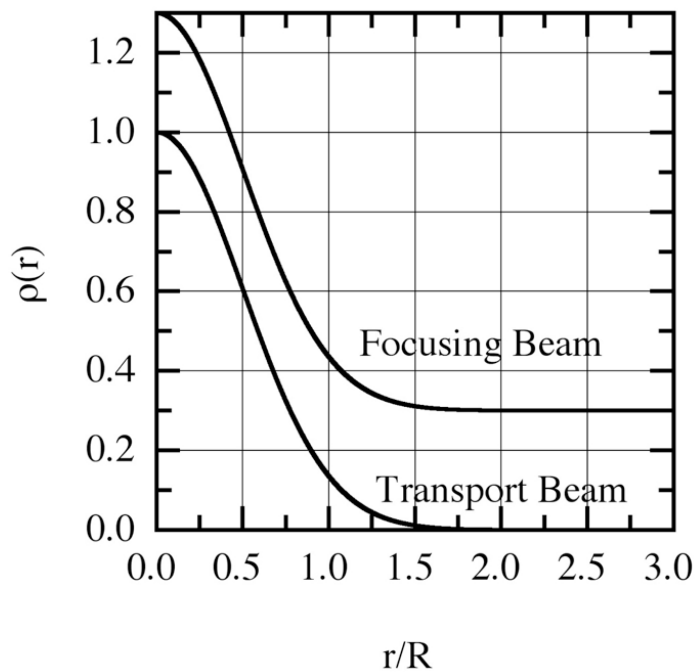

Charged particle density of the transported beam with Gaussian distribution, and of the external focusing beam

Quadrupole-Duodecapole Focusing Structure

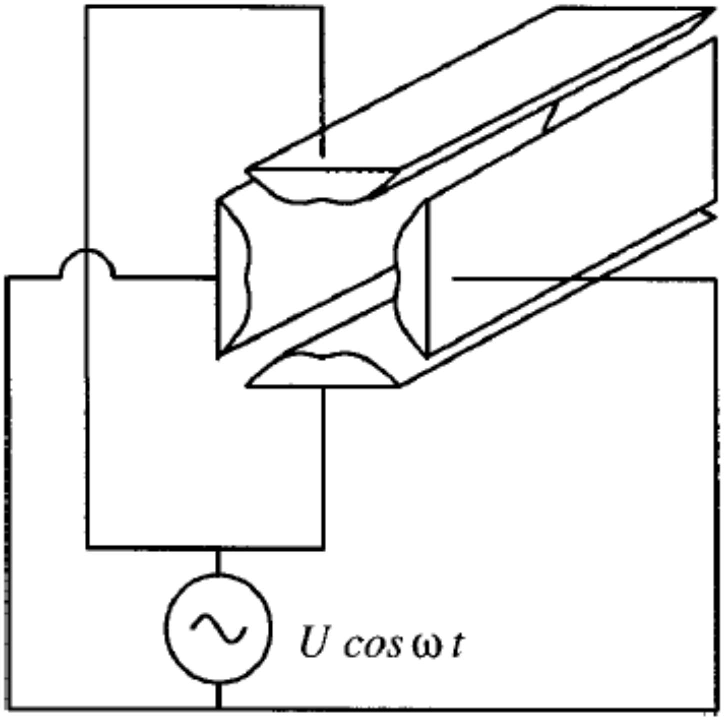

FIG. 6. Proposed four vane quadrupole structure with a duodecapole field component [5].

Potential of the uniform four vanes structure:

$$U(r,\varphi,t)=\left(\frac{G_2}{2}r^2\cos 2\varphi+\frac{G_6}{6}r^6\cos 6\varphi\right)\sin\omega_0 t,$$

The electrical field of the structure is given by

$$\vec{E}(r,\varphi,t)=[-\vec{i}_r(G_2 r\cos 2\varphi+G_6 r^5\cos 6\varphi)$$

$$+\vec{i}_\varphi(G_2 r\sin 2\varphi+G_6 r^5\sin 6\varphi)]\sin\omega_0 t.$$

Effective Potential of Quadrupole-Duodecapole Focusing Structure

an effective scalar potential of the structure [6]

$$U_{\text{ext}}(\vec{r}) = \frac{q}{4m\gamma}\frac{E_0^2(\vec{r})}{\omega_0^2}, \tag{6.3}$$

which describes the averaged motion of particle. For the considered structure, the effective potential is

$$U_{\text{ext}}(r,\varphi) = \frac{mc^2}{q}\frac{\mu_0^2}{\lambda^2}\left[\frac{1}{2}r^2 + \zeta r^6 \cos 4\varphi + \frac{\zeta^2}{2}r^{10}\right], \tag{6.4}$$

where μ_0 is a smooth transverse oscillation frequency and ζ is a ratio of field components:

$$\mu_0 = \frac{qG_2\lambda^2}{\sqrt{8}\pi mc^2\sqrt{\gamma}}, \quad \zeta = \frac{G_6}{G_2}. \tag{6.5}$$

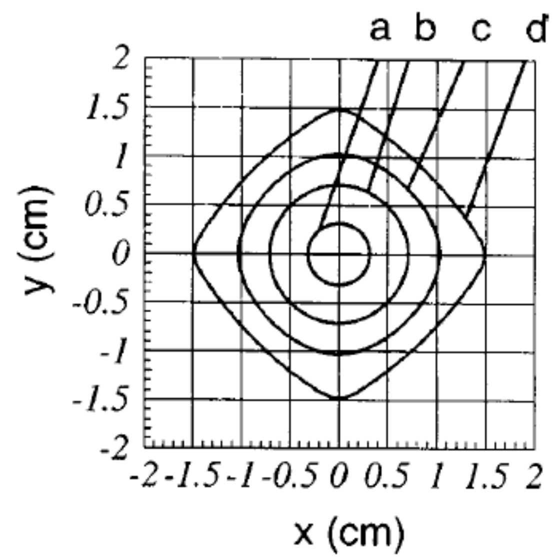

FIG. 7. Lines of equal values of the function $C = \frac{1}{2}r^2 + \zeta r^6 \cos 4\varphi + (\zeta^2/2)r^{10}$ for $\zeta = -0.03$: (a) $C = 0.05$, (b) $C = 0.25$, (c) $C = 0.5$, and (d) $C = 0.85$.

Space-Charge Density of the Matched Beam

The space charge distribution of a matched beam can be derived from Poisson's equation via a known space charge potential of the beam

$$\rho_b = -\epsilon_0 \Delta U_b = \frac{\epsilon_0}{1+\delta} \gamma^2 \Delta U_{\text{ext}} . \qquad (4.26)$$

Application of Eq. (4.26) gives an expression for the self-consistent space charge distribution of the beam in the structure:

$$\rho_b = \rho_0 (1 + 10 \zeta r^4 \cos 4\varphi + 25 \zeta^2 r^8), \qquad (6.6)$$

$$\rho_0 = \frac{2\gamma^2}{(1+\delta)} \frac{mc^2}{q} \frac{\epsilon_0 \mu_0^2}{\lambda^2} . \qquad (6.7)$$

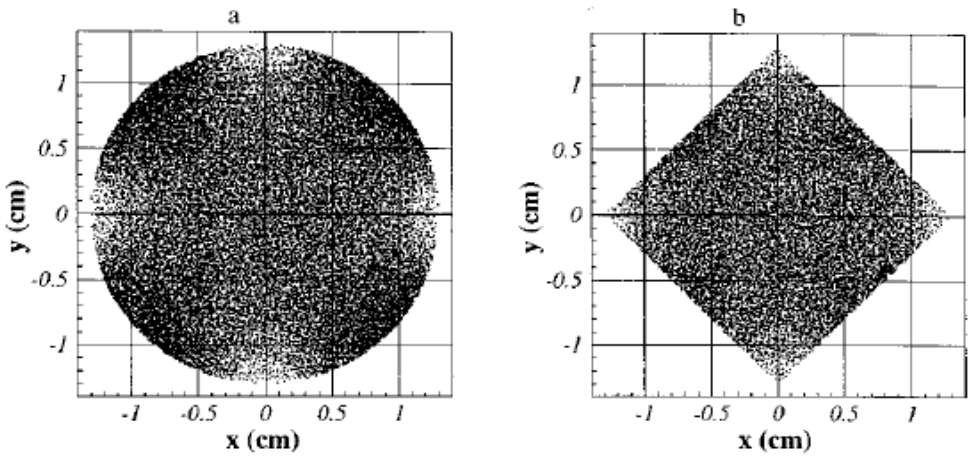

FIG. 8. Self-consistent particle distribution $\rho_b = \rho_0 (1 + 10 \zeta r^4 \cos 4\varphi + 25 \zeta^2 r^8)$ of the matched beam in a quadrupole channel with a duodecapole component with parameter $\zeta = -0.03$: (a) without truncation, (b) with truncation.

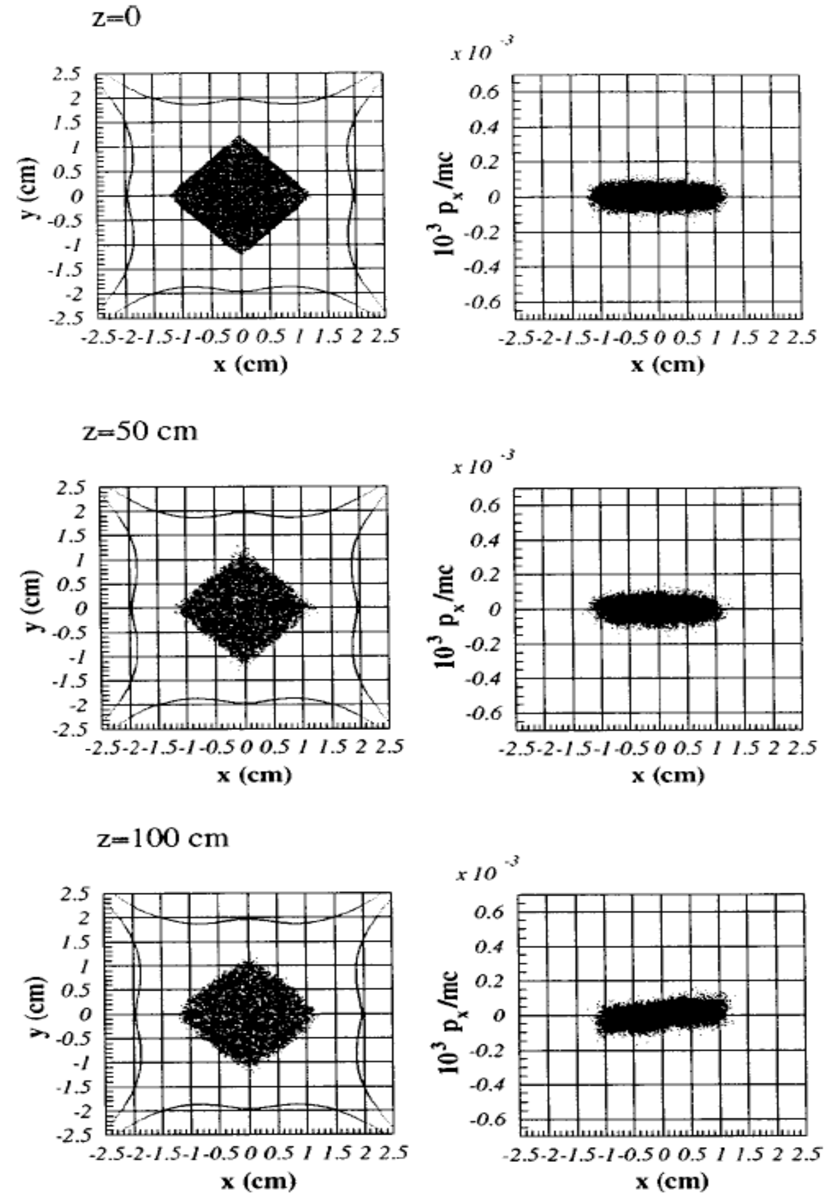

FIG. 9. Emittance conservation of the 150 keV, 100 mA, 0.06π cm mrad proton beam with a matched distribution function (6.14) in a four vane quadrupole structure with field gradient $G_2 = 48$ kV/cm^2 and duodecapole component $G_6 = -1.3$ kV/cm^6.

FODO Quadrupole - Duodecapole Channel for Suppression of Halo Formation

Effective potential of quadrupole-duodecapole structure:

$$U_{eff} = (\frac{\mu_o \beta c}{L})^2 [\frac{r^2}{2} + \varsigma r^6 \cos 4\theta + \varsigma^2 \frac{r^{10}}{2}]$$

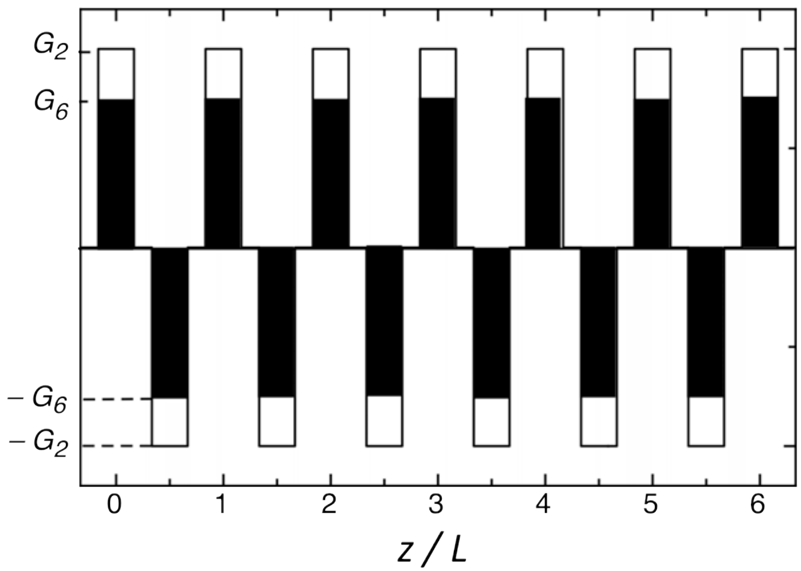

Ratio of field components $\varsigma = \frac{G_6}{G_2}$

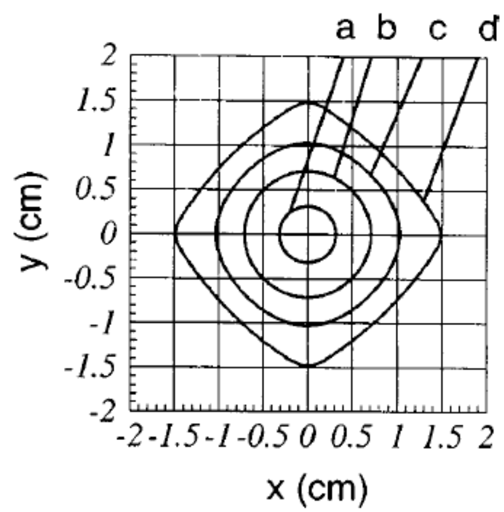

FODO channel with combined quadrupole $G_2(z)$ and duodecapole $G_6(z)$ field components

FIG. 7. Lines of equal values of the function $C=\frac{1}{2}r^2+\zeta r^6 \cos 4\varphi+(\zeta^2/2)r^{10}$ for $\zeta=-0.03$: (a) $C=0.05$, (b) $C=0.25$, (c) $C=0.5$, and (d) $C=0.85$.

(Y.B. et al NIM-A 816, 2016, p.78–86)

FODO Quadrupole - Duodecapole Channel for Suppression of Halo Formation

Quadrupole Channel

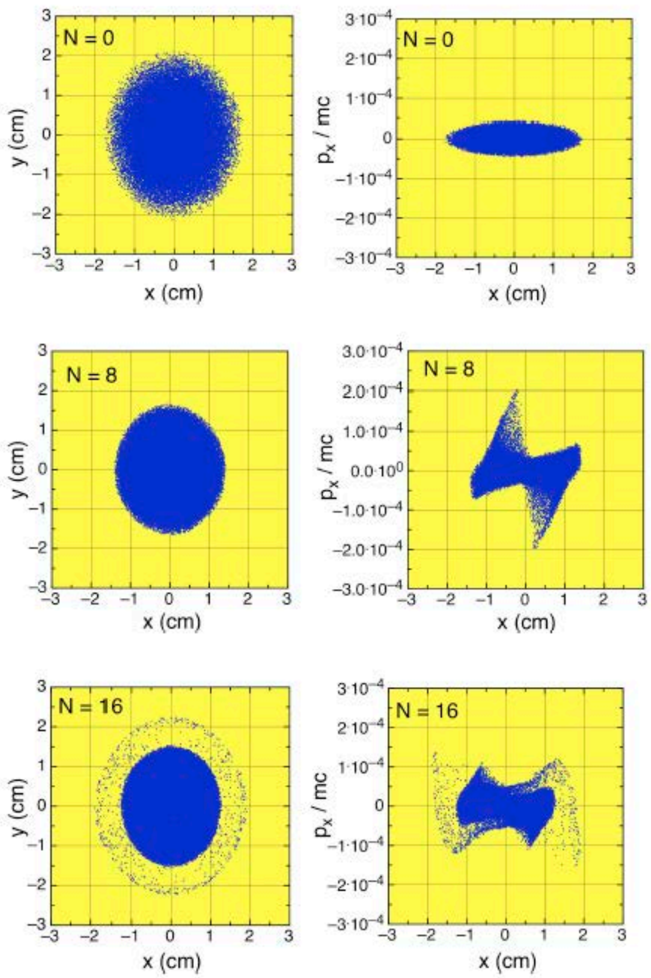

Quadruple-Duodecapole Channel

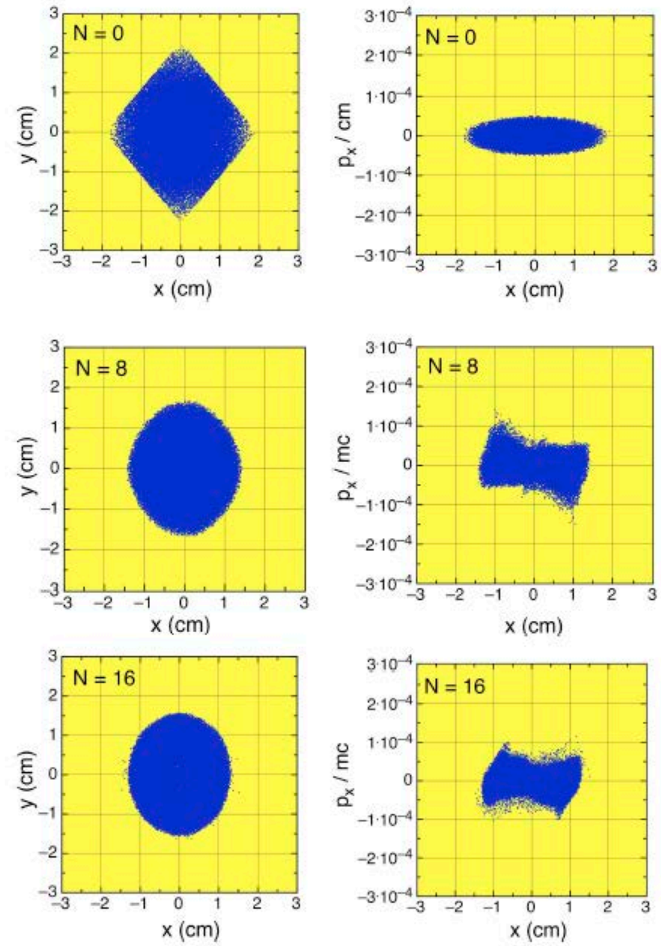

Beam energy	**35 keV**
Beam current	**11.7 mA**
Beam emittance	**0.05 cm mrad**
FODO period	**15 cm**
Lens length	**5 cm**

Quadrupole field gradient 0.03579 T/cm

Quadrupole field gradient 0.03579 T/cm
Duodecapole component G_6 = -1.76e-04 T/cm^5 adiabatically decline to zero at the distance of 7 periods. Numbers indicate FODO periods.

Suppression of Space Charge Induced Beam Halo Formation

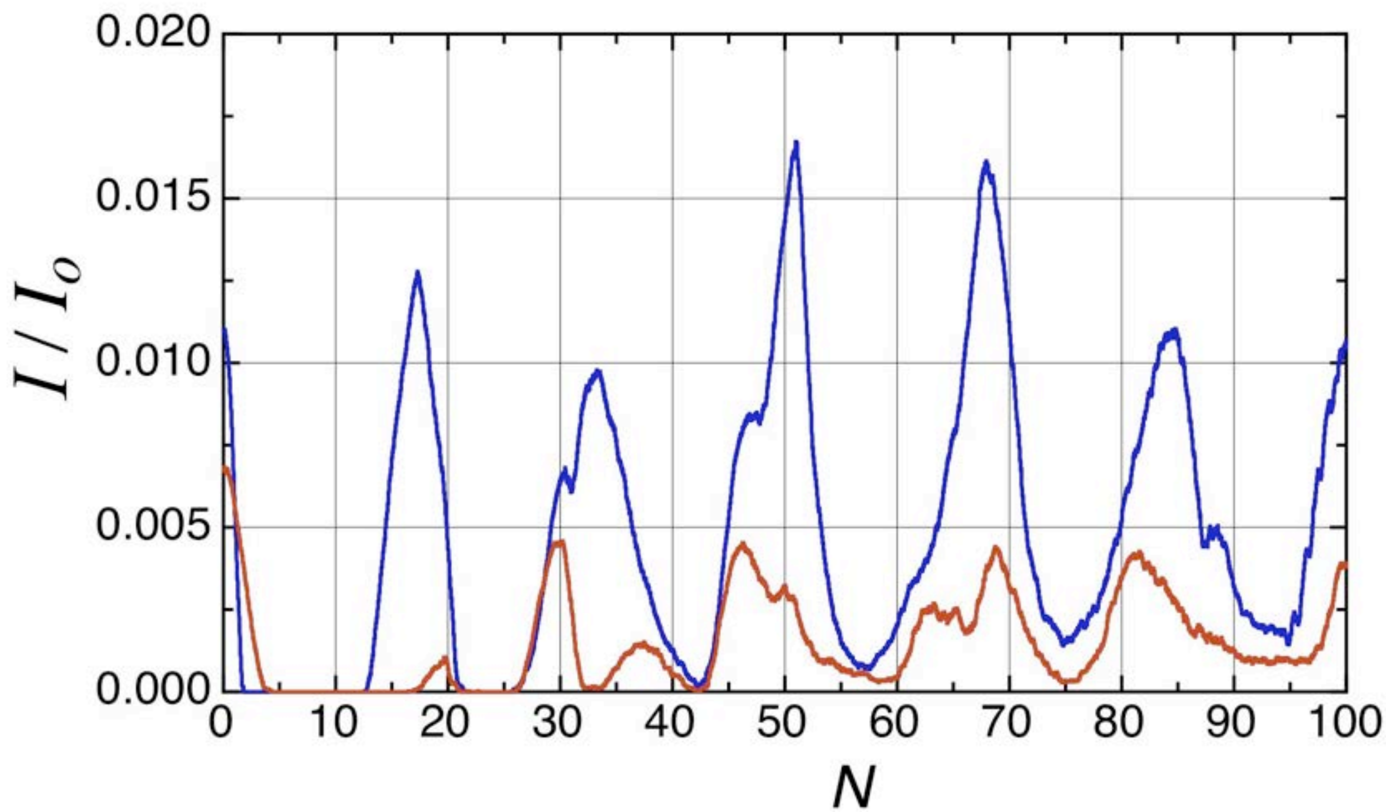

Fraction of particles outside the beam core $2.5\sqrt{<x^2>}$ x $2.5\sqrt{<y^2>}$ as a function of FODO periods: (blue) quadrupole channel, (red) quadrupole-duodecapole channel.

Particle Studio Simulation of Halo Formation in Quadrupole Channel

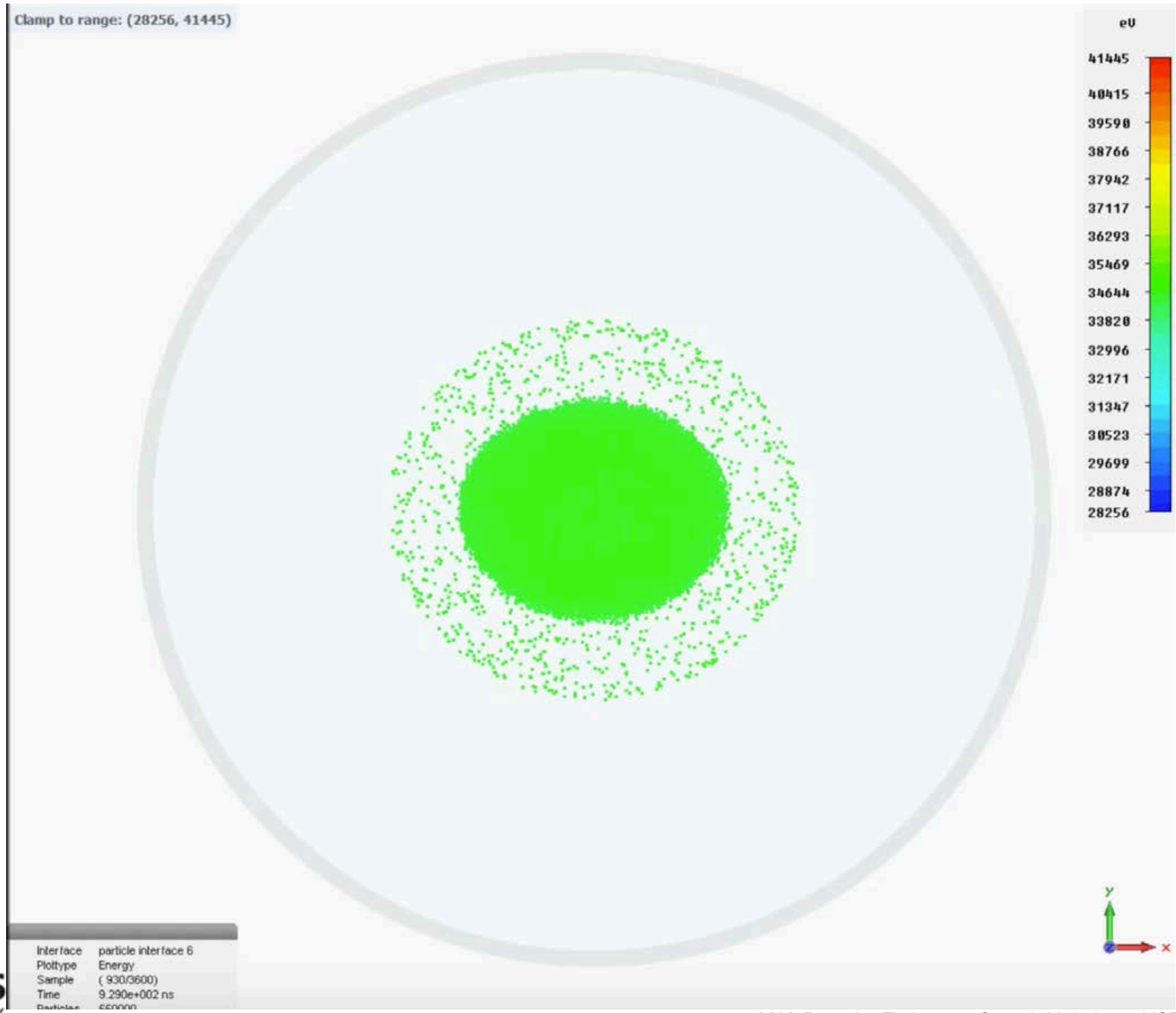

Particle Studio Simulation of Halo Suppression in Quadrupole-Duodecapole Channel

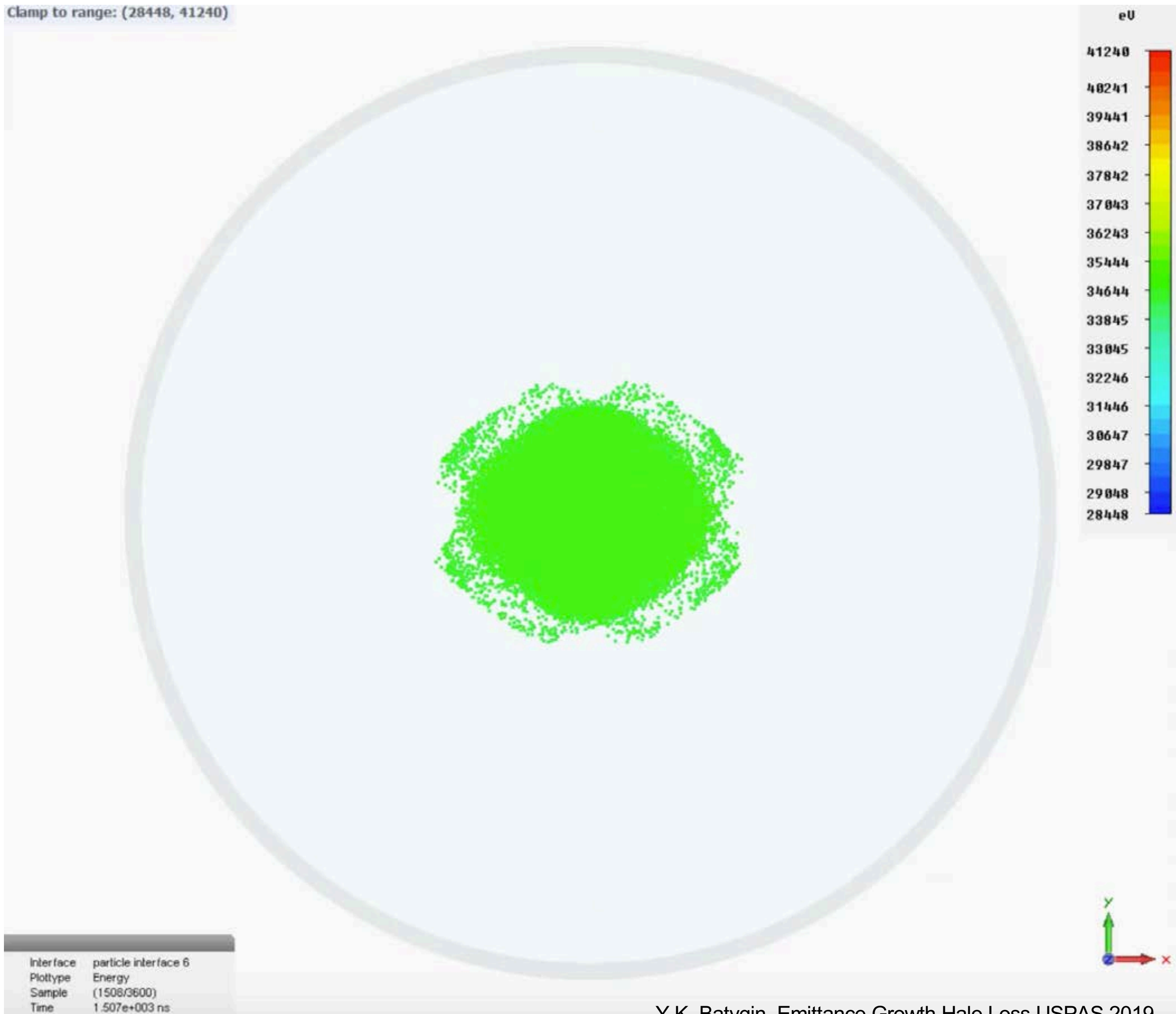

Final Particle Distributions in Focusing Channels

Quadrupole Channel

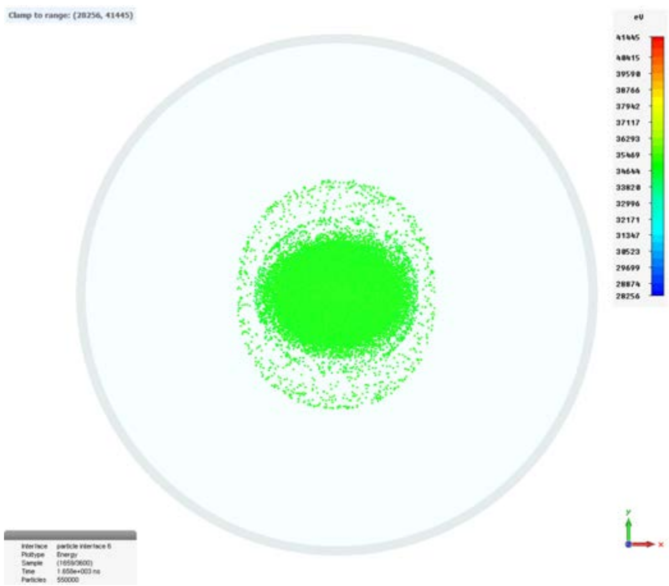

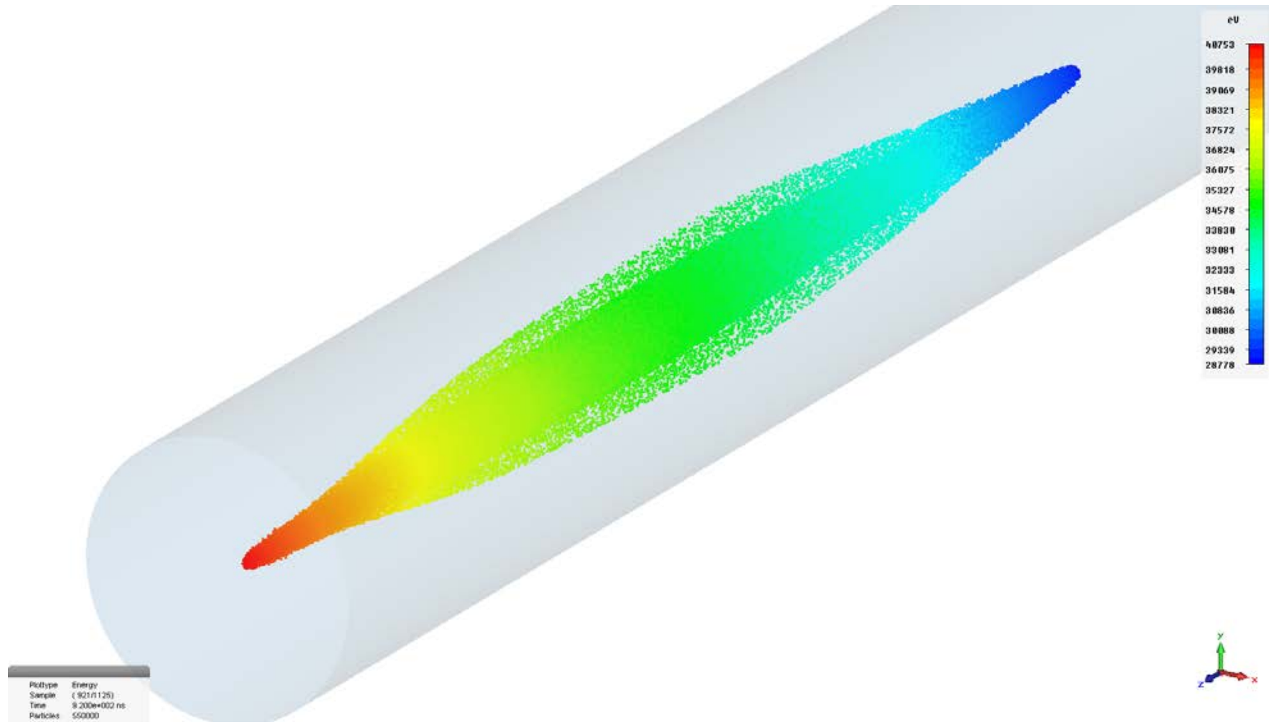

Quadruple-Duodecapole Channel

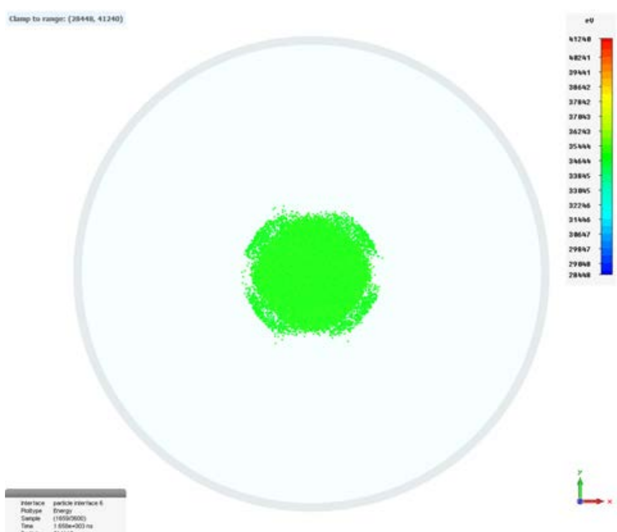

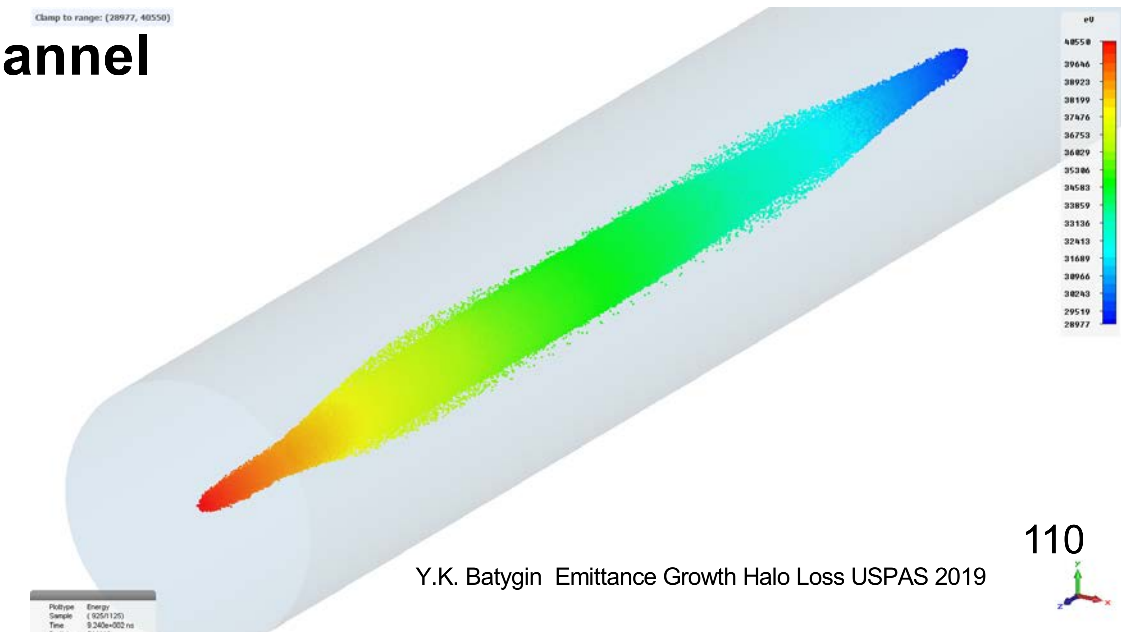

High-Power Accelerators

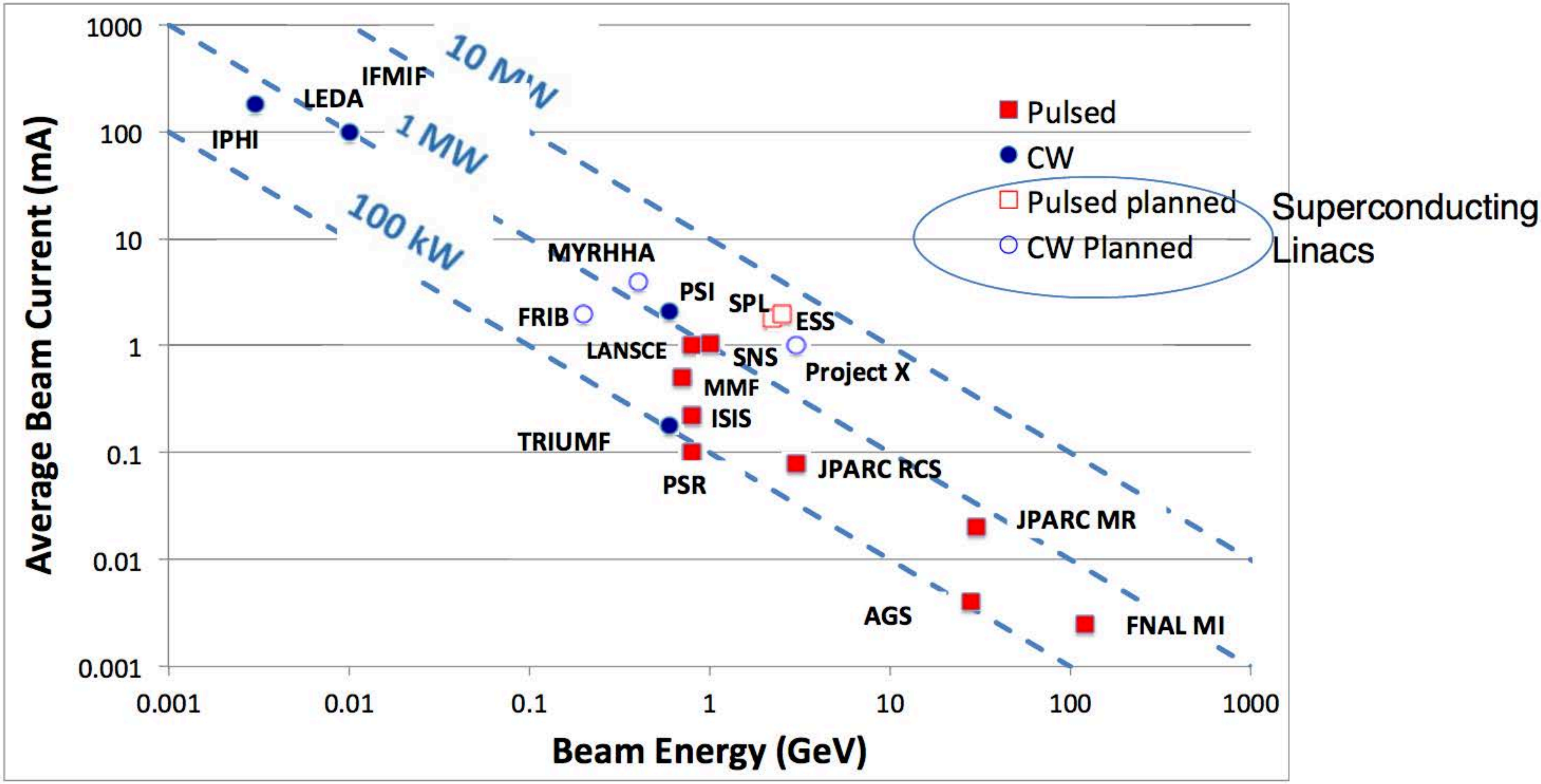

High-Power Accelerators (cont.)

Table 4. Overview of existing and planned superconducting proton linacs.

Machine	SC cavity types	f_{RF} of SC cavities (MHz)	Cavity geometric β	Energy (GeV)	P_{beam} (MW)	f_{rep} (Hz)	I_{pulse} (mA)	Application
SNS	Elliptical	805	0.61/0.81	1	1.4	60	$26^{\dagger}$	Neutron production
*Project X	HWR, spoke, ell.	162.5/325/650/1300	0.094/0.19/0.43/0.61/0.9/1.0	1/3/8	1/3/0.4	CW	1–5	Neutrino driver
*ESS	Spoke, ell.	352/707	0.5/0.65/0.86	2	5	14	61	Neutron production
*EURISOL	HWR, spoke, ell.	176/352/704	0.09/0.15/0.3/0.47/0.65/0.78	1–2	5	CW	6	RIB
*Myrrha	Spoke, ell.	352/704	0.35/0.47/0.65	0.6	2.4	CW	4	ADS
*HP-SPL	Ell.	704	0.65/1.0	5	4	50	$40^{\dagger}$	Neutrino driver
*LP-SPL	Ell.	704	0.65/1.0	4	0.14	2	$20^{\dagger}$	LHC injector
*India ADS	Spoke/ell.	325/650	t.b.c./0.61/t.b.c.	1	30	CW	30	ADS
*China ADS	HWR/ spoke/ell.	162.5/325/650	0.12/0.21/0.4/0.63/0.82	1.5	15	CW	10	ADS

(P.Ostroumov, F. Gerigk, Reviews of Accelerator Science and Technology, 2013)

The LANSCE Accelerator Provides Unique Flexible Time-Structured Beams From 100 to 800 MeV

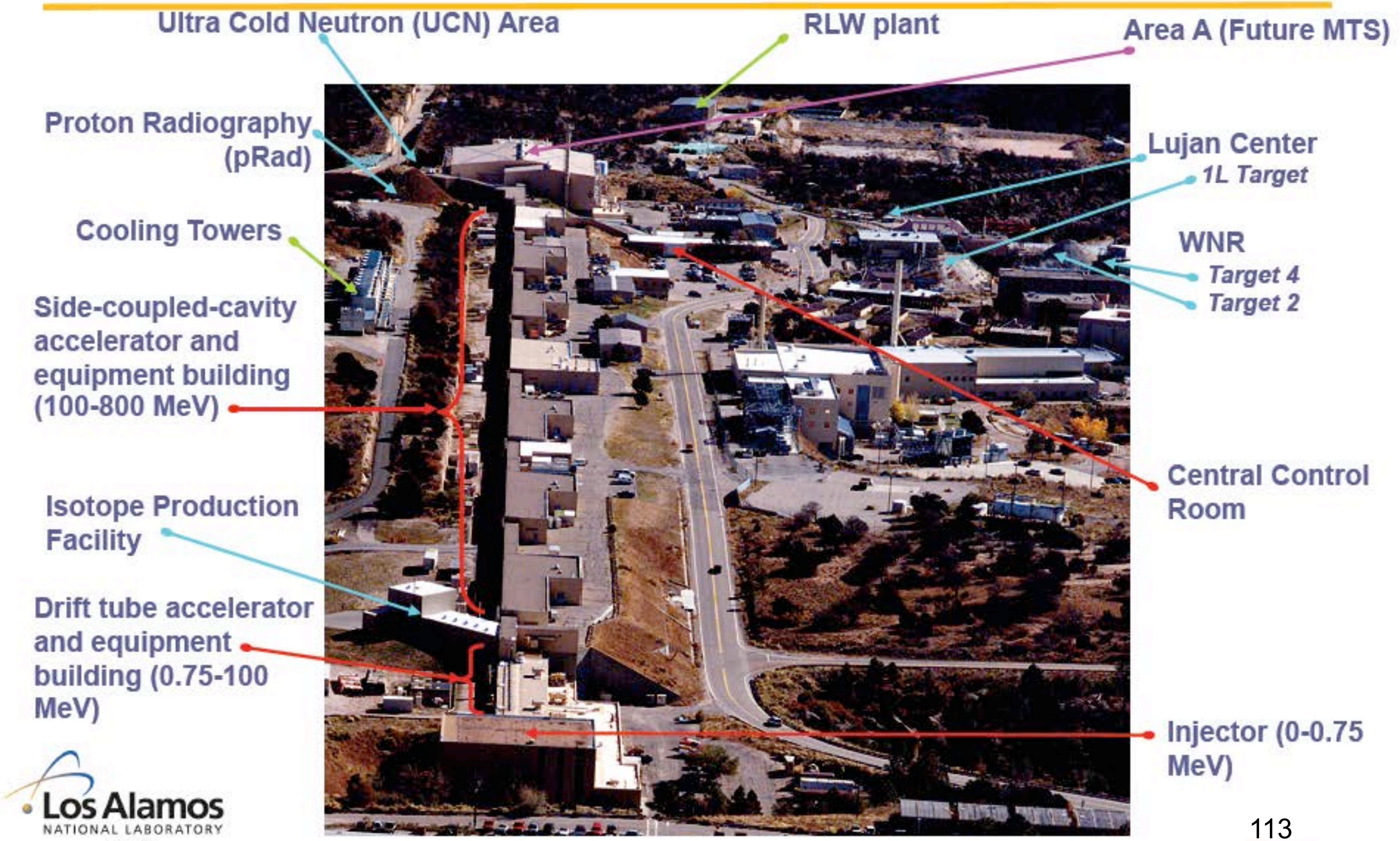

LANSCE Facility Overview

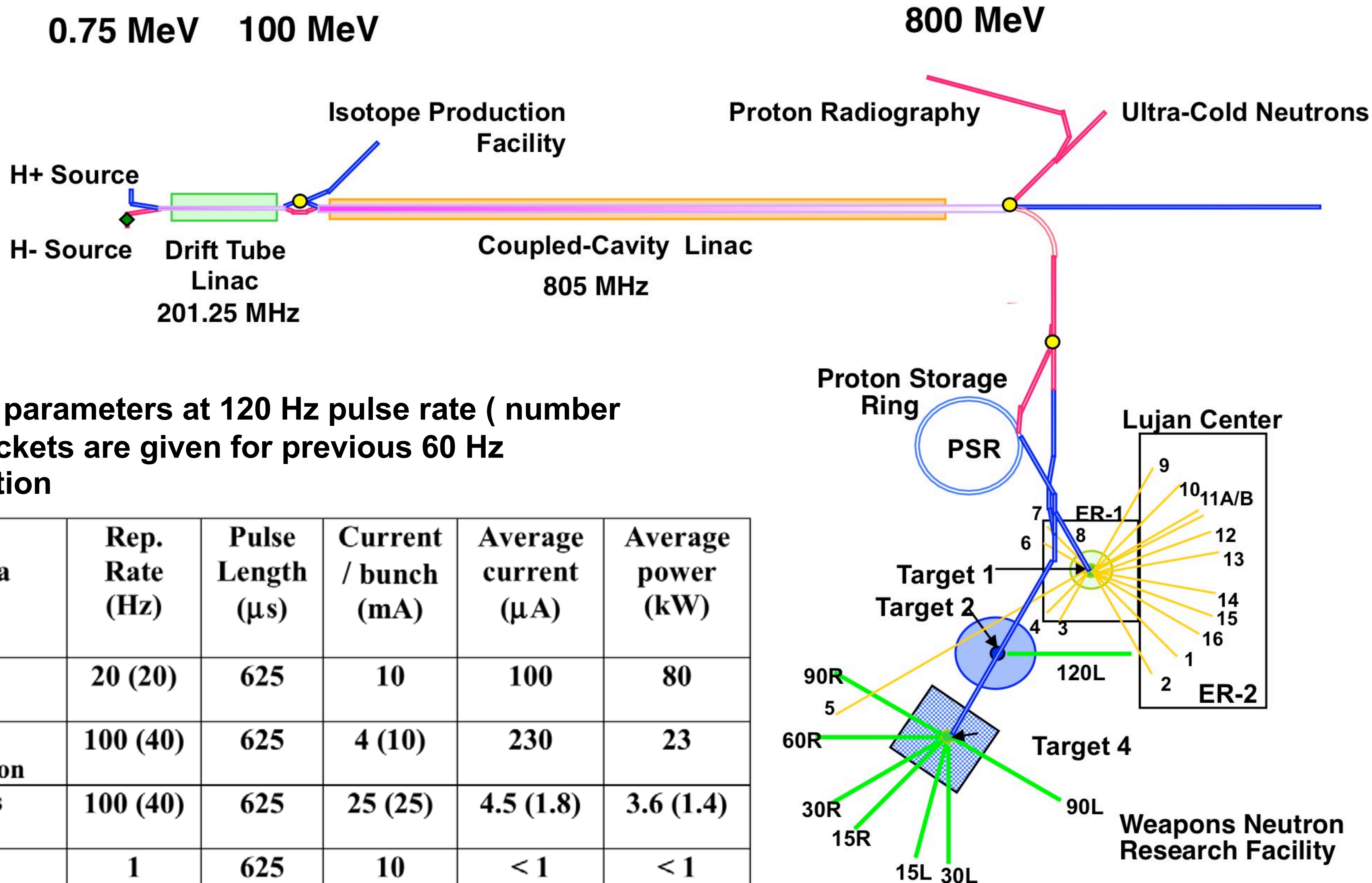

Beam parameters at 120 Hz pulse rate (number in brackets are given for previous 60 Hz operation

Area	Rep. Rate (Hz)	Pulse Length (μs)	Current / bunch (mA)	Average current (μA)	Average power (kW)
Lujan Center	20 (20)	625	10	100	80
Isotope Production	100 (40)	625	4 (10)	230	23
Weapons Neutron	100 (40)	625	25 (25)	4.5 (1.8)	3.6 (1.4)
Proton Radiography	1	625	10	< 1	< 1
Ultra-Cold Neutrons	20 (20)	625	10	10	8

LANSCE Accelerating Structures

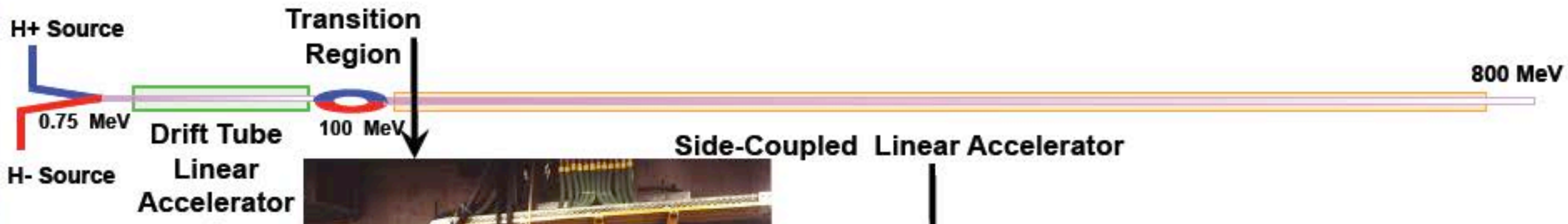

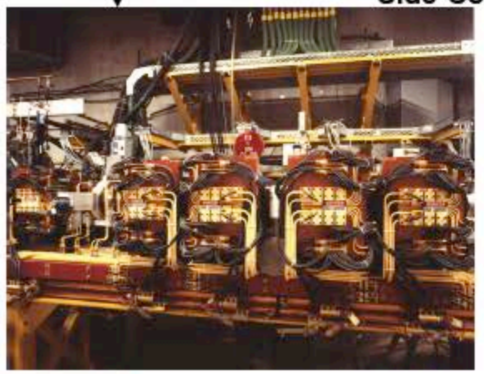

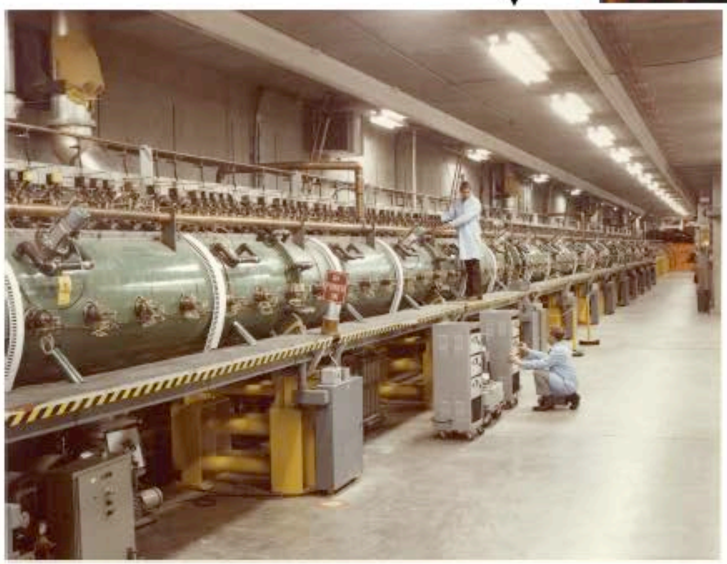

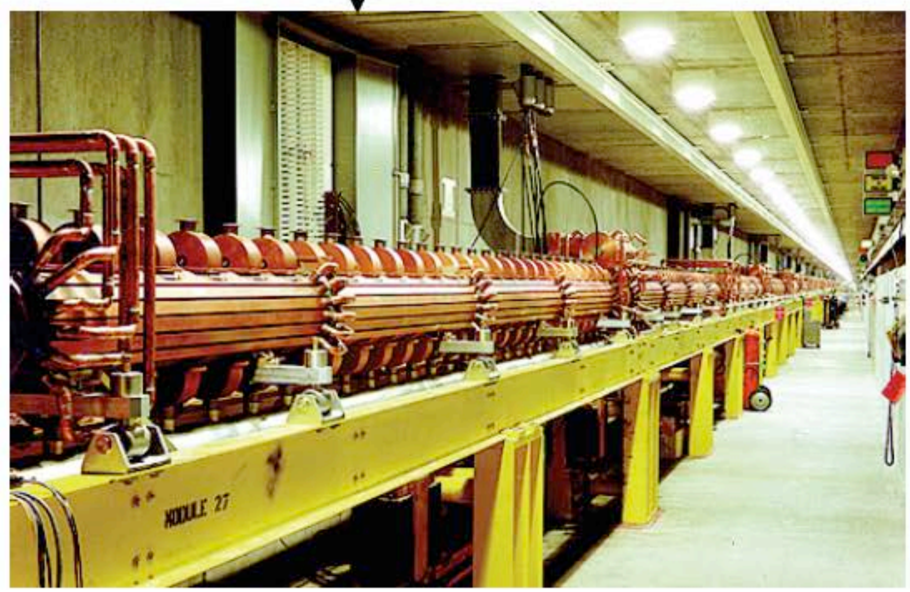

J-PARC Accelerator Facility

The J-PARC accelerator consists of a 400-MeV injector linac, a 3-GeV Rapid Cycling Synchrotron (RCS) and a 50-GeV main ring synchrotron. A high intensity proton beam is delivered to the materials and life science facility, the hadron experimental hall and the neutrino beam line.

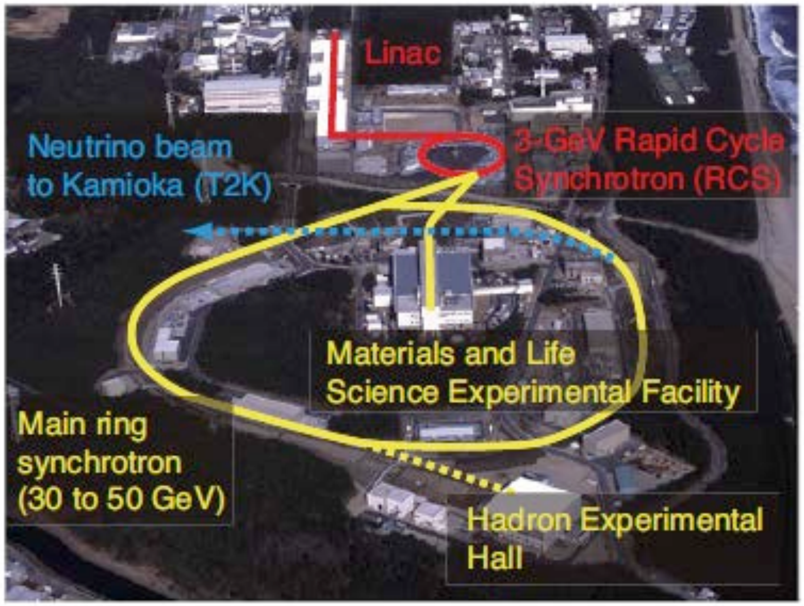

Figure 1: Bird's eye view of the J-PARC.

The 400-MeV energy upgrade of the J-PARC linac started from March 2009. The linac beam energy is at present 181 MeV, limiting the beam power of the 3-GeV Rapid-Cycling Synchrotron (RCS) to 600 kW at most by the space-charge effect. The 400-MeV injection is therefore vital for its 1-MW operation. This energy upgrade requires 25 modules of Annular-ring Coupled Structure (ACS) in total, 25 high-power RF sources, low-level RF

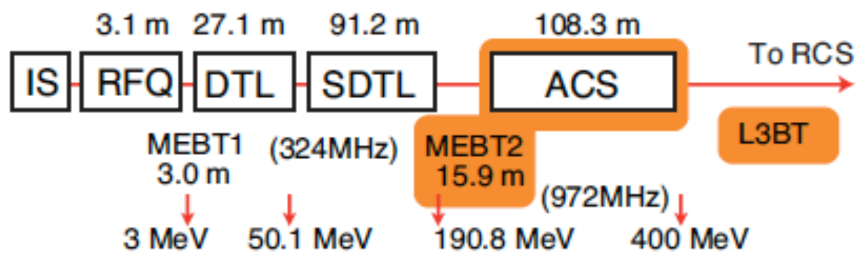

Figure 2: Schematic configuration of the linac.

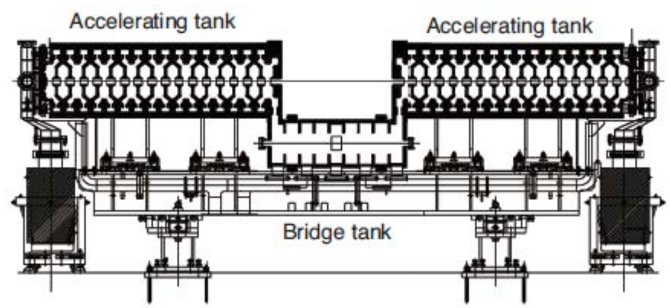

Figure 3: Layout of an ACS accelerating module. Two ACS tanks are coupled by one bridge tank.

European Spallation Source

Table 1: ESS Accelerator Main Parameters

Average beam Power	5 MW
Peak beam power	125 MW
Pulse Length	2.86 ms
Peak beam current	62.5 mA
Repetition rate	14 Hz
Duty cycle	4%

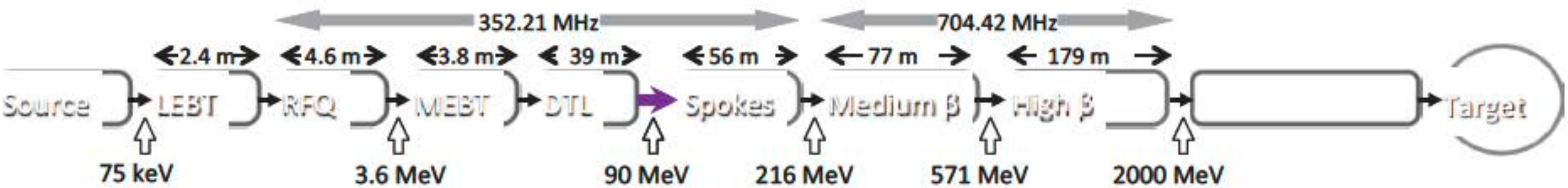

Figure 2: A block diagram of the ESS accelerator.

Linac 4 at CERN

Table 1: Main Linac4 design parameters

Output Energy	160	MeV
Bunch Frequency	352.2	MHz
Repetition Frequency	1.1 (max. 2)	Hz
Beam Pulse Length	0.4 (max. 1.2)	ms
Beam Duty Cycle	0.08	%
Chopper Beam-on Rate	62	%
Linac pulse current	40	mA
N. of particles per pulse	1.0	$\times 10^{14}$
Transverse emittance	0.4	π mm mrad
Maximum RF duty cycle	10	%

As the first step of a long-term programme aiming at an increase in the LHC luminosity, CERN is building a new 160 MeV H^- linear accelerator, Linac4, to replace the ageing 50 MeV Linac2 as injector to the PS Booster (PSB). Linac4 is an 86-m long normal-conducting linac made of an H^- source, a Radio Frequency Quadrupole (RFQ), a chopping line and a sequence of three accelerating structures: a Drift-Tube Linac (DTL), a Cell-Coupled DTL (CCDTL) and a Pi-Mode Structure (PIMS).

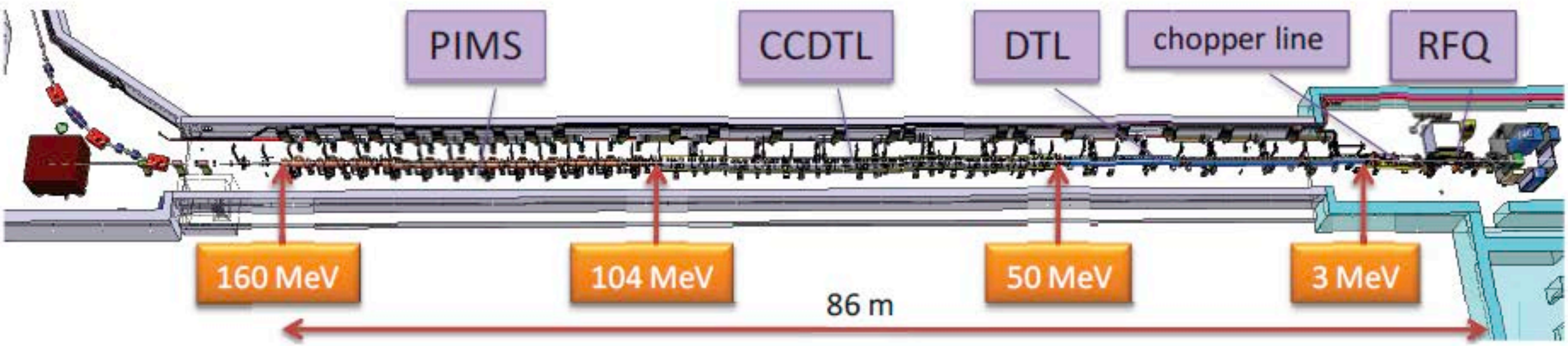

Figure 1: Linac4 layout.

Side-Coupled DTL and Pi-Mode Structure (PIMS)

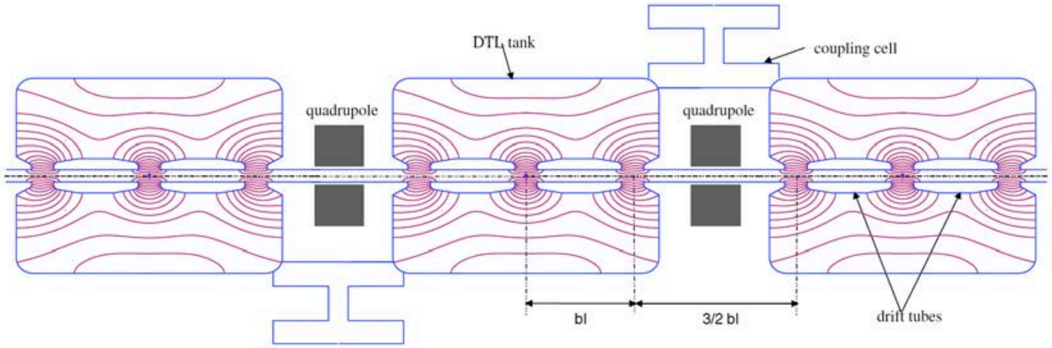

Figure 2.27: Scheme of a CCDTL module showing electric field lines

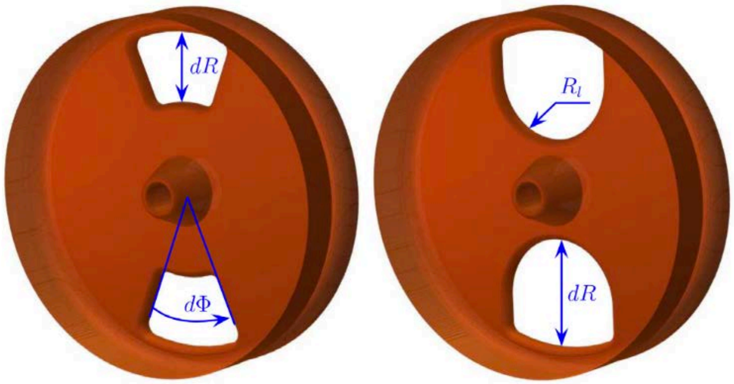

Figure 2: Different coupling slot shapes: left: standard shape, right: modified shape.

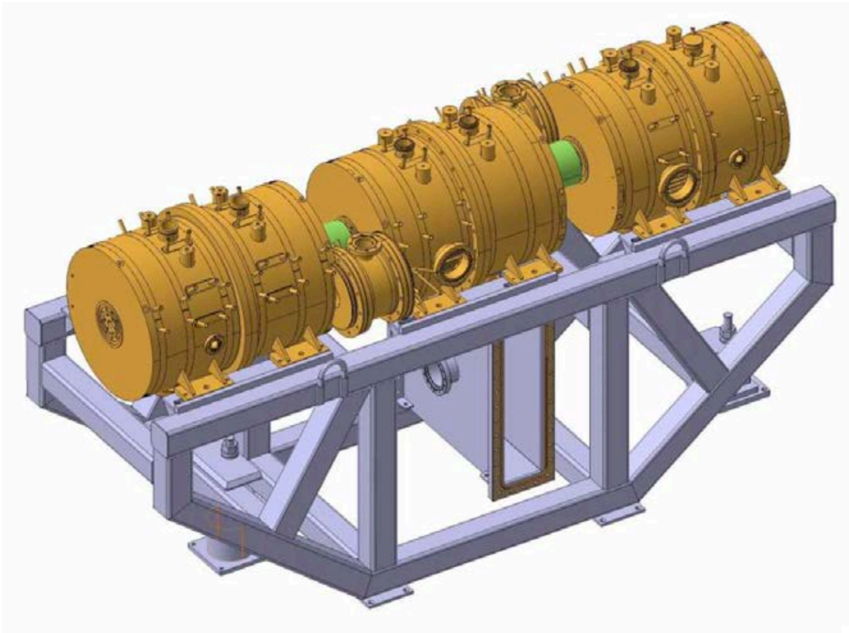

Figure 2.29: 3D view of a CCDTL module with support and waveguide coupler

Figure 8: First module of the Linac4 RFQ after brazing.

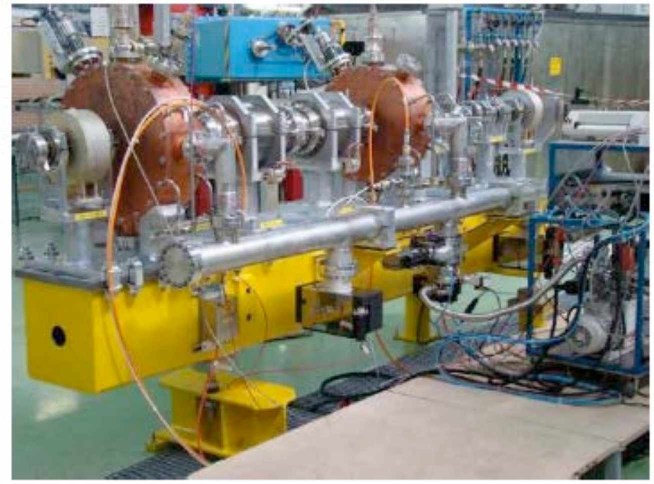

Figure 9: The Linac4 chopper line.

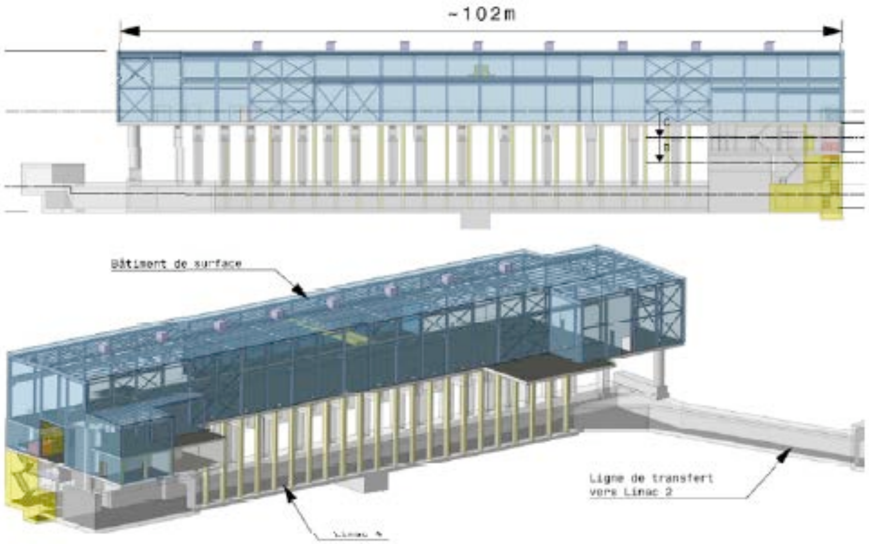

Figure 4: Side and 3D view of tunnel and surface building.

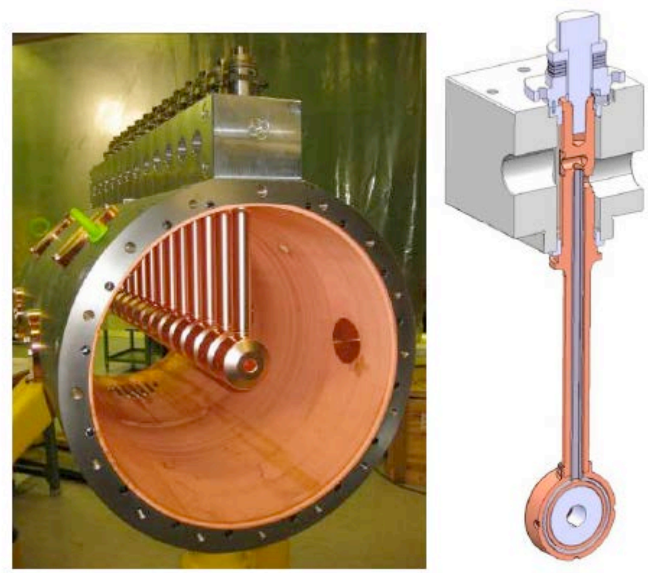

Figure 11: DTL prototype and drift tube assembly.

CHINA SPALLATION NEUTRON SOURCE

Table1: CSNS Design Parameters

Project Phase	**I**	**II**
Beam Power on target [kW]	100	500
Proton energy t [GeV]	1.6	1.6
Average beam current [μ A]	62.5	312.5
Pulse repetition rate [Hz]	25	25

The accelerator complex of China Spallation Neutron Source (CSNS) mainly consists of an H- linac of 80 MeV and a rapid-cycling synchrotron of 1.6 GeV. It operates at 25 Hz repetition rate with an initial proton beam power of 100 kW and is upgradeable to 500kW. The project will start construction in September 2011 with a construction period of 6.5 years. The CSNS accelerator is the first

The approved budget from the central government is increased to \$ 260 M from \$ 215 M in 2010. The local government will support additional \$ 77 M, free land and some infrastructure. CSNS will be located at Dong Guan

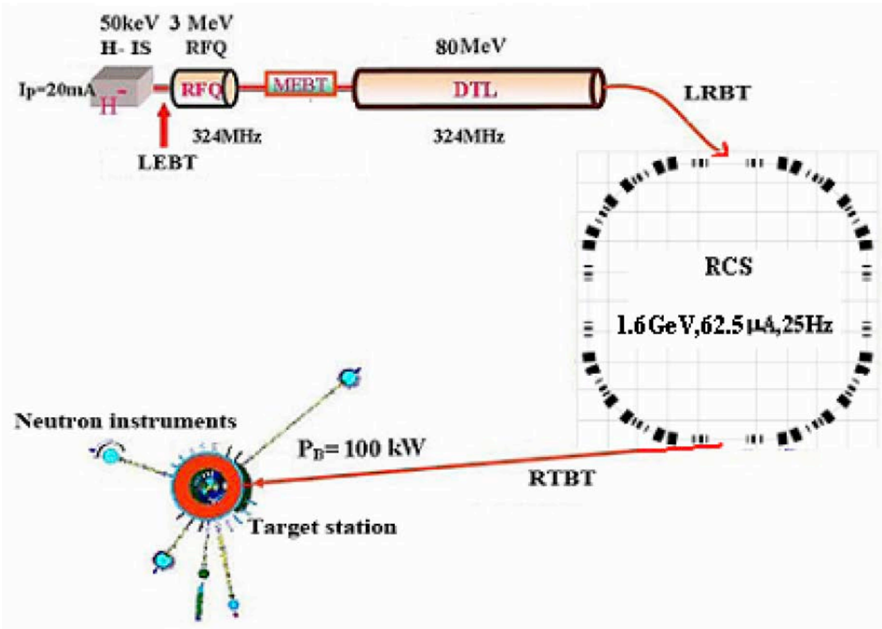

Figure 1: Schematics of the CSNS complex.

COMMISSIONING OF CSNS ACCELERATORS

Figure 8: DTL-1 installed in the tunnel.

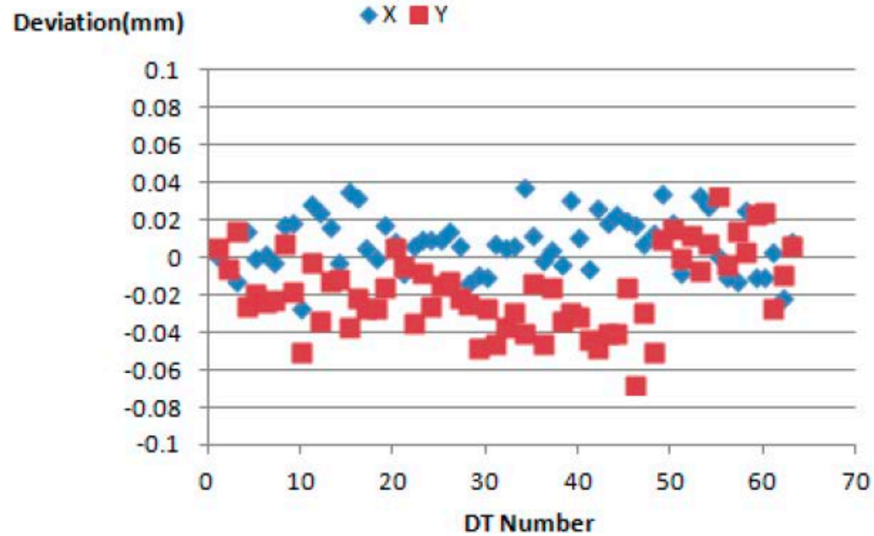

Figure 6: Alignment error of DTL-1 drift tubes.

Figure 10: The dipoles and quadrupoles installed in the tunnel.

CHINA-ADS FACILITY

Schematic figure of ADS driver linac

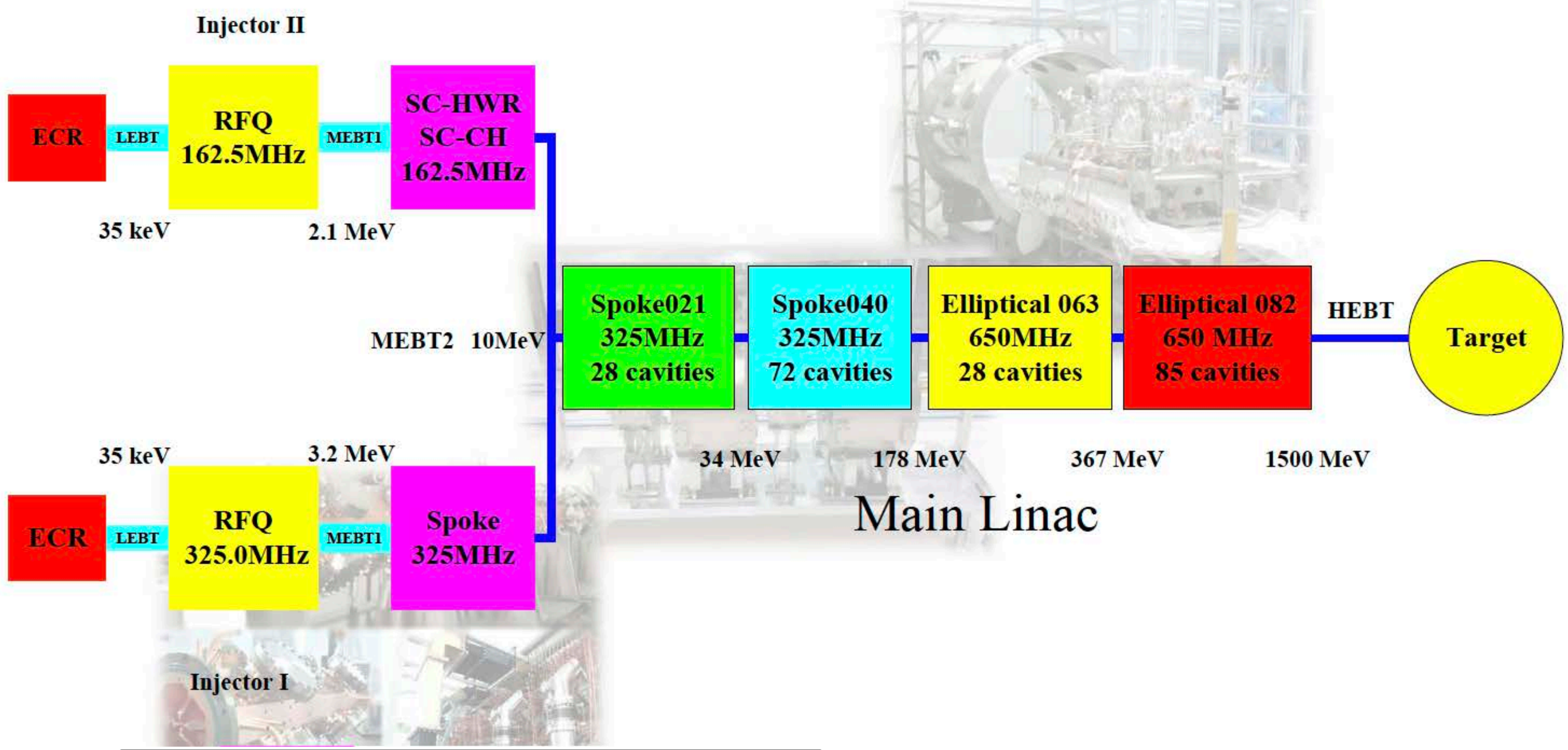

Particle	Proton	
Energy	1.5	GeV
Current	10	mA
Beam power	15	MW
rf frequency	(162.5)/325/650	MHz
Duty factor	100	%
Beam loss	<1	W/m
Beam trips/year [1]	<25000	1 s < t < 10 s
	<2500	10 s < t < 5 m
	<25	t > 5 m

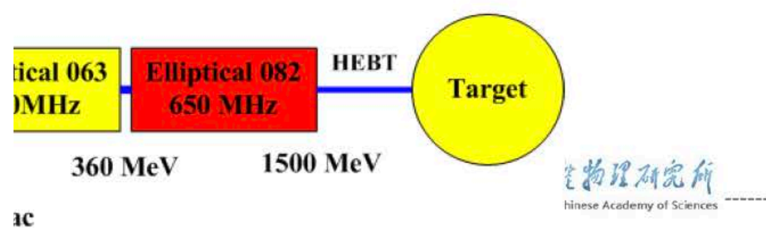

COMMISSIONING OF THE CHINA-ADS INJECTOR-I TESTING FACILITY

Injector-I Specifications	
Particle	H^+
Output Energy (MeV)	10
Current (mA)	10
Beam power (kW)	100
Duty factor (%)	100
RF frequency (MHz)	325

IFMIF/EVEDA Project

IFMIF, the International Fusion Materials Irradiation Facility, is an accelerator-based neutron source that will use Li(d,xn) reactions to generate a flux of neutrons with a broad peak at 14 MeV equivalent to the conditions of the Deuterium-Tritium reactions in a fusion power plant. (EVEDA: Engineering Validation and Engineering Design Activities).

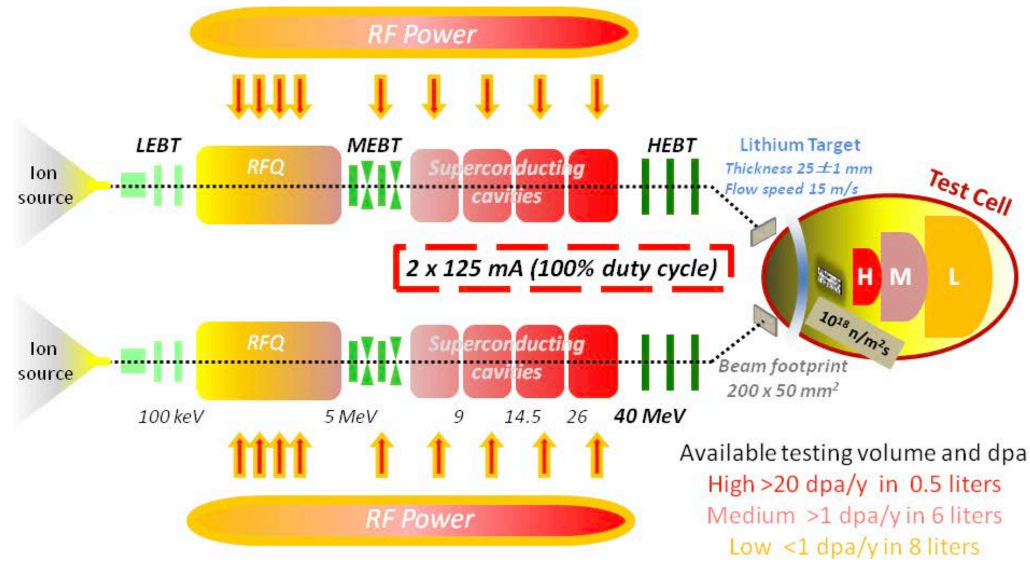

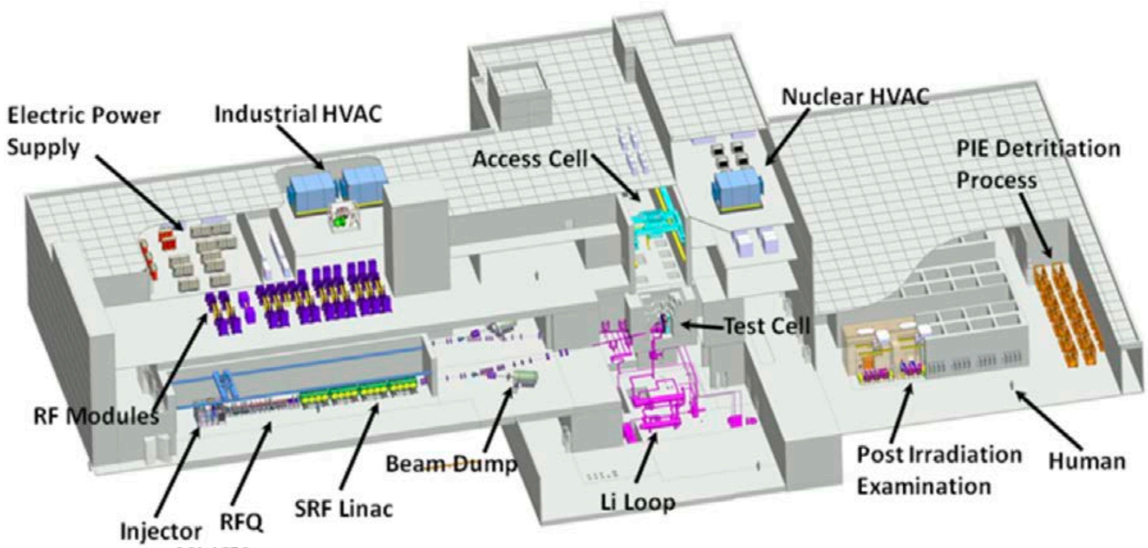

HIGH CURRENT PROTOTYPE ACCELERATOR OF IFMIF/EVEDA

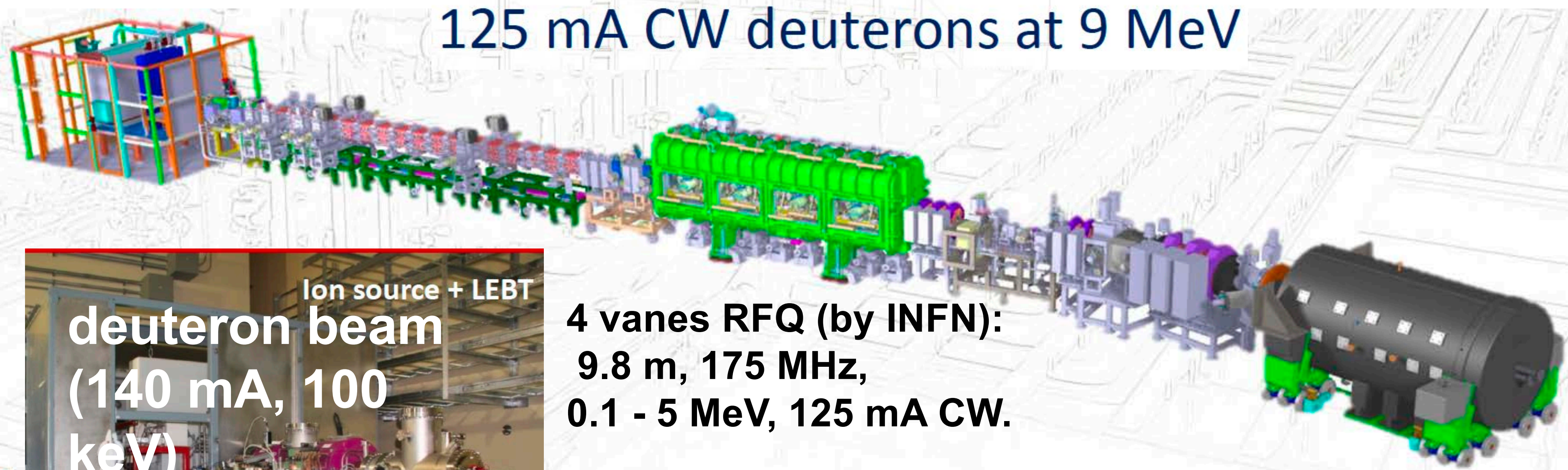

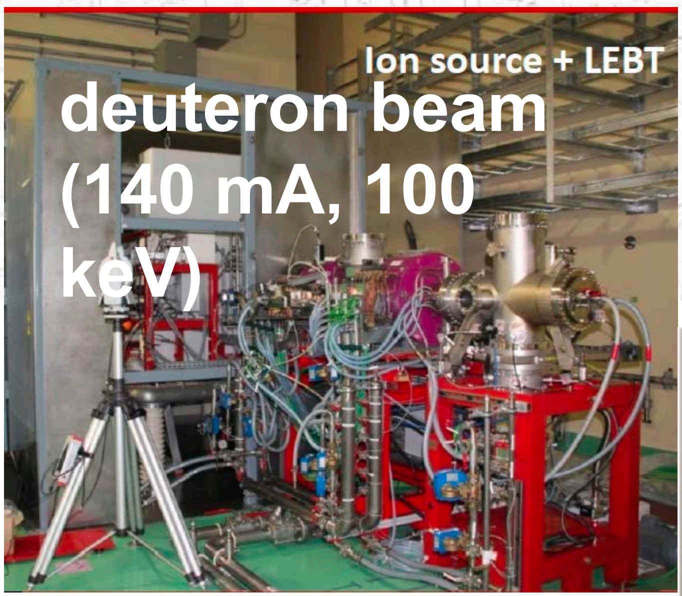

4 vanes RFQ (by INFN):
9.8 m, 175 MHz,
0.1 - 5 MeV, 125 mA CW.

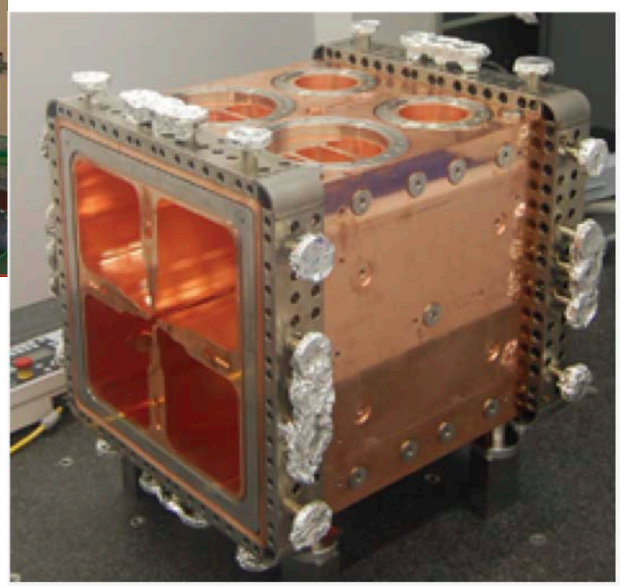

First RFQ module completed (Module 16)